Universidade do Minho
Escola de Ciências

Paulo Jorge Magalhães Cardoso

A study of the electrical properties
of carbon nanofiber polymer composites

Paulo Cardoso A study of the electrical properties of carbon nanofiber polymer composites

UMinho | 2012

fevereiro de 2012

Universidade do Minho
Escola de Ciências

Paulo Jorge Magalhães Cardoso

A study of the electrical properties
of carbon nanofiber polymer composites

Tese de Doutoramento
Física

Trabalho efetuado sob a orientação do
Professor Doutor Senentxu Lanceros-Méndez

e co-orientação do
Professor Doutor Ferrie Wander Joseph van Hattum

fevereiro de 2012

DECLARAÇÃO

Paulo Jorge Magalhães Cardoso

Endereço electrónico: pjmcardoso@gmail.com

Telefone: +351253510100

Número do Bilhete de Identidade: 10478145 9 ZZ7

Título dissertação:

A study of the electrical properties of carbon nanofiber polymer composites

Orientador:

Professor Doutor Senentxu Lanceros-Méndez

Co-Orientador:

Professor Doutor Ferrie Wander Joseph van Hattum

Ano de conclusão: 2012

Designação do Ramo de Conhecimento do Doutoramento:

Física

Nos exemplares das teses de doutoramento ou de mestrado ou de outros trabalhos entregues para prestação de provas públicas nas universidades ou outros estabelecimentos de ensino, e dos quais é obrigatoriamente enviado um exemplar para depósito legal na Biblioteca Nacional e, pelo menos outro para a biblioteca da universidade respectiva, deve constar uma das seguintes declarações:

Universidade do Minho, ____/____/_____

Assinatura: _____

Acknowledgements

Abstract

The interest of industry on using carbon nanofibers (CNF) as a possible alternative to carbon nanotubes (CNT) to produce polymer based composites is due to their lower price, the ability to be produced in large amounts and the their usefulness as a reinforcement filler in order to improve the matrix properties such as mechanical, thermal and electrical. Polymers like epoxy resins already have good-to-excellent properties and an extensive range of applications, but the reinforcement with fillers like CNF, which has high aspect ratio (AR) and surface energy, has the potential to extend the range of applications. The Van der Waals interactions between nanofillers, such as CNF, promote the clustering effect which affects their dispersion in the polymer and may interfere with some properties of the nanocomposites. In this sense, it is very important to use appropriate dispersion methods which are able to disentangle the nanofillers to a certain degree, but avoiding the reduction of the nanofibers AR as much as possible. In fact, the methods and conditions of nanocomposites processing have also influence on the filler orientation, dispersion, distribution and aspect ratio. To the present day, there is a lack of complete information in the literature about the relation between structure and properties, in particular electrical properties, for polymer nanocomposites.

The main objective of this work is to study the electrical properties of composites based on CNF and epoxy resin using production methods which can be easily implemented in industrial environments and that provide different dispersion levels, investigating therefore the relationship between dispersion level and electrical response. Some of the requirements for such methods are the adaptability to the industrial processes and facilities which allow large scale productions and provide a good relation between quality and cost of the composite materials. In this work, morphological, electrical and electromechanical studies were performed in epoxy resin composites with vapor-grown carbon nanofibers (VGCNF). First, the electrical properties of VGCNF/epoxy resin composites produced with a simple method were studied. Then, it was investigated the relation between the electrical properties and the dispersion level of VGCNF/epoxy composites produced with different methods, which were selected to provide different levels of dispersion. The level of nanofiber dispersion of the composites produced with the different methods and filler contents was analyzed by transmission optical microscopy (TOM) and greyscale analysis (GSA) and then

compared to the electrical conductivity measurements. After this study, the influence of different methods of VGCNF dispersion on the electrical conduction mechanism of the composites was investigated. Then, these composites were submitted to electromechanical tests in order to apply them as piezoresistive sensors. The last study of this work was dedicated to an initial comparison between the epoxy composites with VGCNG and multi-walled carbon nanotubes (MWCNT), in terms of electrical and morphological properties.

As the main outcomes of the present work, it can be concluded that a better cluster dispersion seems to be more suitable than good filler dispersion for achieving larger electrical conductivities and lower percolation thresholds. It is also concluded that hopping conductivity is a relevant mechanism for determining the overall conductivity of the composites and that the CNF/epoxy composites are appropriate materials for piezoresistive sensors in particular at concentrations close to the percolation threshold.

Resumo

O interesse da indústria em usar as nanofibras de carbono (CNF) como uma possível alternativa aos nanotubos de carbono (CNT) para produzir compósitos em base polimérica deve-se ao seu baixo preço, facilidade de serem produzidos em grandes quantidades e a sua utilidade como cargas de reforço para aperfeiçoaras propriedades mecânicas, térmicas e elétricas da matriz. Polímeros tais como as resinas epóxidas, já possuem propriedades boas ou até mesmo excelentes e têm uma gama elevada de aplicações, mas o seu reforço com cargas como as CNF, que têm valores elevados de razão entre comprimento e diâmetro (AR) e também de energia de superfície, tem o potencial de estender a gama de aplicações. As interacções de Van der Waals entre cargas nanométricas (nanocargas), tais como as CNF, promovem o efeito de aglomeração que afeta a sua dispersão no polímero e poderá interferir com algumas propriedades dos nanocompósitos. Neste sentido, é muito importante usarem-se métodos de dispersão apropriados que sejam capazes de libertar (desemaranhar) as nanocargas até um determinado grau, de forma a evitar a redução do AR tanto quanto possível. De facto, os métodos e condições de processamento dos nanocompósitos também têm influência nas cargas em termos de orientação, dispersão, distribuição e AR. Hoje em dia existe uma falta de informação generalizada na literatura acerca da relação entre a estrutura e as propriedades dos nanocompósitos poliméricos, em particular nas propriedades eléctricas.

O objectivo principal deste trabalho é o estudo das propriedades eléctricas dos compósitos baseados em CNF e resina epóxida usando métodos de produção que possam ser facilmente implementados num ambiente industrial e que permitam vários níveis de dispersão, investigando desta forma a relação entre o nível de dispersão e a resposta eléctrica. Alguns dos pressupostos para esses métodos, são a sua adaptabilidade aos processos e instalações industriais que permitam produções em larga escala e proporcionem uma boa relação entre a qualidade e o custo dos materiais compósitos. Neste trabalho, foram desenvolvidos estudos morfológicos, elétricos e eletromecânicos em compósitos de resina epóxida com nanofibras de carbono de crescimento por vaporização (VGCNF). Primeiramente foram estudadas as propriedades elétricas de compósitos de resina epóxida com VGCNF produzidos a partir de um método simples. De seguida, foi investigada a relação entre as propriedades elétricas e o nível de dispersão de VGCNF nos compósitos de resina epóxida, produzidos com diferentes

métodos, os quais foram seleccionados de forma a proporcionarem diferentes níveis de dispersão. O nível de dispersão das nanofibras em compósitos produzidos com diferentes métodos e concentrações de cargas foi analisado através da microscopia ótica de transmissão (TOM) e da análise da escala de cinzentos (GSA), sendo posteriormente comparados os resultados com as medições de condutividade elétrica. Depois deste estudo, foi investigada a influência dos diferentes métodos de dispersão nos mecanismos de condução eléctrica dos compósitos. Seguidamente, estes compósitos foram submetidos a testes eletromecânicos de forma a poderem ser aplicados como sensores piezoresistivos. O último estudo deste trabalho foi dedicado a uma comparação inicial entre os compósitos de resina epóxida com VGCNF e os com nanotubos de carbono multi-parede (MWCNT), em termos de propriedades elétricas e morfológicas.

Dos principais resultados deste trabalho pode-se concluir que uma melhor dispersão dos aglomerados parece ser mais adequada do que uma boa dispersão das nanocargas para alcançar condutividades eléctricas elevadas e limiares de percolação reduzidos. Também é possível concluir que a condução por efeito de "hopping" é um mecanismo relevante para determinar a condutividade global dos compósitos e que os compósitos de resina epóxida e CNF são materiais apropriados para serem aplicados como sensores piezoresistivos, particularmente para concentrações próximas do limiar de percolação.

Table of contents

List of figures

List of tables

List of symbols

υ - Poisson ratio

β - Critical exponent dependent on the system dimension

<Ve> - Excluded volume

a - Disorder strength, distance between two bending points

A - Electrode area

A_T - Effective cross-sectional area involving the part of conducting electricity

b - Domain volume divided by the volume filler

d - Barrier width, sample thickness

D - Cylinder average diameter

d_0 - Tunneling distance (between CNF)

dB - Decibel

dl - Variation in length

dR - Resistance change

dz – Displacement in z-axis direction

E_a - Tunnel activation energy

E_g - Band gap energy

g/cm^3 - Gram per centimeter cubic

g/m^2 - Gram per meter squared

g/mol - Gram per mole

G_{cut} - Effective system conductance

G_{cut} - System effective conductance before being conductive

G_{eff} - Composite conductance

Hz - Hertz

I - Electrical current

K_B - Boltzmann constant

Kg - Kilogram

KHz - Kilohertz

L - Cylinder average length

l_{opt} - Optimal path between two vertices

L_T - Effective length involving the part of conducting electricity

m - Charge carriers mass

m^2/g - Meter squared per gram

mbar - Milibar

MHz - Megahertz

min - Minute

mm - Millimeter

nm - Nanometer

N_{max} - Maximum number of fillers in the domain

º - Degrees (angle)

ºC - Degrees Celsius

R - Steady-state material electrical resistance

R - Surface resistance

$R(\varepsilon)$ - Composite resistance under tensile strain (ε)

R_0 - Composite resistance for $\varepsilon = 0$

R^2 - Linear regression coefficient

R_B - Junction resistance

R_m - Proportional constant

rpm - Rotations per minute

R_T - Intrinsic resistance

R_t - Proportional constant

s - Superconductivity critical exponent

S/cm - Siemens per centimeter

t - Conductivity critical exponent

T - Temperature

tan(δ) - Dielectric loss

V - Electrical voltage, filler volume

$V(T)$, φ - Temperature modified barrier height

vol.% - Volume percentage

W/(m.K) - Watt per meter and Kelvin

wt.% - Weight percentage

x_0 - Scale over which the wave function decays

x_{ij} - Distance between two fillers

α - Degree of cure

δ_{max} - Maximum value for the minimum distance between cylinders

ΔR_D - Resistance change due to the geometrical effect

ΔR_I - Resistance change due to the intrinsic piezoresistive effect

ε - Tensile strain

ε_{eff} - Composite (effective) dielectric constant

ε_{ij} - Dielectric constant between two fillers

$\varepsilon_{ij}/(K_B T)$ - Thermal hopping term

ε_{matrix} - Matrix dielectric constant

μm - Micrometer

σ - Conductivity

σ_0 - Dimension coefficient

σ_{AC} - Alternating current conductivity

$\sigma_{conductor}$ - Conductor (filler) conductivity

σ_{eff} - Composite conductivity

σ_{matrix} - Matrix conductivity

Φ - Concentration (filler)

Φ_c - Percolation threshold

ω - Frequency

Ω.cm - Ohm times centimeter

ħ - Planck constant

List of abbreviations

^{13}C NMR- ^{13}C solid-state nuclear magnetic resonance

ABS- Acrylonitrile-butadiene-styrene

AC- Alternating current

ACM- Polyacrylate

AFM - Atomic force microscopy

AR - Aspect ratio

ASI- Applied Sciences, Inc.

BR- Butadiene rubber

CAS- Chemical abstract service

CCVD- Catalytic carbon vapor deposition

CMNC- Ceramic matrix nanocomposites

CNF- Carbon nanofibers

CNT- Carbon nanotubes

CSM- Chlorosulfonated polyethylene

CVD- Chemical vapor deposition

DC- Direct current

DETA- Diethylenetriamine

DETDA- Diethyltoluenediamine

DGEBA- Diglycidyl ether of bisphenol-A

DGEBF- Diglycidyl ether of bisphenol-F

DSC- Differential scanning calorimetry

DWCNT- Double-walled carbon nanotubes

EPDM- Ethylene propylene diene monomer

EPM- Ethylene propylene monomer

ESR- Electron spin resonance

ETFE- Ethylene-tetrafluoroethylene

FEP- Fluorinated ethylene propylene

FTIR- Fourier transformed infrared spectroscopy

GF- Gauge factor

GMRL- General motors research laboratories

GSA- Greyscale analysis

HRTEM- High-resolution transmission electron microscopy

IIR- Butyl rubber

LCP- Liquid crystal polymer

MDA - Methylene dianiline

MMNC - Metal matrix nanocomposites

MWCNT- Multi-walled carbon nanotube

NBR- Acrylonitrile butadiene copolymers

NMR- Nuclear magnetic resonance

PA- Polyamide

PAN- Polyacrylonitrile

PBI- Polybenzimidazole

PBT- Polybutyleneterephthalate

PC- Polycarbonate

PE- Polyethylene

PEEK- Polytherether ketone

PEI- Polyetherimide

PET- Polyethylene terephthalate

PFA- Perfluoroalkoxy

PI- Polyimide

PMMA- Polymethylmethacrylate

PMNC- Polymer matrix nanocomposites

POM- Polyoxymethylene or polyacetal

POSS- Polyhedral oligomeric sislesquioxanes

PP- Polypropylene

PPE- Polyphenylene ether

PPS- Polyphenylene sulfide

PS- Polystyrene

PSR- Polysulfide rubber

PSU- Polysulfone

PTFE- Polytetrafluoroethylene

PVC- Polyvinyl chloride

PVD- Physical vapor deposition

PVDF- Polyvinylidene fluoride

ROM - Rule-of-mixtures

RTM- Resin transfer molding

SAN- Styrene acrylonitrile

SANS- Small angle neutron scattering

SAXS- Small angle X-ray

SBR- Styrene butadiene rubber

SEM- Scanning electron microscopy

SiR- Silicone rubber

SPM - Scanning probe microscopy

SSA - Specific surface area

STM- Scanning tunnelling microscopy

SWCNT- Single-walled carbon nanotube

Td- Decomposition temperature

TEM- Transmission electron microscopy

TETA- Triethylene-tetramine

Tg- Glass transition temperature

TOM- Transmission optical microscopy

USA- United States of America

USSR- Union of Soviet Socialist Republics

UV-VIS - Ultraviolet-visible

VGCF- Vapor-grown carbon fibers

VGCNF- Vapor-grown carbon nanofibers

WAXS - Wide-angle X-ray scattering

XPS- X-ray photoelectron spectroscopy

XRD- X-xay diffractometry

1. Introduction

1.1- Objective

The focus of the research on polymer nanocomposites has been mainly on carbon nanotubes (CNT) as reinforcement filler rather than carbon nanofibers (CNF), as CNT have fewer microstructural defects, resulting in better properties, besides having smaller dimensions and lower density than CNF. However, there are several methods used to treat those defects [1-6] and for biological applications, for instance, CNF can be more attractive than CNT [7]. The largest advantages of using CNF instead of CNT are their lower price and their ability to be produced in large scale which encourage further research on composites with CNF, mainly for industrial productions [8].

The main objective of this thesis is to study the electrical properties of composites based on CNF and epoxy resin using methods of production adjusted to the industrial requirements, in order to be applied in specific applications, in particular as piezoresistive sensors. Some of these requirements are the use of preparation methods which can be adapted to the industrial processes and facilities, allowing a large scale production and a having a good relation between the quality and the cost of the final product.

To achieve this goal, the first section of the work is devoted to the investigation of the electrical properties of composites made of vapor-grown carbon nanofibers (VGCNF) and epoxy resin which are produced with a very simple method, inexpensive and less demanding that other ones used in this thesis. In the second section it is studied the relation between the electrical properties and the dispersion level of VGCNF/epoxy composites produced with different methods, where the selected methods of VGCNF dispersion were intended to provide different levels of dispersion. The level of dispersion of the composites produced with the different methods at different filler contents was quantified by transmission optical microscopy (TOM) and greyscale analysis (GSA) and compared with the electrical conductivity of the composites. Further, the influence of the different methods of VGCNF dispersion on the mechanism of electrical conduction of the composites was theoretically analyzed. The possible application of these composites as piezorestive sensors was also investigated. Finally, an analysis of the main differences between the epoxy composites prepared with CNF and CNT, in terms of electrical and morphological properties, was performed. The main goal is to build a bridge between the study presented in this work about CNF

composites and future similar studies that can be performed in CNT composites based on the same matrix.

1.2- Structure and methodology

This thesis is divided in eight chapters. The first chapter is dedicated to the introduction of the thesis, with the presentation of the objectives, structure and methodologies of the work. The second chapter reviews the state of the art related to the subject of the thesis and from the third to the seventh chapter the most important results of the work and the corresponding discussions are presented, while the eighth chapter is focused on the final conclusions of the work and in possible future research directions.

The state of the art is divided in two main sections. The first one presents a literature review on polymer nanocomposites, making a general approach to the different types of nanofillers, polymer bases, production, properties and applications of polymer nanocomposites, as well as a brief mention to other types of nanocomposite matrices. The second section is dedicated specifically to the CNF/epoxy composites, presenting the main preparation methods, their main properties, in particular the electrical properties and applications.

The chapters corresponding to the results and discussions are five. The first one is the third chapter of this thesis and consists on the study of the main electrical conduction mechanism of composites reinforced with VGCNF dispersed in the matrix using a simple blender mixing method, in order to produce composites with nine filler contents, from 0 to 3 wt.%. The composite electrical properties such as alternating current (AC) and direct current (DC) measurements were performed, and also scanning electron microscopy (SEM) images were taken in order to have a first insight of the morphology of the composites.

The fourth chapter is focused on a quantitative analysis of the dispersion ability of four different methods for the preparation of VGCNF/epoxy composites. The dispersion methods used were the blender mixing, capillary rheometry mixing, 3 roll milling and planetary centrifuge mixing. The relationship between dispersion and DC conductivity of the composites was also evaluated. For the dispersion analysis, four nanofiber concentrations ranging from 0.1 to 3.0 wt.% were prepared for each method, while the DC measurements were performed for eight concentrations, ranging from 0 to 4.0 wt.%. The dispersion was analyzed by TOM and GSA.

In the fifth chapter, the composites were subjected to deeper studies in terms of the electrical conduction mechanism.

The sixth chapter presents a study of the piezoresistive response of composites prepared with the dispersion methods already presented. The composite response was measured as a function of carbon nanofiber loading for the different dispersion methods. Strain sensing by variation of the electrical resistance was tested through 4-point bending experiments, and the dependence of the gauge factor (GF) on the deformation and velocity of deformation was calculated as well as the stability of the electrical response.

The seventh chapter focuses on the comparative study of the electrical properties and the nanofillers dispersion level of epoxy resin based composites with VGCNF and multi-walled carbon nanotube (MWCNT). A blender was used to disperse the nanofillers within the matrix, producing samples with concentrations of 0.1, 0.5 and 1.0 wt.% for both nanofillers. The dispersion of the nanofillers was analyzed using SEM and TOM, in association with the GSA. The electrical conductivity and the dielectric constant were also evaluated.

The eighth chapter of this thesis, as previously mentioned, is dedicated to the final conclusions of this work as well as to the indication of future research works in this area.

References

1.   Lafdi, K., et al., Effect of carbon nanofiber heat treatment on physical properties of polymeric nanocomposites: part I. J. Nanomaterials, 2007. 2007(1): p. 1-6.

2.   Cortés, P., et al., Effects of nanofiber treatments on the properties of vapor-grown carbon fiber reinforced polymer composites. Journal of Applied Polymer Science, 2003. 89(9): p. 2527-2534.

3.   Kumar, S., et al., Study on mechanical, morphological and electrical properties of carbon nanofiber/polyetherimide composites. Materials Science and Engineering: B, 2007. 141(1-2): p. 61-70.

4.   Patton, R.D.P., Jr C. U. Wang, L. Hill, J. R., Vapor grown carbon fiber composites with epoxy and poly(phenylene sulfide) matrices Composites Part A: Applied Science and Manufacturing, 1999. 30(9): p. 1081-1091.

5.   Ahn, S.-N., et al., Epoxy/amine-functionalized short-length vapor-grown carbon nanofiber composites. Journal of Polymer Science Part A: Polymer Chemistry, 2008. 46(22): p. 7473-7482.

6.   Lozano, K. and E.V. Barrera, Nanofiber-reinforced thermoplastic composites. I. Thermoanalytical and mechanical analyses. Journal of Applied Polymer Science, 2001. 79(1): p. 125-133.

7.   Al-Saleh, M.H. and U. Sundararaj, A review of vapor grown carbon nanofiber/polymer conductive composites. Carbon, 2009. 47(1): p. 2-22.

8.   Sun, L.H., et al., Preparation, Characterization, and Modeling of Carbon Nanofiber/Epoxy Nanocomposites. Journal of Nanomaterials, 2011: p. 8.

2. State-of-the-art

The state of the art presents a literature review on polymer nanocomposites, making a general approach to the different types of nanofillers, polymer bases, production, properties and applications of polymer nanocomposites, as well as a brief mention to other types of nanocomposite matrices. It is also presented theCNF/epoxy composites preparation methods, properties, mainly the electrical properties, and applications.

2.1- Polymer nanocomposites

2.1.1- Introduction

Nanocomposites result from the combination of at least one nanomaterial with one or more separated components in order to introduce new functionalities in the matrix and/or to reinforce some of their characteristics. Nanocomposites can be classified in three different categories: ceramic (CMNC), metal (MMNC) and polymer (PMNC) matrix nanocomposites which examples are presented in table 2.1 [1].

Table 2.1 - Different kinds of nanocomposites [1].

Class	Examples
Metal	$Fe-Cr/Al_2O_3$, Ni/Al_2O_3, Co/Cr, Fe/MgO, Al/CNT, Mg/CNT
Ceramic	Al_2O_3/SiO_2, SiO_2/Ni, Al_2O_3/TiO_2, Al_2O_3/SiC, $Al2O_3/CNT$
Polymer	Thermoplastic/thermoset polymer/layered silicates, polyester/TiO_2, polymer/CNT, polymer/layered double hydroxides

In a nanocomposite, nanoparticles (clay, metal, carbon nanotubes, etc.) act as fillers in a matrix that can be a polymer matrix. The development of polymer nanocomposites with organic or inorganic fillers has been of large importance over the last two decades. To overcome the limitations of traditional micrometer-scale polymer composites, nanocomposites contain fillers with at least one of its dimensions in the nanoscale range (<100 nm) [2]. Commercial applications of polymer nanocomposites are in sporting goods, aerospace components, automobiles, among others [3].

Nanocomposites are examples of real applications of nanotechnology which is growing fast, although it still has the image of a future that is yet to come. For instance, Geoff Ogilvy won the United States of America (USA) Open golf tournament in 2006 using a club made of epoxy resin strengthened with a nanomaterial [4]. Nanocomposites incorporate fillers such as metal, carbonaceous (carbon black, carbon nanotubes and nanofibers), mineral or other nanoparticles, which have the ability to enhance significantly the properties of the matrix. Polymer-based nanocomposites are by far the most commercialised class of nanocomposites worldwide.

Microscopy has been essential to the development of nanotechnology and, in particular, of nanomaterials, by improving the characterization of the relationship between a controllable starting composition with the structure and improved properties of the obtained nanomaterial [5]. At the same time, the prediction and characterization of the properties at the nanoscale via modeling and simulation has been facilitated by the fast growth of computer technology, which plays an important and irreplaceable role in providing physical insights into the performance of polymer nanocomposites [6]. The combination of the characteristics of nanomaterials, such as mechanical properties, nanofiller size and content make them outstanding materials. Moreover, it is possible to produce and process polymer nanocomposites using the same procedures as for conventional polymer composites. Compared to conventional micro and macro composites, nanocomposites exhibit enhancements in mechanical, thermal, optical, physico-chemical and other properties, at low filler contents [7, 8]. Besides the filler content, the component structure, interfacial interactions and properties are also key factors for the properties of all heterogeneous polymer systems [9]. The difference in the aspect ratio and surface-to-volume ratio of the nanofillers in comparison to higher dimension fillers is one of the key issues [10]. For particles and fibers, the surface area per unit volume is inversely proportional to the diameter of the material. Therefore, if its diameter is smaller, the surface area per unit volume is higher [11].

Figure 2.1 shows the usual particle geometries and the corresponding ratios of area versus volume.
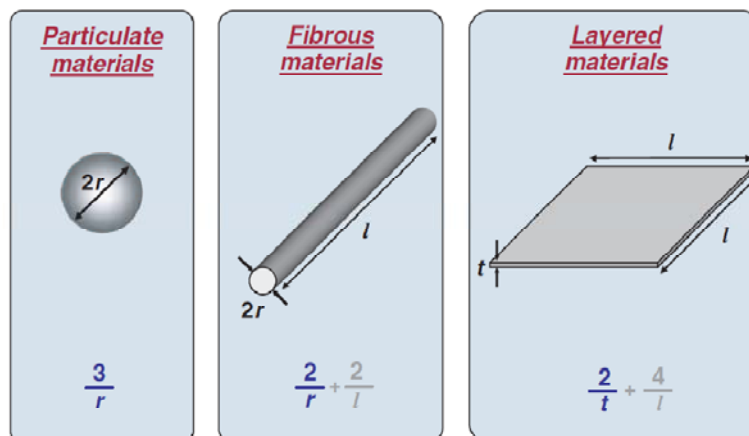
Figure 2.1 - Geometries of particle reinforcements and the corresponding surface versus volume ratio [12].

The change from the micrometer to nanometer range in layer thickness, particle or fibrous material diameter will affect the surface area/volume ratio by three orders of magnitude [12]. Nanoparticles, fullerenes, nanotubes, nanofibers, and nanowires are classified by their geometries as particle, layered, and fibrous materials [12, 13]. Carbon nanofibers and nanotubes are examples of fibrous materials whereas carbon black, silica nanoparticle and polyhedral oligomeric sislesquioxanes (POSS) can be classified as nanoparticle fillers for reinforcement [13]. The nanocomposite properties have an outstanding influence of the size scale of its component phases and the degree of mixing between the two phases. The composite properties may be considerably influenced by the method of preparation and the nature of the used components, such as polymer matrix, layered silicate or nanofiber and cation exchange capacity [14]. Figure 2.2 shows the differing dispersion levels of three main types of composites for layered silicate materials.
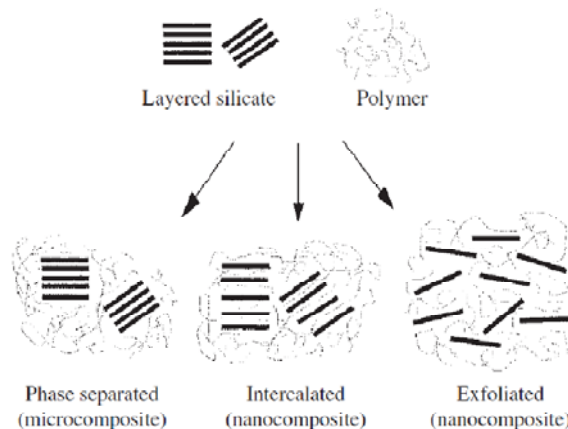
Figure 2. 2 -Scheme of the three main types of layered silicates in polymer matrix [8].

If the polymer is incapable of intercalating or penetrating between the silicate sheets, the result is a phase-separated composite and the properties are similar to those of traditional microcomposites. In an intercalated structure, if the extended polymer chains penetrate between the silicate layers, the result is a well-ordered multilayer morphology with alternating layers of polymeric and inorganic nanofillers. When the dispersion of silicate layers in a continuous polymer matrix is uniform and complete, it is obtained an exfoliated or delaminated structure [8]. The dispersion level of the nanofillers in a polymer matrix is very important and a homogeneous dispersion plays a key role, mostly in mechanical properties. The interfacial strength between filler and

polymer matrix is very important for a good adhesion between the two phases to prevent early failures. Optical, magnetic, electronic, thermal, wear resistance, barrier to diffusion, water resistance and flame retardancy properties can be strongly affected by nanoparticle dispersion in polymer matrices [2]. Although the addiction of nanofillers improves some properties of the polymer matrix, several issues remain largely unresolved even from an empirical perspective. These main issues are the qualitative and quantitative characterization of the dispersion and distribution of nanofillers; the polymer properties, which includes the chain conformation, nonlocal dynamics and local motions; and how these collectively affect the enhancement of the hybrid macroscale properties [15].

2.1.2- Nanomaterials

Nanomaterials are structured components with at least one dimension less than 100 nm. Materials with one dimension in the nanoscale are layers, such graphite, layered silicate, and other layered minerals. Materials that are nanoscale in two dimensions are fibrous, such as nanowires, carbon nanofibers and nanotubes. Materials that are three dimensionally nanoscaled are particles, for example silica, metal, colloids, quantum dots and other organic and inorganic nanoparticles. Nanocrystalline materials are also nanoparticles, which consist of nanoscale grains [12, 16].

2.1.2.1- Layered nanomaterials

Surface and thin film technology have been strongly developed in recent years. Many devices produced in the industry of integrated circuits are based on thin films and the use of film thicknesses at the atomic level is viable and even routine. Monolayers are routinely processed and used in chemistry. The fabrication of monolayers and its properties are reasonably well known from the atomic level to higher levels, even for layers with a high level of complexity.

Clay and graphite composites are two classes of nanoplatet-reinforced composites and in their bulk state, both of them exist as layered materials. For an efficient use of these nanomaterials, a good and efficient separation and dispersion of the layers throughout the matrix is important. The inclusion of clay nanomaterials in polymer matrices improve the strength, stiffness, toughness, thermal stability and

expansion and also reduce the gas permeability. Clay materials such as montmorillonite, saponite, and synthetic mica are commonly used as layered nanomaterials.

The exfoliated graphite or graphene sheet is another layered material and its thickness is almost the same as exfoliated clay. The graphene sheet has a low electrical resistivity, so the polymer composite conductivity is improved when the graphene content reaches the percolation threshold [12]. Graphene consists of a single layer with carbon atoms arranged in a dense honeycomb crystal lattice and its thickness ranges from 0.35 to 1 nm [17]. The platelet thickness measured by Novoselov et al. was from 1 to 1.6 nm [18].

2.1.2.2- Fibrous nanomaterials

In recent years, fibrous nanomaterials such as nanotubes and nanowires got the research interest of the scientific community, mostly because of their novel mechanical and electrical properties. Examples of fibrous nanomaterils are the carbon nanotubes and nanofibers, inorganic nanotubes, nanowires and biopolymers.

CNT are extended tubes of rolled graphene sheets. There are two types of CNT: single-walled carbon nanotubes (SWCNT) and multi-walled carbon nanotubes (MWCNT) and both have usually several micrometres length and few nanometres in diameter. CNT have assumed an important role in the context of nanomaterials, because of their novel properties. The outstanding properties of CNT allow a range of potential applications, such as sensors, nanoelectronics, display devices and the reinforcement of composites.

Soon after CNT, inorganic nanotubes and fullerene-like nanomaterials were discovered and nanocomposites with superior resistance to shockwave impact, tribological properties, catalytic reactivity and storage capacity of hydrogen and lithium were developed.

Nanowires are self-assembled linear arrays of dots or ultrafine wires which can be made from a wide range of materials. Semiconductor nanowires containing gallium nitride, silicon and indium phosphide show outstanding electronic, optical and magnetic properties.

In terms of physical properties, fibrous nanomaterials like carbon nanofibers (CNF) fill the gap between conventional carbon fibers and carbon nanotubes. The

average diameter varies between 5 and 10 μm for conventional carbon fibers and 1 and 10 nm for carbon nanotubes. Its reduced diameter provides a larger surface area with fiber surface functionalities [19]. Usually CNF have an average aspect ratio larger than 100, the length reaching 100 μm and the diameter between 100 and 200 nm. Although the most common structure of CNF is the truncated cones, there are other morphologies such as cones and stacked coins, among others [3]. Applied Sciences, Inc. (ASI) developed Pyrograf-III carbon nanofiber for aerospace applications such as fire retardant coatings, aircraft engine anti-icing, lightning strike protection, conductive aerospace adhesives, thermo-oxidative resistant structures and solid rocket motor nozzles [20-22].

Carbon nanofibers

In the seventies and eighties of the twentieth century researchers started to realize that conventional carbon fibers produced from polyacrylonitrile (PAN) and petroleum pitch could be incorporated in composites, giving excellent properties [23]. France, Japan, the USA and the Union of Soviet Socialist Republics (USSR) made some efforts to produce less expensive vapor-grown carbon fibers (VGCF) from hydrocarbons with the same size and properties of these conventional fibers. These macroscopic 7-10 μm VGCF were produced from iron catalyst particles in an atmosphere of hydrogen mixed with methane or benzene and were recognized as originating from filaments of carbon thickened by chemical vapor deposition (CVD) [24].

Some papers from General Motors Research Laboratories (GMRL) described the development of a process to produce VGCNF continuously using liquid [25] and gaseous [26] catalysts and in 1991 began the commercialization of VGCNF due to a collaboration with ASI. These nanofibers have a stacked-cup morphology, are produced with different thicknesses of surface vapor-deposited carbon and different surface and debulking treatments at prices close to (USA) dollars 200/kg. Many groups investigated and worked with these nanofibers because the price is relatively low and they are easy to obtain in large quantities. Meanwhile, in Japan, some companies such as Sumitomo, Mitsui, Showa Denko, and Nikkiso have developed the capacity to produce

considerable quantities of VGCNF and their application for Li-ion batteries were investigated [27].

In 1991 SWCNT were discovered and accepted as a promising reinforcement material for mechanical and electrical applications, thus many organizations tried to develop a method to produce carbon nanotubes in a practical way [28]. SWCNT have been available only in small quantities and very expensive, which has hindered the potential of these nanofillers as a promising reinforcement for composites. Despite these obstacles, CNT have received more research attention than VGCNF because CNT have smaller diameter, lower density and better mechanical and electrical properties, as previously mentioned. Nevertheless, VGCNF can be seen as an excellent alternative to CNT because they are less expensive and readily available, and they could be used to build research knowledge which might be transferred to CNT. Within the class of CNT, SWCNT are more expensive than MWCNT [29]. Figure 2.3 presents the setup used by ASI to produce VGCNF.
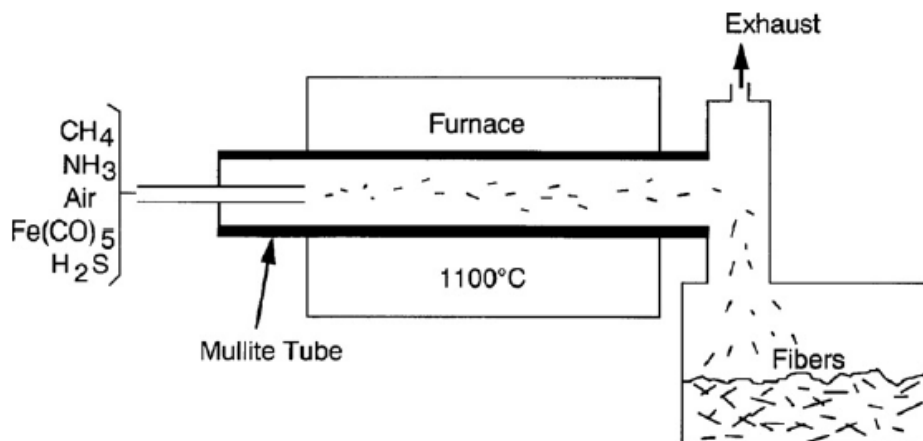
Figure 2. 3- Setup of the process used by ASI for manufacturing VGCNF [24].

The method presented in Figure 2.3 uses natural gas as the feedstock and catalytic iron particles as a catalyst, which comes out of iron pentocarbonyl decomposition. The addiction of hydrogen sulphide promotes the dispersion and activation of the iron catalyst particles, producing carbon nanofibers in the reactor at a temperature close to 1100 ºC (degrees Celsius).

Figure 2.4 shows transmission electron microscopy (TEM) micrographs of the VGCNF structure from a single and double layer in the left and right images, respectively.
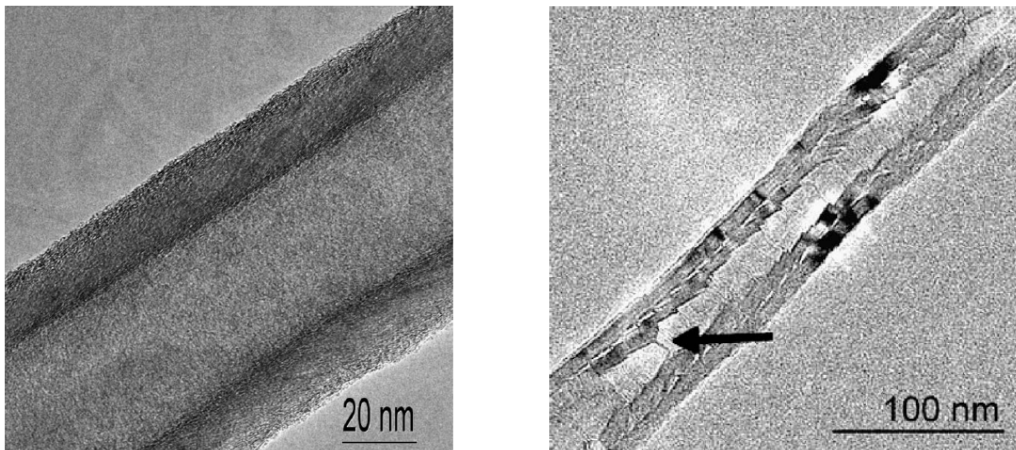
Figure 2. 4- TEM images of the structure of VGCNF with: (left) a single layer [24], and (right) a double layer [30].

Figure 2.4 shows in the left TEM image, a single layer VGCNF with stacked graphite planes with an angle of approximately 25º from the longitudinal axis of the fiber, and in the right TEM image, a double layer VGCNF with stacked graphite planes at a certain angle from the longitudinal axis. Both nanofibers present a hollow core, their stacked graphite planes are nested with each other and have different structures including parallel, bamboo-like and cup-stacked [12, 30-32].

Fig. 2.5 shows schemes representing the structure of VGCNF with a single and double layer.
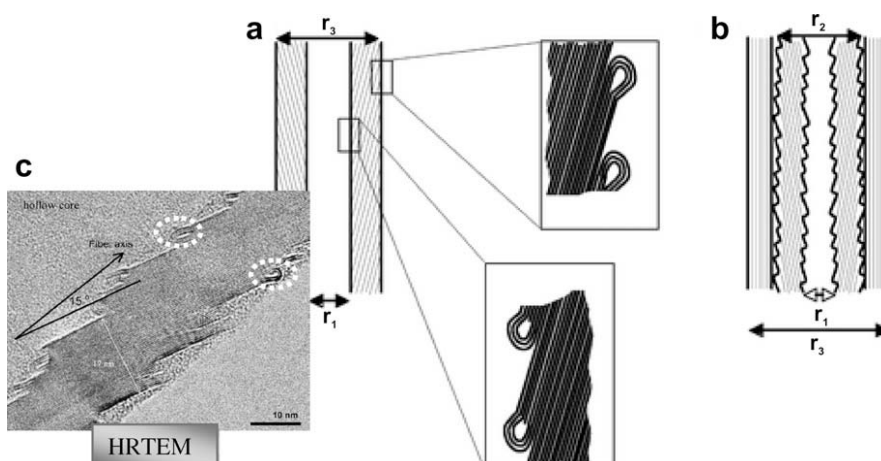
Figure 2. 5- Scheme of the structure of (a) a VGCNF with a single layer and (b) a double layer VGCNF, (c) a HRTEM of the side-wall of a single layer VGCNF [30].

The inset of Figure 2.5 is a high-resolution transmission electron microscopy (HRTEM) of the side-wall of a single layer VGCNF showing the presence of loops at the inner and outer surfaces, where two loops have been enclosed on both sides of the side-wall. The loops are marked in HRTEM image as white ellipses for guiding the eye. The single layer VGCNF have inner and outer diameters of 25 and 60 nm, respectively, while the inner and outer diameters of double layer VGCNF are 20 and 83 nm, respectively. The VGCNF with double layer has a larger diameter and the grapheme planes in the outer layer are parallel to the fiber axis, but the inside layer has the same truncated cone morphology of the single layer VGCNF.

VGCNF in the post-production form are frequently covered with amorphous carbon layers which deteriorate their electrical conductivity. Therefore, it is necessary to use a treatment to remove those outer less conductive carbon layers, which improve the nanofillers crystallinity. There are some techniques used for these purpose, such as debulking, surface treatment and functionalization and also heat treatment.

One of the debulking processes consists in ball milling the VGCNF to decrease the clusters to a size that facilitates the mixing with the matrix, but it is not able to process larger volumes of nanofillers to fulfill industrial needs, although it is effective in the breakdown of the VGCNF clusters. Other debulking techniques have been applied to VGCNF for the same purposes, such as single and twin screw extrusion, but these techniques easily break the nanofillers, damaging the final composites properties.

VGCNF surface treatments such as etching in air near 400 ºC, soaking in sulfuric/nitric acid mixtures or in peracetic acid have proved to be useful. These treatments can add enough oxygen so that 25% of the nanofillers surface contains oxygen atoms [33]. Baek et al. demonstrated that the in-situ polycondensation of an aromatic (ether-ketone) on the VGCNF surface increase its compatibility with aromatic and aliphatic matrices and improves the fiber dispersion [34]. The method to modify the VGCNF surface which is probably the most efficient and less expensive is to change the reactant mix inside the reactor where the fiber growth takes place.

The heat treatment above 2800 ºC of VGCNF with a filamentary core of conically nested graphene planes promotes their recrystallization into disconnected conical crystallites. With this treatment the carbon crystallinity increases but decreases the mechanical and electrical properties of the resulting nanocomposites. For this kind of VGCNF treatment, the suitable temperature to achieve the best mechanical and

electrical properties is 1500 ºC, but this value may vary slightly depending on the particular application. The intrinsic resistivity at room temperature for VGCNF grown near 1100 ºC is 2×10^{-3} Ω.cm, while for graphitized VGCNF is 5×10^{-5} Ω.cm, which is near the resistivity of graphite [24].

Further details on the historical development, production processes and main properties of CNF can be found in the review papers [29] and [24].

The CNF used in this work are the VGCNF Pyrograf III[TM], PR-19-XT-LHT, supplied by Applied Sciences Inc. [35]. PR-19 has an average diameter of approximately 150 nm, a surface area of 15 to 20 g/m^2 and a chemically vapor deposited (CVD) carbon layer on the surface of the fiber over a catalytic layer, as shown in Figure 2.6.
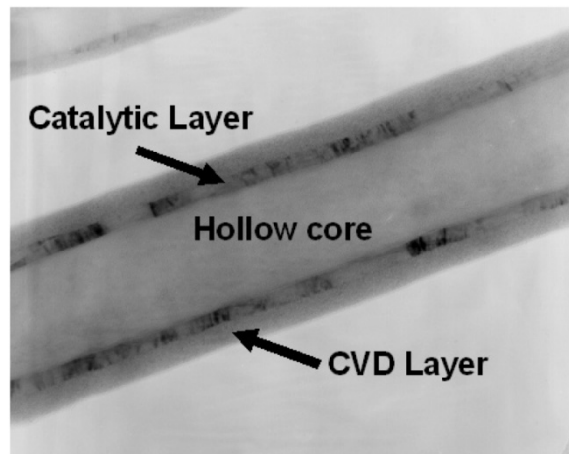
Figure 2. 6- TEM micrograph showing a longitudinal cut along the PR-19 VGCNF axis [35].

The LHT category is produced by the heat treatment of the nanofiber at 1500 ºC, converting any chemically vapor deposited carbon present on the surface of the fiber to a short range ordered structure, which increases the nanofiber intrinsic conductivity. This kind of VGCNF is used preferably to improve mechanical and electrical properties of the composites.

Carbon nanotubes

After the discovery of CNT in 1991 by Iijima [36], researchers from areas such as physics, chemistry, electrical and materials engineering have been dedicated time and resources to study this kind of nanofillers [29]. CNT have low mass density, are highly flexible and have large aspect ratio, typically higher than 1000, in addition to exceptionally high tensile moduli and strengths [37]. Carbon nanotubes are long cylinders of carbon atoms connected with covalent bonds and, in some cases, the cylinder extremities are capped by hemifullerenes. CNT are classified as being SWCNT or MWCNT. It is assumed that SWCNT are made of a single graphene sheet rolled into a seamless cylinder with 1-2 nm in diameter, where graphene is a monolayer of sp2-bonded carbon atoms. These carbon atoms have a part of the sp3 orbital, which increases as the radius of the cylinder curvature decreases. MWCNT are made of nested graphene cylinders coaxially disposed around a hollow core with approximately 0.34 nm separations between the graphene cylinders [38], which are bonded by weak Van der Waals forces [39]. Double-walled carbon nanotube (DWCNT) is a special case of MWCNT because it has two concentric graphene cylinders. It is expected that DWCNT exhibit higher flexural modulus than SWCNT because it has two layers instead of one and also because it has higher toughness than standard MWCNT due to their smaller size [40]. The carbon nanotube diameter, form and chirality determine their properties [41]. A representation of SWCNT and MWCNT is shown in Fig. 2.7.
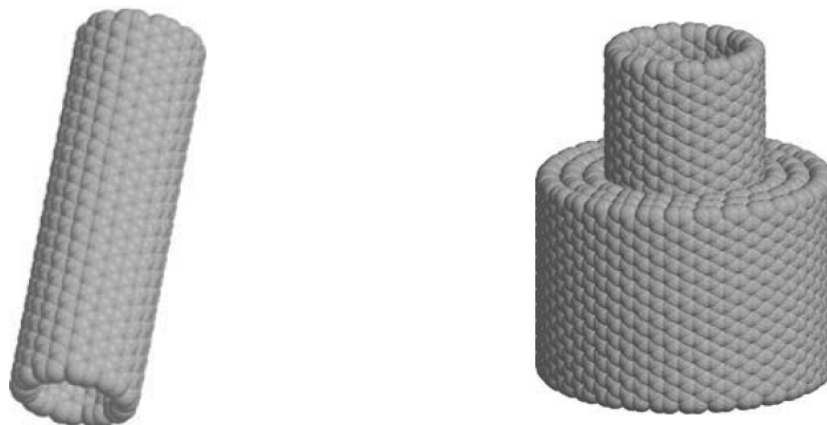
Figure 2. 7- Representation of a (left) SWCNT and (right) MWCNT [42].

MWCNT and SWCNT can be produced by arc discharge, laser ablation,CVD and spinning process [43, 44]. The three most common methods to produce CNT using spinning processes are: from a lyotropic liquid crystalline suspension of CNT, in a process of wet-spinning analogous to that used for polymeric fibers; from previously made MWCNT, grown on a substrate as semi-aligned carpets and finally from SWCNT and MWCNT aerogel as produced in the chemical vapor deposition reactor. The SWCNT average diameter is approximately 1.2-1.4 nm whereas for MWCNT the average diameter varies from several to hundred nanometers. The CNT lengths range from several tens of nanometers to some micrometers [45]. The properties of the CNT/polymer composites vary significantly due to the distribution of the diameter, length and type of nanotubes.

Most available forms of CNT are fragile and isotropic and contain several species despite their intrinsic rigidity and high anisotropy. It is necessary to use pre-processing techniques on the carbon nanotubes to prepare for processing them on a macroscopic scale [46]. It is common to use the following steps: purification to eliminate non-nanotube material, deagglomeration for dispersing individual nanotubes and chemical functionalization for improving CNT/matrix interactions for processability and property enhancement. Several methods are used to prepare nanocomposites with CNT as nanofillers, such as melt-mixing, in-situ polymerization and solution processing, among other methods [47].

The CNT used in this work are the NANOCYL^{TM} NC7000, which are thin MWCNT processed via catalytic carbon vapor deposition (CCVD). A main application for this type of MWCNT is to produce low electrical percolation threshold nanocomposites with high performance as electrostatic dissipative plastics or coatings. NC7000 are available in powder form, have an average diameter of 9.5 nanometers, 1.5 microns average length, 90 % carbon purity, 10 % of metal oxide and a surface area of 250 to 300 m^2/g .

2.1.2.3- Particulate nanomaterials

Quantum effects and relative surface area are the two main factors which distinguish the properties of nanomaterials. These factors can modify or improve their reactivity, electrical and strength properties. Decreasing the particle size places a greater

proportion of atoms in its surface, which decreases the amount of atoms inside the particle. Therefore, in comparison with micro and macro scaled particles, nanoparticles have a higher surface area per unit mass. For example, as the size of structural components of materials like crystalline solids decreases, there is a higher interface area within the material, which can deeply influence its electrical and mechanical properties. Another example is the effect of the application of growth and catalytic chemical reactions to nanomaterial surfaces, because it causes a higher reactivity in nanomaterials than in larger particles [16].

Examples of particulate nanomaterials are metal particles, spherical silica, semiconductor nanoparticles (quantum dots), titanium dioxide and zinc oxide, fullerenes (Carbon 60 - C_{60}) and dendrimers (spherical polymeric molecules) [16, 23].

2.1.3- Polymers

Polymers are long-chain molecules with very high molecular weight which is frequently in the order of hundreds of thousands (g/mol), reason why they are also referred to as macromolecules. Natural products like cotton, proteins, starch and wool were the first polymers to be used and the synthetic polymers were produced in the early beginning of the last century. Bakelite was the first synthetic polymer to be discovered and then nylon, being these polymers the first important synthetic polymers with enormous potential as new materials. However, researchers became aware of the limitations to understand the correlation between the physical properties and the chemical structures [48].

A large number of polymers crystallize (commonly referred to as "semi-crystalline" polymers) and the shape, size and crystallite arrangement is correlated to the way in which the crystallization occurred. Effects like annealing are very important for the final molecular arrangement. Other polymers are amorphous, sometimes because of the high complexity level of their chains which does not allow a regular packing. The beginning of the motion of molecular chains indicates the glass transition [48].

Besides the distinction between amorphous and semi-crystalline, polymers can be classified in different ways. One way to classify the polymers is according to the process of polymerization used for their production. The polymers can also be classified according to their structure as being linear, branched or network polymers and also

based on their intrinsic structure and properties as thermoplastics, elastomers (rubbers) or thermosets. Naturally, the last two sets of classifications are correlated due to the strong link between structure and properties [49].

2.1.3.1- Thermoplastics

The majority of polymers used in applications are thermoplastic [49]. This class of polymers consists on branched or linear molecules which melt when heated and, using this property, this type of polymer can be molded using heat. When the thermoplastic melts, a mass of tangled molecules is formed but in the cooling process they can form a glass or crystallize. Even if the crystallization process happens, it is only partially because the rest becomes more mobile, also referred to non-crystalline or amorphous state. In certain cases and for some temperature region, the thermoplastics form a liquid-crystal phase [49]. The thermoplastics can be classified according to their performances, consumption level and degree of specificity. Polyethylene (PE), polypropylene (PP), polyvinyl chloride (PVC), polystyrene (PS) are examples of commodity thermoplastics; acrylonitrile-butadiene-styrene (ABS) and styrene acrylonitrile (SAN) are known as copolymers with more specific applications. Polyamide (PA), polycarbonate (PC), polymethylmethacrylate (PMMA), polyoxymethylene or polyacetal (POM), polyphenylene ether (PPE), polyethylene terephthalate (PET) and polybutyleneterephthalate (PBT) are some examples of engineering thermoplastics; while polysulfone (PSU), polyetherimide (PEI) and polyphenylene sulfide (PPS), are engineering thermoplastics with more specific performances. Thermoplastics like ethylene-tetrafluoroethylene (ETFE), polytherether ketone (PEEK), liquid crystal polymer (LCP), polytetrafluoroethylene (PTFE), perfluoroalkoxy (PFA), fluorinated ethylene propylene (FEP), polyimide (PI) and polyvinylidene fluoride (PVDF) are for high-tech uses and have limited consumption. Finally, polybenzimidazole (PBI) is a thermoplastic for highly targeted uses with a very restricted consumption [50].

2.1.3.2- Elastomers

Elastomers or rubbers are network polymers with cross-links which can be stretched to high dimensions and have a reversible behaviour. Without stretching, the

elastomers have molecules reasonably well curled in a random way but when stretched, they are elongated and unfolded. Therefore, the molecular chains are less random, the entropy of the material is lower and the decrease in entropy causes a retractive force. When the elastomer is stretched, the cross-links of the molecules guarantee that their relative positions are recovered. The cooling process promotes a partial vitrification or crystallization of the elastomer while in the heating process the elastomer does not melt due to existence of the cross-links [49]. Among elastomers are, for instance, the synthetic rubbers. Examples of synthetic rubbers are acrylonitrile butadiene copolymers (NBR), butadiene rubber (BR), butyl rubber (IIR), chlorosulfonated polyethylene (CSM), ethylene propylene diene monomer (EPDM), ethylene propylene monomer (EPM), polyacrylate (ACM), polysulfide rubber (PSR), silicone rubber (SiR) and styrene butadiene rubber (SBR), among others [51].

2.1.3.3- Thermosets

Thermosets are dense three-dimensional network polymers which are densely cross-linked and typically rigid. It is not possible to melt this class of polymers at any temperature and it can even disintegrate if above a specific temperature level. The name is derived from the fact that, for the first polymers of this class, it was necessary to heat them to induce the cross-linking or curing process. Nowadays, this denomination is used also for polymers where the cross-linking process occurs without heating. Epoxy resins like araldites, polyesters, phenol-formaldehyde and urea-formaldehyde resins are examples of thermosets [49].

Usually, thermoset resins are monomers with low molecular weight or oligomers with functional groups for cross-linking reactions. The curing process or polymerization of these resins can be achieved by addition or condensation reaction to accomplish a highly cross-linked three-dimensional structure. During curing process, it is desirable to use resins that do not produce volatile products in order to prevent the emergence of voids in molded parts. Resins are classified as A, B or C-stage resins depending on the curing phase and correspond to unreacted, partially reacted and completed cured, respectively.

Thermosetting resins may be low or high viscous liquids or solids, depending on their structure. High viscous resins need the use of pressure or high temperatures to wet

efficiently the fillers while the low viscous resins do not need them. To decrease the resins viscosity it is common to use reactive diluents.

Typical thermoset resin properties are ease of processing, thermal and thermo oxidative stability, high decomposition temperature (Td), high glass transition temperature (Tg), low water absorption, good mechanical properties and retention of properties in hot wet environment. Thermoset resins have applications in defense, aerospace, and electronic industries [52].

Epoxy resins

Epoxy resins are pre-polymers with relatively low molecular weight which have the ability to be processed under different conditions. Cured resins have good thermal, electrical and mechanical properties, high corrosion and chemical resistance and also remarkable adhesion to several substrates. Typically, the major drawbacks are the high curing time and poor performance in hot and wet environments. For the preparation of epoxy resins, many materials can be used which provides different kind of resins with a manageable and high performance. Generally, these resins are prepared by reaction of a phenol or polyfunctional amine with epichlorohydrin in the presence of a strong base [52].

The diglycidyl ether of bisphenol-A (DGEBA) remains to be the most used type of epoxy resin. Fig. 2.8 presents the diglycidyl ether of bisphenol-F (DGEBF) which is another type of epoxy resin [53].
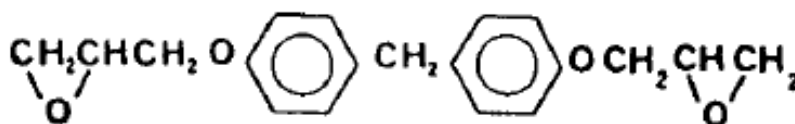
Figure 2. 8- Representation of the chemical formula of bisphenol-F epoxy resin [53].

EPON™ Resin 862, produced by Hexion Specialty Chemicals, is a DGEBF liquid epoxy resin with low viscosity, manufactured from epichlorohydrin and bisphenol-F and contains no diluents or modifiers. When this resin is cross-linked with suitable curing agents, it can achieve superior mechanical, electrical, adhesive and

chemical resistance properties. The Chemical Abstract Service (CAS) registry number is 28064-14-4 and the chemical designation is bisphenol-F/epichlorohydrin epoxy resin [54].

The EPIKOTE™ Resin 862, produced by Resolution Performance Products, consists of a bisphenol-F epoxy resin used for fabricating composite parts using resin transfer molding (RTM) or filament winding. Low viscosity and very long working life at room temperature make this resin versatile and easy to process. The CAS registry number, properties and applications of this epoxy resin are the same of EPON™ Resin 862 [55].

Curing agents

The cross-linking of epoxy resins into a three-dimensional network results on the improvement of its properties and performance. To choose the curing agent it is necessary to take into account the desired processing method and conditions (curing temperature and time), chemical and physical properties, environmental and toxicological limitations as well as the cost. The epoxy group is notably reactive due to its three-membered ring structure which can be accelerated by various nucleophilic and electrophilic reagents. Curing agents can be co-reactive, functioning as an initiator of the epoxy resin homopolymerization, or catalytic which acts as a comonomer in the polymerization process. Several curing agents have been used in the curing process of epoxy resins which contains active hydrogen atom like aromatic, polyamide and aliphatic amines, anhydrides, polyamides, polysulphides, dicyandiamide, isocyanate, mercaptans, urea formaldehyde and melamine-formaldehydes, among others [52].

ETHACURE® 100 Curative, produced by Albemarle Corporation, is an effective curing agent for epoxies and polyurethanes which might also be employed as a chain extender for polyurethane and polyuria elastomers, especially in Reaction Injection Molding (RIM) and spray applications. This curing agent can also be used as a chemical intermediate, antioxidant for elastomers, lubricants and industrial oils. The CAS registry number of Ethacure 100 curative is 68479-98-1 and the denomination is diethyltoluenediamine (DETDA) [56].

EPIKURE™ Curing Agent W, produced by Resolution Performance Products, consists of an aromatic amine used for the production of composite parts using RTM or

filament winding. This curing agent does not contain methylene dianiline (MDA). The CAS registry number, properties and applications of this curing agent are the same of Ethacure 100 curative [55].

Curing of epoxy resins

The epoxy resins curing process is related to a state change, from a liquid mixture with low molecular weight to a cross-linked network. The system molecular mobility decreases during the curing process because of the cross-linking of several molecular chains, which results on a network with a molecular weight tending to infinite. The irreversible and very fast transformation from a viscous liquid to an elastic gel is named as gel point. Gelation usually occurs between 55 and 80% conversion, meaning that the degree of cure (α) is between 0.55 and 0.80. Beyond the gel point, the reaction continues to produce one infinite network with considerable increase in the cross-link density, Tg and final physical properties.

When the glass transition of the network corresponds to the cure temperature, the vitrification of the growing chains (network) takes place. The vitrification is a transition which is reversible and may happen at any phase of the curing process, where the curing process can be resumed using heat to devitrify the epoxy resin with incomplete cure. Oxirane and amine ring reaction is highly exothermic.

Curing time depends on the type and amount of curing agent. When diethylenetriamine (DETA) or triethylene-tetramine (TETA) are used for curing DGEBA, pot life at ambient temperature is less than an hour, but takes 6 hours using m-phenylene diamine.

In this work, EPIKOTE™ Resin 862 and ETHACURE® 100 Curative were used to produce a group of samples and the other group of samples used EPON™ Resin 862 and EPIKURE™ Curing Agent W.

Properties and applications of cured epoxy resins

Cured epoxy resins have distributed molecular weights and segment lengths between the cross-linking points and there is also a distribution of monomers and unreacted functional groups captured or fixed spatial dispositions throughout the

network. Therefore, the macroscopic Tg variation is close to 50 ºC, but to decrease this range it can be used a slow and constant cooling rate which introduces a relaxation peak. There may be a relation between the Tg of a cross-linked polymer and the total conversion, cross-linked chain stiffness and the free volume trapped inside the network.

The mechanical properties of cured epoxy resins are related to the chemical structure of both epoxy resin and curing agent and also to the corresponding stoichiometry, cure network, cross-link density of the cured network, strain rate and test temperature.

Cured epoxy resins are good insulators and have a low dielectric constant. They have been applied to produce adhesives, laminates, sealants, coatings, etc. The anhydride cured epoxy resins have excellent mechanical, chemical and electrical properties which make them suitable for electrical and electronic applications. Epoxy resins are also used as binders in materials for construction and crack fillers in concrete structures. Epoxy based prepregs have been used to produce aircraft components like stabilizers, rudders, wing tips, landing gear doors, elevators, ailerons and radomes, among others. Approximately 28% of epoxy resins production is for composite and laminate industries, being the coating industry the other major user of epoxy resins.

Further details on thermosets, main properties and applications can be found in [52].

2.1.4- Production, characterization and applications of nanocomposites

To produce nanocomposites, the first task is to choose the fabrication method [3]. Many of the processing techniques used to produce microcomposites are also used to produce the three types of nanocomposites (CMNC, MMNC and PMNC).

The most common methods used to produce CMNC are the spray pyrolysis, polymer precursor route, conventional powder method, vapor techniques like physical vapor deposition (PVD) and CVD, and chemical methods like sol-gel process, template synthesis, colloidal and precipitation approaches. Regarding the MMNC, the most used processing techniques are the rapid solidification, liquid metal infiltration, vapor techniques, spray pyrolysis, electrodeposition and chemical methods (sol-gel and colloidal processes). The most important methods used to produce PMNC are the in-situ intercalative polymerization, intercalation of polymer or pre-polymer from solution,

melt intercalation, template synthesis, direct mixture of particulates and polymer, sol-gel process and in-situ polymerization [1].

To produce outstanding nanocomposites it is necessary to have an excellent adhesion between the matrix and the filler, which is determined by both physical and chemical phenomena happening in the filler/matrix interface. A weak filler/matrix adhesion causes fails in the interfaces that are reflected in the deterioration of the composite properties such as mechanical, for instance [24].

The dispersion of the nanofillers in the matrix has a strong influence on composites physical properties. The nanofillers tend to form strongly bounded clusters, due to the Van der Waals forces, for instance, and bigger agglomerates may emerge [2]. The dispersion level of nanoparticles has been shown to influence the thermal and mechanical properties [57-59], abrasion resistance, [60], coercive force [61], electrical conductivity [62-66], dielectric constant [67, 68], ionic conductivity [69], UV resistance [70], refractive index [71], among other properties [72, 73].

To characterize the nanocomposites several techniques and equipments can be used, such as scanning tunnelling microscopy (STM), atomic force microscopy (AFM), Fourier transformed infrared spectroscopy (FTIR), differential scanning calorimetry (DSC), nuclear magnetic resonance (NMR), X-ray photoelectron spectroscopy (XPS), X-ray diffractometry (XRD), small angle X-ray and neutron scattering (SAXS/SANS), SEM, TEM, TOM, electron spin resonance (ESR), Raman spectroscopy, ultraviolet-visible (UV-VIS) spectra and ^{13}C solid-state nuclear magnetic resonance (^{13}C NMR) [2]. Beyond these techniques, there are also the theoretical simulations and calculations which are used to predict nanocomposite properties.Tables 2.2, 2.3 and 2.4 show potential applications of some ceramic, metal and polymer based nanocomposites, respectively.

Table 2.2 - Potential applications of ceramic matrix nanocomposite systems [1].

Nanocomposites	Applications
SiO_2/Fe	High performance catalysts, data storage technology
ZnO/Co	Field effect transistor for the optical femtosecond study of interparticle interactions
$BaTiO_3/SiC$, PZT/Ag	Electronic industry, high performance ferroelectric devices
SiO_2/Co	Optical fibres
SiO_2/Ni	Chemical sensors
Al_2O_3/SiC	Structural materials
Si_3N_4/SiC	Structural materials
$Al_2O_3/NdAlO_3$ & $Al_2O_3/LnAlO_3$	Solid-state laser media, phosphors and optical amplifiers
TiO_2/Fe_2O_3	High-density magnetic recording media, ferrofluids and catalysts
Al_2O_3/Ni	Engineering parts
$PbTiO_3/PbZrO_3$	Microelectronic and micro-electromechanical systems

Table 2.3 - Potential applications of metal matrix nanocomposite systems [1].

Nanocomposites	Applications
Fe/MgO	Catalysts, magnetic devices
Ni/PZT	Wear resistant coatings and thermally graded coatings
Ni/TiO^2	Photo-electrochemical applications
Al/SiC	Aerospace, naval and automotive structures
Cu/Al$_2$O$_3$	Electronic packaging
Al/AlN	Microelectronic industry
Ni/TiN, Ni/ZrN, Cu/ZrN	High speed machinery, tooling, optical and magnetic storage materials
Nb/Cu	Structural materials for high temperature applications
Fe/Fe$_{23}$C$_6$/Fe$_3$B	Structural materials
Fe/TiN	Catalysts
Al/Al$_2$O$_3$	Microelectronic industry
Au/Ag	Microelectronics, optical devices, light energy conversion

Table 2.4 - Potential applications of polymer matrix nanocomposite systems [1].

Nanocomposites	Applications
Polycaprolactone/SiO_2	Bone-bioerodible for skeletal tissue repair
Polyimide/SiO	Microelectronics
PMMA/SiO	Dental application, optical devices
Polyethylacrylate/SiO_2	Catalysis support, stationary phase for chromatography
Poly(p-phenylene vinylene)/SiO2	Non-liner optical material for optical waveguides
Poly(amide-imide) / TiO_2	Composite membranes for gas separation applications
Poly(3,4-ethylene-dioxythiophene) /V_2O_5	Cathode materials for rechargeable lithium batteries
Polycarbonate/SiO_2	Abrasion resistant coating
Shape memory polymers/SiC	Medical devices for gripping or releasing therapeutics within blood vessels
Nylon-6/LS	Automotive timing-belt – TOYOTA
PEO/LS	Airplane interiors, fuel tanks, components in electrical and electronic parts, brakes and tires
PLA/LS	Lithium battery development
PET/clay	Food packaging applications. Specific examples include packaging for processed meats, cheese, confectionery, cereals and boil-in-the-bag foods, fruit juice and dairy products, beer and carbonated drinks bottles
Thermoplastic olefin/clay	Beverage container applications
Polyimide/clay	Automotive step assists - GM Safari and Astra Vans
Epoxy/MMT	Materials for electronics
SPEEK/laponite	Direct methanol fuel cells

Numerous applications already exist and many more are yet to come for these materials, opening new possibilities for the future. Therefore all the three types of nanocomposites provide opportunities and incentives gaining the interest of diverse economic sectors worldwide in these new materials.

Further details on production, properties and applications of nanocomposites can be found in the review paper [1].

2.2- Carbon nanofiber/epoxy composites

2.2.1- Introduction

Research on polymer nanocomposites has been focused mainly on CNT rather than CNF as the reinforcement filler, because CNT have fewer microstructural defects than CNF which result in better overall properties as well as smaller dimensions and lower density. However, there are several methods used to treat those defects, such as heat treatment [74], acid treatment [75, 76], plasma treatment [77] and surface functionalization [78, 79]. The largest advantages of using CNF instead of CNT is its lower price and ease of production in large amounts, encouraging further research on composites with CNF mainly for industrial productions [80].

Epoxy resins properties are recognized as being good-to-excellent, allowing an extensive range of applications [81]. The incorporation of fillers with high aspect ratio like CNF improves the epoxy mechanical and electrical properties and the range of applications for this type of nanocomposite is naturally extended [29]. CNF have been used as fillers in order to improve electrical properties of epoxy composites, due to the high electrical conductivity of CNF [82, 83]. In fact, it was observed a noticeable increase in electrical conductivity when CNF volume fraction exceeded the percolation threshold.

The high aspect ratio and high surface energy of CNF, associated with the Van der Waals interactions between them, promotes the clustering effect which leads to an inhomogeneous dispersion. However, significant efforts have been made in order to unbundle CNF clusters using methods such as diluting the matrix with solvents [62, 77] and the combination of sonication and mechanical mixing [82].

The quality of dispersion of nanofillers in polymer-based composites is intrinsically related to the efficiency of the dispersion method in improving the

properties of nanocomposites such as electrical, mechanical and thermal, amongst others. The homogeneous dispersion of nanofillers in the polymer matrix and the adhesion quality between polymer and filler are crucial for some composite properties, because a weak adhesion results in the decline of composite properties such as premature failure [2]. The methods and conditions of nanocomposites processing have influence in filler dispersion, distribution, aspect ratio and orientation [29].

In last years, the structural heterogeneity of polymers composites and their phase separation on a nanometer scale have been studied using several experimental methods and techniques, some of them based on mathematical or statistical tools. Some of the most used experimental techniques for evaluation of the nanofillers dispersion are TEM and SEM. Other techniques like AFM, XRD, ESR and Raman spectroscopy, are also used for evaluation of nanofillers dispersion [2].

There is a lack of complete information in the literature about the relation between structure and properties for polymer nanocomposites. One of the main reasons is because it is difficult to characterize the aspect ratio of nanofillers before and after the mixing process without using destructive techniques in order to quantify the level of nanofiller dispersion [29]. As a consequence of this fact, till now seems that no one could establish a clear relation between dispersion and electrical properties of nanocomposite and, consequently, there are no definite conclusions on this subject [15].

2.2.2- Preparation methods

Processing methods and conditions influence the filler dispersion, distribution, aspect ratio and orientation. In order to accomplish low percolation threshold and improve composites conductivity, the dispersion level of the VGCNF should be very good without damaging the aspect ratio. When the conductive fillers aspect ratio is reduced, one of the major and direct changes in composite properties is the increase of the electrical percolation threshold concentration. Another consequence is the increase of the filler content necessary to reach some electromagnetic interference shielding effect (EMI SE) [24].

In order to produce composites based on thermosets and VGCNF, different methods can be used such as dilution of the epoxy resin in tetrahydrofuran [84] and acetone[81], high shear mixing [85] and blending followed by roll milling [81]. All

methods mentioned previously were succeeded in the VGCNF dispersion, except high shear mixing, because the diffusion of the nanofillers throughout the matrix was not complete, resulting in modest improvements in mechanical properties, despite the enhancement of thermal conductivity [29]. Patton et al. [77] prepared VGCF/epoxy composites with two different methods. In the first, epoxy resin (Epon 830) was diluted with acetone to improve the filler infusion throughout the matrix, while the second method consisted on blending of the fillers with a low viscosity resin (Clearstream 9000), followed by two hours of roll milling. Both methods were successful, tripling or quadrupling the flex modulus and more than doubling the flex strength.

Recently, Sun et al. [80] prepared VGCNF/epoxy composites using sonication followed by mechanical stirring, where the nanofillers were chemically purified and sonicated before being mixed with the matrix.

2.2.3- Morphology

2.2.3.1- Surface modification and characterization techniques

The control of the CNF surface chemistry is crucial because it defines their functionality and, consequently, their applications too. The hydrophobicity, surface charge and chemical reactivity of CNF can be changed through chemical and physical modifications. The literature on this subject mentions that surface coatings improve the chemical stability and mechanical strength of CNF and also additional functionalities such as the variation of electrical conductivity or selective activation of specific surface regions, using microfabrication routes. Chemical vapor deposition of thin film coatings and electro or electroless plating, are examples of surface coating techniques. The second method of CNF surface modification corresponds to the chemical and biochemical functionalization. Chemical functionalization consists on covalent attachment of functional groups which is commonly used to increase dispersibility, wettability and surface reactivity of CNF, enabling further biochemical functionalization.

Some of the most common and relevant surface characterization techniques found in the literature are the infrared and electron spectroscopies, scanning probe and electron microscopies, atom probe analysis, temperature-programed desorption and ion spectrometry [86].

There is a recent work carried on by Nie et al. [87] about the effect of the VGCNF functionalization on some properties of the VGCNF/epoxy resin composites. This functionalization consisted in a multistage process which includes oxidation, reduction and silanization. Composites with functionalized and original (as received) VGCNF were produced in order to compare their chemical, mechanical, thermal and electrical properties. The composites with functionalized VGCNF show better dispersion of functionalized nanofillers in the epoxy polymer matrix, as indicated by SEM images. The functionalization of the VGCNF also improved the mechanical and thermal properties, while the electrical conductivity was reduced.

2.2.3.2- VGCNF dispersion in thermosets

Properties and performance of polymer nanocomposites have a strong relation with dispersion and distribution of the VGCNF in the polymer matrix. VGCNF tend to form clusters because of the intermolecular Van der Waals interactions between them. These interactions forces prejudice the nanofillers dispersion which may affect in a negative way some of the composites properties.

Dispersion and distribution are different concepts. For instance, a good dispersion of CNF in an epoxy matrix happens when there is no agglomeration effect, meaning that nanofillers can only touch other fillers in a reduced contact area, without needing to occupy uniformly the entire matrix, which may lead to a bad distribution. A good dispersion and good distribution occurs when the nanofillers uniformly occupy the entire matrix with no agglomerations. Figure 2.9 illustrates the four possible combinations of bad or good dispersion and distribution.
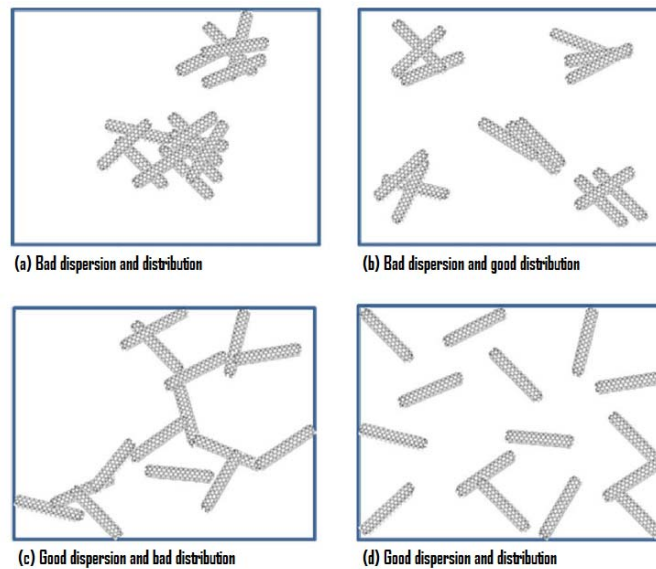
Figure 2. 9- Schematic sketches showing the four combinations of good/bad distribution/dispersion [29].

Al-Saleh et al. mention that a good VGCNF dispersion in a polymer matrix, without reducing the aspect ratio, improves the composites conductivity and leads to a decrease on the concentration necessary to achieve the percolation threshold. It is also mentioned that a good distribution may not be required to produce a conductive network throughout the polymer [29]. Regarding the nanofillers dispersion, some studies mention that a good dispersion of the nanofillers throughout the composite is inconvenient for the formation of electrical conductive networks [64, 88].

Recently, Karippal et al. [89] used a twin screw extruder to disperse CNF in epoxy resins, studying the effect of amine functionalization of the nanofillers on mechanical, thermal and electrical properties and also on the dispersion. Regarding the dispersion, SEM examinations showed that functionalization resulted in better dispersion of the CNF, besides the improvement in mechanical, thermal and electrical properties.

2.2.3.3- Nanofillers dispersion analysis

To visualize the nanofillers dispersion in the host matrix, several characterization techniques have been used such as TOM, scanning probe microscopy (SPM), SEM and TEM [90]. TEM can only provide direct information on nanofillers dispersion for very small volumes of the sample and may not be representative at the macroscopic level, which is achieved using TOM [91]. On the other hand, the disadvantage of TOM is that this technique can only reach length scales of a few microns. The quantification of the nanofillers dispersion or distribution in the matrix requires the use of specific image techniques and mathematical tools. For instance, the mixing quality of VGCNF/epoxy nanocomposites can be adequately evaluated using TOM and GSA, yielding a quantitative description of the CNF dispersion in the matrix [92-94]. The quantification of CNF dispersion in epoxy nanocomposites can also be made through the nanomechanical characterization [95] and SANS, associated with TEM and dynamical mechanical studies [96].

2.2.4- Electrical properties

The intrinsic resistivity of VGCNF grown at a temperatures close to 1100 ºC and measured at room temperature is $2x10^{-3}$ Ω.cm, whereas for the case of graphitized VGCNF is $5x10^{-5}$ Ω.cm, which is close to the graphite resistivity. These values are in agreement with the resistivity values expected taking into account the noticed VGCNF graphitization indices [97].

The class of polymer influences considerably the filler content necessary to achieve the percolation threshold, being that the polymer crystallinity, polarity, surface tension and molecular weight are the main factors influencing the percolation threshold [98, 99]. According to Al-Saleh et al. [29], there is a tendency for an increase of percolation threshold tension as the polymer surface increases and the higher the polymer surface tension the lower the interfacial tension between polymer and filler. When the interfacial tension between polymer and filler is low, the fillers are easily wetted by the polymer matrix which facilitates an efficient distribution throughout the matrix and, consequently, increases the percolation threshold. Moreover, high polymer-filler interfacial tension increases fillers agglomeration effect, promoting the emergence of a conductive network throughout the polymer matrix. In the same way, increasing the

polymer polarity causes the increase of percolation threshold due to the improvement of the interaction polymer-filler which will distribute the filler more efficiently. Composites change from insulating to conductive materials when critical filler content is reached. This concentration is known as the percolation threshold and at this point the composite electrical conductivity increases strongly by several orders of magnitude. At this critical filler concentration a continuous conductive network is formed throughout the polymer and if the filler content continues increasing, the effect in the overall electrical resistivity is quite lower, as presented in Figure 2.10 [29].
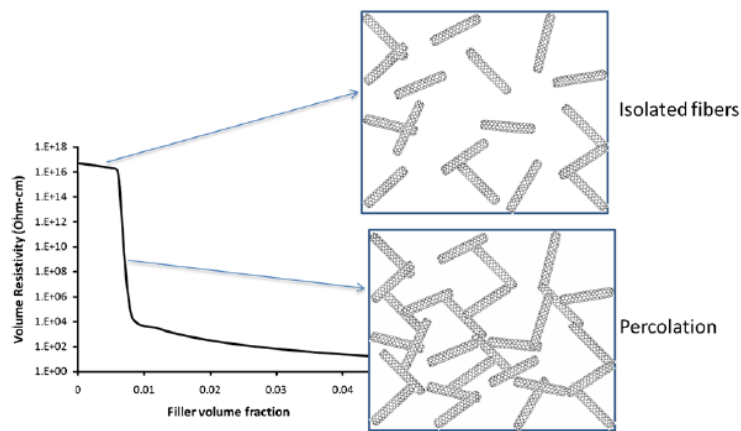
Figure 2. 10- Schematic sketch showing typical electrical resistivity as a function of filler loading of high aspect ratio filler/polymer system [29].

Al-Saleh et al. also mention that if composite electrical resistivity continues to decrease strongly at filler contents above the percolation threshold, it means that the conduction network has not been formed yet. In this way, the percolation threshold is not caused by the formation of a nanofillers network throughout the matrix, but because of the tunneling effect. This effect is the dominant mechanism of the electrical conductivity for some cases. In a recent study made by Sun and co-workers [80] on VGCNF/epoxy resin composites, it was found an increase in the electrical conductivity of four and seven orders of magnitude for filler contents of 0.0578 and 0.578 vol.% (volume percentage), respectively. It was also found an electrical percolation threshold (critical concentration) of 0.057 vol.%.

2.2.4.1- Electrical conductivity mechanisms

Percolation theory

The percolation theory is a powerful theory that has been used to study the mechanisms behind the formation of networks. This theory can be used to analyze how networks are formed during the polymerization process, forest fires, phase transitions and electrical conduction in composites [100]. The application of the percolation theory to study the conductive behavior of composites made of a polymer matrix with conductive fillers, is based on some important assumptions and concepts. One of the most important assumptions is that the electrical conduction is based on the physical contact between the conductive fillers. The fundamental concepts in the percolation theory are the percolation threshold (Φ_c) and the existence of correlation length ruling critical phenomena. The percolation threshold or critical concentration is defined as the concentration (Φ) at which an infinite cluster emerges in an infinite lattice. When $\Phi > \Phi_c$, a cluster spreads throughout the system, whereas for $\Phi < \Phi_c$ the system is made of many small isolated and disconnected clusters. According to Stroud and Bergman [101], the dielectric constant in composites with metallic fillers in an insulating matrix is defined by equation 2.1, being that there is a divergence at Φ_c.

$$\varepsilon_{eff} \propto \varepsilon_{matrix} |\Phi - \Phi_c|^{-s} \qquad (2.1)$$

Stroud and Bergman also demonstrate that composite conductivity is given by equation 2.2, for $\Phi > \Phi_c$.

$$\sigma_{eff} \propto \sigma_{matrix} |\Phi - \Phi_c|^{-t} \qquad (2.2)$$

Equations 2.1 and 2.2 present coefficients t and s which are called the conductivity and superconductivity critical exponents, respectively. The parameters ε_{eff} and σ_{eff} are the composite dielectric constant and conductivity, respectively, while ε_{matrix} and σ_{matrix} are the matrix dielectric constant and conductivity, respectively. The values for the conductivity exponent t were determined by Kirkpatrick [102] and for a 3D system it is 1.5 +/- 0.2, although more recent works reported values close to 1.8.

Herrmann and Derrida [103] found that the superconductivity exponent *s* is 0.75 +/-
0.04, using a bond percolation model in 3D system and in conjugation with a transfer
matrix algorithm.

Excluded volume theory

The excluded volume theory is also based on the assumption that the electrical
conduction mechanism is based on the physical contact between the conductive fillers.
The excluded volume theory predicts some bounds for the critical concentration or the
percolation threshold for rod-like fillers. In general, the percolation threshold is defined
as present in equation 2.3.

$$1 - e^{-1.4V/\langle V_e \rangle} \leq \Phi_c \leq 1 - e^{-2.8V/\langle V_e \rangle} \qquad (2.3)$$

In equation 2.3, *V* is the filler volume and Φ_c the critical volume fraction.
Equation 2.3 links the average excluded volume $\langle V_e \rangle$ which is the volume around an
object (filler) in which the center of another similarly shaped object is not allowed to
penetrate averaged over the orientation distribution and the critical concentration. In this
equation, the values 1.4 and 2.8 correspond to the situation where the fillers are
infinitely thin cylinders and spheres, respectively, and both were obtained by
simulation. The derivation of this equation and related discussion can be seen in [104].

The percolation theory associated to the excluded volume theory can be found in
some studies [66, 89, 105] as mathematical tools for the prediction, through
calculations, of some electrical properties of composites made of conductive fillers
immersed in insulating matrices. The excluded volume theory is used to calculate the
critical concentration corresponding to the percolation threshold [106].

A recent review elaborated by Bauhofer et al. [107] presented some
experimental percolation thresholds of polymer composites with CNT as nanofillers and
it was observed a wide range of values for the same type of composite, with the same
matrix (polymer) and nanofillers (CNT). It was also observed a deviation between the
experimental and the calculated bound values, using the formula of the excluded
volume theory. This review also mentions a deviation between the standard and
experimental values of the critical exponent *t* which is calculated using the conductivity
formula 2.2 from the percolation theory. According to the percolation theory, the critical

exponents*t* and *s* are independent of the type of matrix or filler geometry and only depend on the system dimension. The failure of the percolation theory associated with the excluded volume theory allowed the emergence of other models such as the complex network theory.

Complex network theory

The complex network theory has been used to study systems such as social networks or the World Wide Web and can also be applied to material science. This theoretical model may allow a deeper understanding of basic phenomenon in physics such as the electrical conductivity and percolation threshold in composites made of a polymeric matrix with conductive nanofillers such as CNT or CNF. Some work has been done, through numerical simulations, in order to find a formula which can be used to predict the critical concentration corresponding to the percolation threshold of the electrical conductivity. One of these works was carried on by Silva et al. [108] in which the main objective was to apply the complex network theory to comprehend the electrical conduction mechanism in polymer composites with high aspect ratio fillers. According to this study, the determination of the formula which can be used to calculate the percolation threshold is based on the application of numerical simulations to the theoretical framework of the random graph model developed by Erdös and Rényi [109]. The equation 2.4 was found to predict the percolation thresholds for materials such as polymer composites with cylinder shaped conductive nanofillers with high aspect ratio, like CNT and CNF.

$$\Phi_c = \frac{D^2}{2L\delta_{max}} \quad (2.4)$$

In equation 2.4, Φ_c is the percolation threshold, D is the average diameter of the cylinder (nanofiller), L is the cylinder average length and δ_{max} is the maximum value for the minimum distance between the cylinders, as defined by Simões et al. [110]. The cylinders are mapped to vertices and the edges to the minimum distance between the cylinders, which corresponds to the maximum electric field between the two fillers. The δ_{max} parameter represents this minimum distance for a nanocomposite microstructure (3D) and allows the study of the influence of the matrix on the percolation threshold.

The simulations made by Silva et al. assumed that δ_{max} is 10 nm because this is the value which can be assumed to generate a certain electrical conduction between the nanofillers. Some studies [82, 110, 111] corroborate this assumption although some of them are based on different conduction mechanisms. Equation 2.4 is valid till $\delta_{max} = D$, where the results become equal to the ones calculated with the excluded volume theory [112, 113].

To find the formula which can predict the behavior of the conductivity in composites based on polymers with cylinder shaped nanofillers like CNT and CNF, the model developed by Miller et al. [114, 115] was used. Miller and co-workers developed a formula to calculate to electrical conductivity based on the electron hopping mechanism, which is shown as equation 2.5.

$$\sigma_{ij} = \sigma_0 e^{\left(-\frac{x_{ij}}{x_0} - \frac{\varepsilon_{ij}}{K_B T}\right)} \quad (2.5)$$

In equation 2.5, x_{ij} is the distance between two fillers and x_0 is the scale over which the wave function decays in the matrix, $\varepsilon_{ij}/(K_B T)$ is the thermal hopping term which can be disregarded at room temperature and σ_0 is the dimension coefficient. Equation 2.5 is similar to the formula of conductance distribution [116] which is based on the random graphs (Erdös and Rényi) and random resistor networks [117] theoretical frameworks. Equation 2.6 results from the adaptation of the conductance distribution formula to the specifications of the electrical conduction mechanism of a nanocomposite based on polymer with conductive fibrous nanofillers.

$$G_{eff} = G_{cut} e^{\left(\frac{-a}{(b\Phi)^{1/3}}\right)} \quad (2.6)$$

In equation 2.6, b is the volume of the domain divided by the filler volume and G_{cut} is the effective system conductance before a bond with maximum conductance is added or removed from the system. The parameter a is the disorder strength which controls the broadness of the distribution of linked weights [118]. Numerical simulations using equation 2.6 to calculate the electrical conductivity as a function of volume fraction for pristine and functionalized VGCNF polymer composites resulted in a relationship described in equation 2.7.

$$\log(\sigma) \propto \Phi^{-\frac{1}{3}} \qquad (2.7)$$

The relation presented in equation 2.7 is valid for composites regardless of the fact of having functionalized or pristine VGCNF. Regardless of the difference on the physical mechanisms, there is a resemblance between equation 2.7 and the expression of the (fluctuation-induced) tunneling effect. The electrical conductivity expression developed by Connor et al. [119] is presented in equation 2.8.

$$\sigma_{DC} \propto e^{-2\chi_T d} \quad (2.8)$$

In equation 2.8, d is the barrier width, $\chi_T = (2mV(T)/\hbar^{2})^{-1/2}$, where m is mass of the charge carriers, $V(T)$ is the temperature modified barrier height and $\hbar$ is the Plank's constant.

The complex network theory assumes a weighted disorder network in which the fillers are vertices and edges are the gaps between fillers and, in terms of electrical conductivity, the weights of the edges indicate the difficulty for the electrical charges to transverse it. This way, the optimal path between two vertices (l_{opt}) is defined as the single path for which the sum of the weights along the path is minimum and when most of the path links contribute to the sum, the system is said to be in the weak disorder regime. When one link dominates the sum along the path the system is called as the strong disorder regime [118]. In the scope of the random graphs model [109], for the strong disorder regimes $l_{opt} \sim N^{1/3}$ while for the weak disorder regime $l_{opt} \sim ln(N)$. In the weak disorder regime, $a \sim l_{opt}$ and as b is simply the total number of fillers that can exist in the domain N_{max}, equation 2.6 is simplified and results in equation 2.9.

$$G_{eff} = G_{cut} e^{\left(\frac{-l_{opt}}{(N_{max}\Phi)^{1/3}} \right)} \qquad (2.9)$$

According to Strümpler et al. [111], the tunneling effect is a mechanism of electrical conduction which happens when the distance between the nanofillers inside the polymer matrix is inferior to 10 nm. It has been indicated that analyzing the relation between the electrical current I and voltage V, it is possible to find if the composite

conductivity is due to the tunneling effect or direct contact between the nanofillers [120, 121]. If the relation between current and voltage is linear, the dominant conduction mechanism is the direct contact between nanofillers, indicating the presence of Ohm's law. On the other hand, if the I-V relation is non-liner, other mechanisms may be responsible for the electrical conduction occurring in the composite. For instance, if the I-V relation is ruled by a power law, the dominant conduction mechanism is the tunneling effect [121, 122].

Further details on the electrical conductivity mechanisms can be found in [106, 108].

2.2.5- Other properties

Besides the electrical properties, CNF/epoxy composites have many other interesting properties such as mechanical, thermal and electromagnetic interference shielding effectiveness which are attracting for many applications [29].

A study made by Lafdi and Matzek [123] consisted on the fabrication of composites with Epon resin 862 and three types of VGCNF. The composites with the highly surface oxidized VGCNF achieved the higher modulus increased which is approximately a factor of three higher than the modulus of the resin samples, while the composites with high temperature graphitized VGCNF accomplished the best increase in thermal diffusivity. The nanofibers dispersion in the matrix became difficult above 12 wt.% of filler content which prejudiced the mechanical properties, but not the thermal properties. Ishikawa et al. [124] used CNF to reinforce the resin matrix placed between the plies of a composite in order to increase the compressive strength. This operation resulted in a reasonable increase of the compressive strength due to a reinforcement of 20 to 35 wt.% of VGCNF, although the change in compressive modulus was unexpectedly small. The preparation of composites with high loadings was by the stirring method followed by vacuum deaeration. A study made by Rana and co-workers [125] investigated the mechanical behavior of CNF reinforcement on epoxy resins. The CNF were uniformly dispersed throughout the composite at a very low concentration (0.07 wt.%), resulting in enhancements of 24 % in breaking stress, 98% in Young modulus and 144% in work of rupture.

Patton and co-workers [126] found that the low erosion and char rates of composites made from VGCNF and phenolic resin under a plasma torch at 1650 ºC might be propitious to produce solid rocket motor nozzles. If the length of the VGCNF is shortened, lower thermal conductivities can be obtained in comparison to the competing continuous carbon fibers. Patton et al. [77] also measured the thermal conductivity of composites with VGCNF and epoxy resin and for 40 vol.% filler content values up to 0.8 W/(m.K) were found. However, this value is not so extraordinary in comparison to the value for neat resin, which is 0.26 W/(m.K), and this disappointing increase is due to the difficulty in the transference of thermal energy among nanofibers. The study by Lafdi and Matzek [123], also mention that the thermal conductivity increased from 0.2 W/(m.K) for epoxy resin to 2.8 W/(m.K) for composites with 20 wt.% of VGCNF content. These results mean that it is not necessary to have a good coupling between the filler and the matrix in order to accomplish high thermal conductivity, although mechanical properties such as stiffness and strength are prejudiced. Prolongo and co-workers [127] studied the thermal and mechanical properties of epoxy composites with amino-functionalized CNF. They found out that the addition of nanofillers increases the coefficient of thermal expansion and glassy storage modulus of nanocomposites although the α-relaxation temperature decreases. It is also mentioned that dispersion level clearly affects the thermo-dynamical mechanical properties of the epoxy nanocomposites.

2.2.6- Applications

The conductivity of VGCNF/epoxy resin composites is high enough to allow a reasonable good electromagnetic interference shielding effect. A shielding effectiveness of 45 dB at 200 MHz was achieved by Donohue and Pittman [128] for samples with 1.8 mm thickness and 15 wt.% content of temperature heat-treated VGCNF in a vinyl ester matrix. The differences on the techniques used to disperse and prepare the composites reflected on the composites characteristics. This finding suggests that dispersion and preparation methods used to produce nanocomposites are some of the key issues for future shielding applications.

Currently there are epoxy resin composites with VGCNF contents of 20 wt.% which are applied as molding compounds, pre-pegs, adhesives and coatings. In the case

of the adhesives, they are supposed to have strength characteristics and good electrical conductivity. These composites are also intended to be applied as components for aerospace, electronics and medicine and also as composite panels in order to replace metal structures which are heavier and less corrosion resistant. The use of VGCNF as reinforcement filler allows improvements in the mechanical properties of epoxy resin in order to fabricate linerless composite pressure vessels, where the development of resins with a high strain and resistant to microcracks improves composites performance.

There are promising applications for VGCNF in the automotive industry, because the use of this nanofiller in the production of polymer composites could improve the shielding of automotive electronics, electrostatic painting of exterior panels and the stiffness of the tires [129]. These applications could make the vehicles with lower fuel consumption, lower environmental emissions, better quality and lower cost. In addition, polymers filled with VGCNFs can be used as sensors for organic vapors [130] and for biological applications. In comparison to SWCNT and MWCNT, VGCNF are more suitable to incorporate in the hollow core of the fiber biological components such as DNA and proteins, because the hollow core diameter is much larger [131].

In a recent review paper, Huang et al. [132] mention the outstanding advantages of carbon nanofiber to be used in the production of electrochemical biosensors. CNF have been successfully used as immobilization matrices in order to construct several oxidase, dehydrogenase and enzyme-based biosensors which evidenced high sensitivity and the enzymatic activity was efficiently maintained. Using the CNF molecular wires allowed the direct transference of the electron from the surfaces of the electrode to the redox sites of enzymes. The substrates of vertically aligned carbon nanofibers (VACNF) could be functionalized with biomolecules like protein and DNA, using a photochemical route or combined chemical and electrochemical route. These molecular functionalization processes of VACNF resulted in structures with outstanding biological and chemical properties, allowing promising applications for chemical sensing and biosensing purposes.

Further details on preparation methods, properties and applications of CNF/epoxy composites can be found in the review papers [24, 29].

References

1. Camargo, P.H.C., K.G. Satyanarayana, and F. Wypych, Nanocomposites: synthesis, structure, properties and new application opportunities. Materials Research, 2009. 12: p. 1-39.

2. Šupová, M., G.S. Martynková, and K. Barabaszová, Effect of Nanofillers Dispersion in Polymer Matrices: A Review. Science of Advanced Materials, 2011. 3(1): p. 1-25.

3. Hussain, F., et al., Review article: Polymer-matrix Nanocomposites, Processing, Manufacturing, and Application: An Overview. Journal of Composite Materials, 2006. 40(17): p. 1511-1575.

4. Bogue, R., Nanocomposites: a review of technology and applications. Assembly Automation, 2011. 31(2): p. 106 - 112.

5. YAO, N. and Z.L. WANG, HANDBOOK OF MICROSCOPY FOR NANOTECHNOLOGY. 2005, BOSTON / DORDRECHT / NEW YORK / LONDON: KLUWER ACADEMIC PUBLISHERS.

6. Liu, J., et al., Static, rheological and mechanical properties of polymer nanocomposites studied by computer modeling and simulation. Physical Chemistry Chemical Physics, 2009. 11(48): p. 11365-11384.

7. Ateeq, R., A. Ilia, and A.Z.S.M.e. al, A REVIEW OF THE APPLICATIONS OF NANOCARBON POLYMER COMPOSITES. NANO: Brief Reports and Reviews, 2011. 6(3): p. 185-203.

8. Alexandre, M. and P. Dubois, Polymer-layered silicate nanocomposites: preparation, properties and uses of a new class of materials. Materials Science and Engineering: R: Reports, 2000. 28(1-2): p. 1-63.

9. Móczó, J. and B. Pukánszky, Polymer micro and nanocomposites: Structure, interactions, properties. Journal of Industrial and Engineering Chemistry, 2008. 14(5): p. 535-563.

10. Vaia, R.A. and H.D. Wagner, Framework for nanocomposites. Materials Today, 2004. 7(11): p. 32-37.

11. Luo, J.-J. and I.M. Daniel, Characterization and modeling of mechanical behavior of polymer/clay nanocomposites. Composites Science and Technology, 2003. 63(11): p. 1607-1616.

12. Thostenson, E.T., C. Li, and T.-W. Chou, Nanocomposites in context. Composites Science and Technology, 2005. 65(3-4): p. 491-516.

13. Schmidt, D., D. Shah, and E.P. Giannelis, New advances in polymer/layered silicate nanocomposites. Current Opinion in Solid State and Materials Science, 2002. 6(3): p. 205-212.

14. Park, C.I., et al., The fabrication of syndiotactic polystyrene/organophilic clay nanocomposites and their properties. Polymer, 2001. 42(17): p. 7465-7475.

15. Kumar, S.K. and R. Krishnamoorti, Nanocomposites: Structure, Phase Behavior, and Properties, in Annual Review of Chemical and Biomolecular Engineering, Vol 1, J.M. Prausnitz, M.F. Doherty, and M.A. Segalman, Editors. 2010, Annual Reviews: Palo Alto. p. 37-58.

16. Society, R. and R.A.o. Engineering, Nanoscience and nanotechnologies: opportunities and uncertainties, T.R. Society, Editor. 2004: London
   p. 7-10.

17. Nemes-Incze, P., et al., Anomalies in thickness measurements of graphene and few layer graphite crystals by tapping mode atomic force microscopy. CARBON, 2008. 46(11): p. 1435-1442.

18. Novoselov, K.S., et al., Electric Field Effect in Atomically Thin Carbon Films. Science, 2004. 306(5696): p. 666-669.

19. Jayaraman, K., et al., Recent Advances in Polymer Nanofibers. J Nanosci Nanotechnol. 2004 Jan-Feb;, 2004. 4(1-2): p. 52-65.

20. Koo, J.H., L.A. Pilato, and G.E. Wissler, Polymer Nanostructured Materials for Propulsion System, in Conference Proceedings for AIAA-2005-3606, 41st AIAA/ASME/SAE/ASEE Joint Propulsion Conference & Exhibit. 2005: Tucson, AZ.

21. Koo, J.H., et al., NANOCOMPOSITE ROCKET ABLATIVE MATERIALS: SUBSCALE ABLATION TEST, in SAMPE Symposium. 2004: Long Beach, CA. p. 15.

22. Koo, J.H., et al., Epoxy Nanocomposites for Carbon Reinforced Polymer Matrix Composites, in SAMPE Symposium. 2005: CA.

23. Anderson, B.W., The impact of carbon fibre composites on a military aircraft establishment. Journal of Physics D: Applied Physics, 1987. 20(3): p. 311.

24. Tibbetts, G.G., et al., A review of the fabrication and properties of vapor-grown carbon nanofiber/polymer composites. Composites Science and Technology, 2007. 67(7-8): p. 1709-1718.

25. Tibbetts, G.G., D.W. Gorkiewicz, and R.L. Alig, A new reactor for growing carbon fibers from liquid- and vapor-phase hydrocarbons. Carbon, 1993. 31(5): p. 809-814.

26. Tibbetts, G.G., et al., Role of sulfur in the production of carbon fibers in the vapor phase. Carbon, 1994. 32(4): p. 569-576.

27. Endo, M., et al., Vapor-grown carbon fibers (VGCFs): Basic properties and their battery applications. Carbon, 2001. 39(9): p. 1287-1297.

28. Thostenson, E.T., Z. Ren, and T.W. Chou, Advances in the science and technology of carbon nanotubes and their composites: a review. Composites Science and Technology, 2001. 61(13): p. 1899-1912.

29. Al-Saleh, M.H. and U. Sundararaj, A review of vapor grown carbon nanofiber/polymer conductive composites. Carbon, 2009. 47(1): p. 2-22.

30. Miyagawa, H., M.J. Rich, and L.T. Drzal, Thermo-physical properties of epoxy nanocomposites reinforced by carbon nanotubes and vapor grown carbon fibers. Thermochimica Acta, 2006. 442(1-2): p. 67-73.

31. Merkulov, V.I., et al., Patterned growth of individual and multiple vertically aligned carbon nanofibers. Applied Physics Letters, 2000. 76(24): p. 3555-3557.

32. Endo, M., et al., Selective and Efficient Impregnation of Metal Nanoparticles on Cup-Stacked-Type Carbon Nanofibers. Nano Letters, 2003. 3(6): p. 723-726.

33. Glasgow, D.G., et al., Surface treatment of carbon nanofibers for improved composite mechanical properties, in SAMPE. 2004: Long Beach, CA - USA. p. 10.

34. Baek, J.-B., C.B. Lyons, and L.-S. Tan, Grafting of Vapor-Grown Carbon Nanofibers via in-Situ Polycondensation of 3-Phenoxybenzoic Acid in Poly(phosphoric acid). Macromolecules, 2004. 37(22): p. 8278-8285.

35. ASI. Applied Sciences Inc.; Available from: http://www.apsci. com/ppi-pyro3.html.

36. Iijima, S., Helical microtubules of graphitic carbon. Nature, 1991. 354(6348): p. 56.

37.   Spitalsky, Z., et al., Carbon nanotube-polymer composites: Chemistry, processing, mechanical and electrical properties. Progress in Polymer Science, 2010. 35(3): p. 357-401.

38.   Awasthi, K., A. Srivastava, and O.N. Srivastava, Synthesis of carbon nanotubes. J Nanosci Nanotechnol, 2005. 5(10): p. 1616-1636.

39.   Kearns, J.C. and R.L. Shambaugh, Polypropylene fibers reinforced with carbon nanotubes. Journal of Applied Polymer Science, 2002.86(8): p. 2079-2084.

40.   Monthioux, M., Filling single-wall carbon nanotubes. Carbon, 2002. 40(10): p. 1809-1823.

41.   Qian, D.D., E. C. Andrews, R., Load transfer and deformation mechanisms in carbon nanotube-polymer composites Appl. Phys. Lett., 2000. 76: p. 2868-2870.

42.   O'Connell, M.J., Carbon Nanotubes - Properties and Applications, M.J. O'Connell, Editor. 2006, CRC Press, Taylor & Francis Group: Boca Raton. p. 21.

43.   Koziol, K., et al., High-Performance Carbon Nanotube Fiber. Science, 2007. 318(5858): p. 1892-1895.

44.   Moniruzzaman, M. and K.I. Winey, Polymer Nanocomposites Containing Carbon Nanotubes. Macromolecules, 2006. 39(16): p. 5194-5205.

45.   Zheng, L.X., et al., Ultralong single-wall carbon nanotubes. Nat Mater, 2004. 3(10): p. 673-676.

46.   Vigolo, B., et al., Macroscopic Fibers and Ribbons of Oriented Carbon Nanotubes. Science, 2000. 290(5495): p. 1331-1334.

47.   Breuer, O. and U. Sundararaj, Big returns from small fibers: A review of polymer/carbon nanotube composites. Polymer Composites, 2004. 25(6): p. 630-645.

48.   Sperling, L.H., Introduction to physical polymer science. 2006, John Wiley & Sons, Inc.: Bethlehem - Pennsylvania.

49.   Bower, D.I., An Introduction to Polymer Physics. 2002, Cambridge University Press: Cambridge, UK. p. 9-12.

50.   Biron, M., Thermoplastics and thermplastic composites. Real Series, ed. E.S. Technology. 2007. 944.

51.   Harper, C.A., Handbook of Plastics, Elastomers & Composites (4th Edition), McGraw-Hill. p. 214.

52.	Varma, I.K. and V.B. Gupta, 2.01 - Thermosetting Resin—Properties, in Comprehensive Composite Materials, K. Editors-in-Chief: Anthony and Z. Carl, Editors. 2000, Pergamon: Oxford. p. 1-56.

53.	Goodman, S.H., 6 - Epoxy Resins, in Handbook of Thermoset Plastics (Second Edition), H.G. Sidney, Editor. 1999, William Andrew Publishing: Westwood, NJ. p. 193-268.

54.	Hexion, S.C., EPON™Resin 862 technical data sheet, S.C. Hexion, Editor. 2005. p. 5.

55.	Resolution, P.P., EPIKOTE™ Resin 862/EPIKURE™ Curing Agent W system, R.P. Products, Editor. 2001. p. 11.

56.	Albemarle, C., ETHACURE® 100 Curative, A. Corporation, Editor. 2001. p. 2.

57.	Coleman, J.N., et al., Small but strong: A review of the mechanical properties of carbon nanotube-polymer composites. Carbon, 2006. 44(9): p. 1624-1652.

58.	Manchado, M.A.L., et al., Thermal and mechanical properties of single-walled carbon nanotubes–polypropylene composites prepared by melt processing. Carbon, 2005. 43(7): p. 1499-1505.

59.	Garg, P., et al., Effect of dispersion conditions on the mechanical properties of multi-walled carbon nanotubes based epoxy resin composites. Journal of Polymer Research, 2011. 18(6): p. 1397-1407.

60.	Dasari, A., et al., Clay exfoliation and organic modification on wear of nylon 6 nanocomposites processed by different routes. Composites Science and Technology, 2005. 65(15-16): p. 2314-2328.

61.	Guo, Z., et al., Fabrication and characterization of iron oxide nanoparticles reinforced vinyl-ester resin nanocomposites. Composites Science and Technology, 2008. 68(6): p. 1513-1520.

62.	Choi, Y.-K., et al., Mechanical and physical properties of epoxy composites reinforced by vapor grown carbon nanofibers. Carbon, 2005. 43(10): p. 2199-2208.

63.	Sandler, J.S., M. S. P. Prasse, T. Bauhofer, W. Schulte, K. Windle, A. H., Development of a dispersion process for carbon nanotubes in an epoxy matrix and the resulting electrical properties. Polymer, 1999. 40(21): p. 5967-5971.

64. Andrews, R., et al., Fabrication of Carbon Multiwall Nanotube/Polymer Composites by Shear Mixing. Macromolecular Materials and Engineering, 2002. 287(6): p. 395-403.

65. Schueler, R., et al., Agglomeration and electrical percolation behavior of carbon black dispersed in epoxy resin. Journal of Applied Polymer Science, 1997. 63(13): p. 1741-1746.

66. Jimenez, G.A. and S.C. Jana, Electrically conductive polymer nanocomposites of polymethylmethacrylate and carbon nanofibers prepared by chaotic mixing. Composites Part A: Applied Science and Manufacturing, 2007. 38(3): p. 983-993.

67. Rao, Y., A. Takahashi, and C.P. Wong, Di-block copolymer surfactant study to optimize filler dispersion in high dielectric constant polymer-ceramic composite. Composites Part A: Applied Science and Manufacturing, 2003. 34(11): p. 1113-1116.

68. Khastgir, D. and K. Adachi, Rheological and dielectric studies of aggregation of barium titanate particles suspended in polydimethylsiloxane. Polymer, 2000. 41(16): p. 6403-6413.

69. Okamoto, M., S. Morita, and T. Kotaka, Dispersed structure and ionic conductivity of smectic clay/polymer nanocomposites. Polymer, 2001. 42(6): p. 2685-2688.

70. Essawy, H.A., N.A. Abd El-Wahab, and M.A. Abd El-Ghaffar, PVC–laponite nanocomposites: Enhanced resistance to UV radiation. Polymer Degradation and Stability, 2008. 93(8): p. 1472-1478.

71. Imai, Y., et al., Transparent poly(bisphenol A carbonate)-based nanocomposites with high refractive index nanoparticles. European Polymer Journal, 2009. 45(3): p. 630-638.

72. Bocchini, S., et al., Influence of nanodispersed hydrotalcite on polypropylene photooxidation. European Polymer Journal, 2008. 44(11): p. 3473-3481.

73. Adhikari, A. and K. Lozano, Effects of carbon nanofibers on the crystallization kinetics of polyethylene oxide. Journal of Polymer Research, 2011. 18(5): p. 875-880.

74. Lafdi, K., et al., Effect of carbon nanofiber heat treatment on physical properties of polymeric nanocomposites: part I. J. Nanomaterials, 2007. 2007(1): p. 1-6.

75.   Cortés, P., et al., Effects of nanofiber treatments on the properties of vapor-grown carbon fiber reinforced polymer composites. Journal of Applied Polymer Science, 2003. 89(9): p. 2527-2534.

76.   Kumar, S., et al., Study on mechanical, morphological and electrical properties of carbon nanofiber/polyetherimide composites. Materials Science and Engineering: B, 2007. 141(1-2): p. 61-70.

77.   Patton, R.D.P., Jr C. U. Wang, L. Hill, J. R., Vapor grown carbon fiber composites with epoxy and poly(phenylene sulfide) matrices Composites Part A: Applied Science and Manufacturing, 1999. 30(9): p. 1081-1091.

78.   Ahn, S.-N., et al., Epoxy/amine-functionalized short-length vapor-grown carbon nanofiber composites. Journal of Polymer Science Part A: Polymer Chemistry, 2008. 46(22): p. 7473-7482.

79.   Lozano, K. and E.V. Barrera, Nanofiber-reinforced thermoplastic composites. I. Thermoanalytical and mechanical analyses. Journal of Applied Polymer Science, 2001. 79(1): p. 125-133.

80.   Sun, L.H., et al., Preparation, Characterization, and Modeling of Carbon Nanofiber/Epoxy Nanocomposites. Journal of Nanomaterials, 2011: p. 8.

81.   May, C.A. and G.Y. Tanaka, Epoxy Resins Chemistry and Technology, ed. M. Dekker. 1987, New York, USA.

82.   Allaoui, A., S.V. Hoa, and M.D. Pugh, The electronic transport properties and microstructure of carbon nanofiber/epoxy composites. Composites Science and Technology, 2008. 68(2): p. 410-416.

83.   Natsuki, T., Q.-Q. Ni, and S.-H. Wu, Temperature dependence of electrical resistivity in carbon nanofiber/unsaturated polyester nanocomposites.Polymer Engineering & Science, 2008. 48(7): p. 1345-1350.

84.   Chyi-Shan, W. and A.M. D, Method of forming conductive polymeric nanocomposite materials, O. University of Dayton (Dayton, Editor. 2004.

85.   Rice, B.P., T. Gibson, and K. Lafdi. DEVELOPMENT OF MULTIFUNCTIONAL ADVANCED COMPOSITES USING A VGNF ENHANCED MATRIX. in 49th International SAMPE symposium proceedings. 2004. Long Beach.

86.   Klein, K.L., et al., Surface characterization and functionalization of carbon nanofibers. JOURNAL OF APPLIED PHYSICS, 2008. 103(6): p. 26.

87.   Nie, Y. and T. Hübert, Effect of carbon nanofiber (CNF) silanization on the properties of CNF/epoxy nanocomposites. Polymer International, 2011. 60(11): p. 1574-1580.

88.   Aguilar, J.O., J.R. Bautista-Quijano, and F. Avilés, Influence of carbon nanotube clustering on the electrical conductivity of polymer composite films. eXPRESS Polymer Letters, 2010. 4(5): p. 292–299.

89.   Karippal, J.J., et al., Effect of amine functionalization of CNF on electrical, thermal, and mechanical properties of epoxy/CNF composites. Polymer Bulletin, 2010. 65(8): p. 849-861.

90.   Peter, T.L. and et al., A quantitative assessment of carbon nanotube dispersion in polymer matrices. Nanotechnology, 2009. 20(32): p. 7.

91.   Xie, S., et al., Quantitative characterization of clay dispersion in polypropylene-clay nanocomposites by combined transmission electron microscopy and optical microscopy. Materials Letters, 2010. 64(2): p. 185-188.

92.   Spowart, J.E.M., B. Miracle, D. B., Multi-scale characterization of spatially heterogeneous systems: implications for discontinuously reinforced metal-matrix composite microstructures. Materials Science and Engineering: A, 2001. 307(1-2): p. 51-66.

93.   Hattum, F.v., et al. Quantitative assessement of mixing quality in nanoreinforced polymers using a multi-scale image analysis method. in 38th ISTC. 2006. Dallas, Texas.

94.   Leer-Lake, C. and e. al., Quantifying Dispersion in Carbon Nano Materials Composites by Grey Scale Analysis. submitted to Comp. Sci. Techn., 2012.

95.   Gershon, A., et al., Nanomechanical characterization of dispersion and its effects in nano-enhanced polymers and polymer composites. Journal of Materials Science, 2010. 45(23): p. 6353-6364.

96.   Yoonessi, M., et al., Neutron scattering, electron microscopy and dynamic mechanical studies of carbon nanofiber/phenolic resin composites. Carbon, 2008. 46(4): p. 577-588.

97.   Finegan, I.C., et al., Surface treatments for improving the mechanical properties of carbon nanofiber/thermoplastic composites. Journal of Materials Science, 2003. 38(16): p. 3485-3490.

98. Huang, J.-C., Carbon black filled conducting polymers and polymer blends. Advances in Polymer Technology, 2002. 21(4): p. 299-313.

99. Miyasaka, K., et al., Electrical conductivity of carbon-polymer composites as a function of carbon content. Journal of Materials Science, 1982. 17(6): p. 1610-1616.

100. Stauffer, D. and A. Aharony, eds. Introduction to percolation theory. 2nd edition ed., ed. T.a. Francis. 1991: London.

101. Stroud, D. and D.J. Bergman, Frequency dependence of the polarization catastrophe at a metal-insulator transition and related problems. Physical Review B, 1982. 25(3): p. 2061-2064.

102. Kirkpatrick, S., Percolation and Conduction. Reviews of Modern Physics, 1973. 45(4): p. 574-588.

103. Herrmann, H.J., B. Derrida, and J. Vannimenus, Superconductivity exponents in two- and three-dimensional percolation. Physical Review B, 1984. 30(7): p. 4080-4082.

104. Celzard, A., et al., Critical concentration in percolating systems containing a high-aspect-ratio filler. Physical Review B, 1996. 53(10): p. 6209.

105. Jimenez, G.A. and S.C. Jana, Oxidized carbon nanofiber/polymer composites prepared by chaotic mixing. Carbon, 2007. 45(10): p. 2079-2091.

106. Silva, J., Theoretical modeling of the electric response of carbon based nanocomposites for advanced applications, in Physics. 2009, Minho: Braga. p. 20.

107. Bauhofer, W. and J.Z. Kovacs, A review and analysis of electrical percolation in carbon nanotube polymer composites. Composites Science and Technology, 2009. 69(10): p. 1486-1498.

108. Silva, J. and et al., Applying complex network theory to the understanding of high-aspect-ratio carbon-filled composites. EPL (Europhysics Letters), 2011. 93(3): p. 37005.

109. Erdös, P. and A. Rényi, On random graphs, I. Publicationes Mathematicae (Debrecen), 1959. 6: p. 290-297.

110. Simoes, R. and et al., Low percolation transitions in carbon nanotube networks dispersed in a polymer matrix: dielectric properties, simulations and experiments Nanotechnology, 2009. 20(3): p. 8.

111. STRÜMPLER, R. and J. GLATZ-REICHENBACH, Conducting polymer composites. Journal of electroceramics, 1999. 3(4): p. 329-346.

112. Balberg, I., et al., Excluded volume and its relation to the onset of percolation. Physical Review B, 1984. 30(7): p. 3933.

113. Bug, A.L.R., S.A. Safran, and I. Webman, Continuum Percolation of Rods. Physical Review Letters, 1985. 54(13): p. 1412-1415.

114. Ambegaokar, V., B.I. Halperin, and J.S. Langer, Theory of hopping conductivity in disordered systems. Journal of Non-Crystalline Solids, 1972. 8-10(0): p. 492-496.

115. Miller, A. and E. Abrahams, Impurity Conduction at Low Concentrations. Physical Review, 1960. 120(3): p. 745-755.

116. Li, G., et al., Transport and percolation theory in weighted networks. Physical Review E, 2007. 75(4): p. 045103.

117. Wu, Z., et al., Current flow in random resistor networks: The role of percolation in weak and strong disorder. Physical Review E, 2005. 71(4): p. 045101.

118. Sreenivasan, S., et al., Effect of disorder strength on optimal paths in complex networks. Physical Review E, 2004. 70(4): p. 6.

119. Connor, M.T., et al., Broadband ac conductivity of conductor-polymer composites. Physical Review B, 1998. 57(4): p. 2286–2294.

120. Yui, H., et al., Morphology and electrical conductivity of injection-molded polypropylene/carbon black composites with addition of high-density polyethylene. Polymer, 2006. 47(10): p. 3599-3608.

121. Bar, H., M. Narkis, and G. Boiteux, The electrical behavior of thermosetting polymer composites containing metal plated ceramic filler. Polymer Composites, 2005. 26(1): p. 12-19.

122. Chekanov, Y., et al., Electrical properties of epoxy resin filled with carbon fibers. Journal of Materials Science, 1999. 34(22): p. 5589-5592.

123. Lafdi, K. and M. Matzek. Carbon nanofbres as a nano-reinforcement for polymeric nanocomposites.in 35th ISTC. 2003. Dayton, OH.

124. Ishikawa, T., et al. 2004: USA.

125. Rana, S., R. Alagirusamy, and M. Joshi, Mechanical behavior of carbon nanofibre-reinforced epoxy composites. Journal of Applied Polymer Science, 2010. 118(4): p. 2276-2283.

126.   Patton, R.D., et al., Ablation, mechanical and thermal conductivity properties of vapor grown carbon fiber/phenolic matrix composites. Composites Part A: Applied Science and Manufacturing, 2002. 33(2): p. 243-251.

127.   Prolongo, S.G., et al., Thermo-physical characterisation of epoxy resin reinforced by amino-functionalized carbon nanofibers. Composites Science and Technology, 2009. 69(3-4): p. 349-357.

128.   Donohoe, J. and C. Pittman. Shielding Effectiveness of Vapor Grown Carbon Nanofiber/Vinyl Ester Composites. in EMC Europe 2004, international symposium on electromagnetic compatibility. 2004. Eindhoven, Netherlands.

129.   Pelsoci, T. Composite manufacturing technologies: applications automotive, petroleum, and civil infrastructure industries. 2004; Available from: http://www.atp.nist.gov/eao/grc04-863/gcr04-863.pdf.

130.   Zhang, B., et al., Gas sensitive vapor grown carbon nanofiber/polystyrene sensors. Materials Research Bulletin, 2006. 41(3): p. 553-562.

131.   Shim, B.S., J. Starkovich, and N. Kotov, Multilayer composites from vapor-grown carbon nano-fibers. Composites Science and Technology, 2006. 66(9): p. 1174-1181.

132.   Huang, J., Y. Liu, and T. You, Carbon nanofiber based electrochemical biosensors: A review. Analytical Methods, 2010. 2(3): p. 202-211.

3. The dominant role of tunneling in the conductivity of carbon nanofiber-epoxy composites

In this work, epoxy composites reinforced with vapor grown carbon nanofibers were prepared by a simple dispersion method and studied in order to identify the main conduction mechanism. The samples show high electrical conductivity values. The results indicate that a good cluster distribution seems to be more important than the fillers dispersion in order to achieve high conductivity values. Inter-particle tunneling has been identified as the main mechanism responsible for the observed behavior.

3.1- Introduction

Epoxy resins are known, in general, for their good-to-excellent properties covering an extensive range of applications[1]. One attempt to increase their application range is to incorporate nanoscale fillers which have intrinsically high electrical conductivity into the epoxy matrix. Among nanoscale modifiers, vapor grown carbon nanofibers (VGCNF) are very suitable as they show similar mechanical, electrochemical properties to the carbon nanotubes (CNT) at a lower price. These facts, together to the relatively easier incorporation and dispersion into polymers also raised the interest in VGCNF to provide solutions to some problems in composite applications[2, 3].

VGCNF can be prepared with diameters in the nanometer scale resulting in high aspect ratios. Pyrograf® III nanofibers (Applied Sciences Inc. (ASI), Ohio, USA), are a highly graphitic sort of VGCNF with stacked-cup morphology[4].

With the goal of obtaining high mechanical and electrical performance in VGCNF/Epoxy composites, the focus has been in the development of processing methods to achieve homogeneous dispersion of the fillers in the epoxy matrix. In particular, acetone solvent/epoxy infusion and mixing[5]; mixing carried out through high intensity ultrasonic irradiation[6]; combination of ultrasonication and mechanical mixing[7]; sonication and conventional stirring[8] and preparation methods involving heat treatment of the fibers[9]have been successfully tested and the effect of VGCNF loading on the electrical and mechanical macroscopic response has been evaluated. In particular, the effect of different dispersion states on the rheological and AC conductivity properties of carbon nanofiber/epoxy suspensions prepared by simple hand-mixing[10]has been reported, and an electrical threshold at 0.5 wt.% loading has been achieved.

Despite the aforementioned efforts, the role of CNT or VGCNF dispersion in the conductivity values and the origin of the conduction mechanism in these types of composites are still under discussion. These problems are addressed in the present letter.

3.2- Material and methods

The VGCNF used in the present study were Pyrograf III[TM], PR-19-LHT-XT, provided by Applied Sciences, Inc. (Cedarville, OH), density of 1.95 g/cm^3. The polymer matrix was a low-viscous epoxy resin (Epikote[TM] Resin 862), density of 1.17 g/cm^3, as supplied by Resolution Performance Products. The epoxy resin was mixed with a hardener Epikure 100 Curative, density of 1.022 g/cm^3, manufactured by Albemarle Corporation. Eight different concentrations of VGCNF in the epoxy resin and a neat sample were prepared. The VGCNF were used as provided by the manufacturer. The preparation method for the composites was the following: first, the VGCNF were hand mixed with the epoxy resin during two minutes, then the hardener was added and hand mixed for two minutes. The ratio was 100 parts of resin for 26.4 parts in weight of hardener. At this stage, all the samples were subjected to a pressure of 20mbar, then cast into a mold and cured at 80 °C and 150 °C for 90 minutes. The samples are rectangular bars with 1 mm thickness, 10 mm width and 70 mm length. Morphology and CNF dispersion were investigated by Scanning Electron Microscopy (SEM) in a Phillips X230 FEG apparatus. Surface and cross section images were taken after coating the samples with a gold layer by magnetron sputtering. The volume electrical resistivity of the samples was obtained by measuring I-V curves at room temperature with a Keithley 487 picoammeter/voltage source.

Measurements of the ε', real part of the dielectric function, and tan δ, dielectric loss, were performed at room temperature in a home-built sample holder with an automatic Quadtech 1929 Precision LCR meter. The applied signal for seven frequencies in the range 100 Hz to 100 kHz was 0.5 V. The samples were coated by thermal evaporation with circular Al electrodes of 5mm diameter onto both sides of the sample.

3.3- Results and Discussion

Scanning electronic microscopy image revealed: a) the VGCNF dispersion (Figure 3.1) achieved with this method is not perfect, showing some clustering effects of the fibers (Figure3.1, right); b) the VGCNF clusters show nevertheless a good distribution along the samples; c) with increasing VGCNF concentration (Figure3.1,

right), in particular in the percolation threshold transition 0.1 wt.% (Figure 3.1, left) to 0.5 wt.% (Figure 3.1, right) a reduction in the fiber-fiber distance is observed.
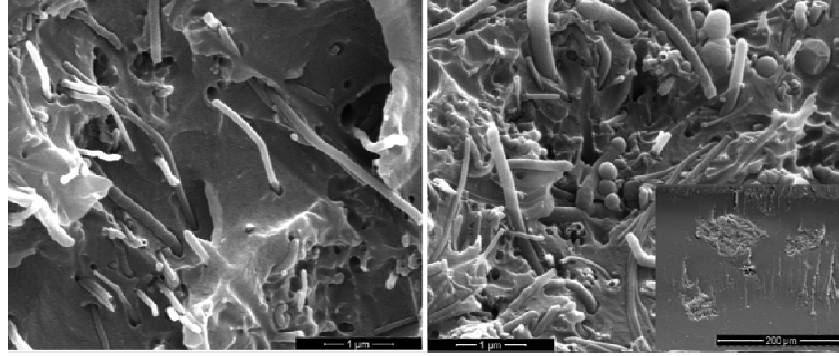
Figure 3. 1- SEM image for (left) 0.1 wt.% and (right) 0.5 wt.%. Right inset: SEM image at a different scale for the same concentration.

The variation of the real and imaginary part of the dielectric function with frequency is shown in figure 3.2. The variation of the DC conductivity with concentration is presented in figure 3.3. The variation of the electrical properties with concentration for polymer/VGCNF composites is usually understood in the framework of the percolation theory[11-13]. The percolation threshold (Φ_c) is defined as the concentration Φ at which an infinite cluster appears in an infinite lattice. For a concentration $\Phi > \Phi_c$ a cluster spans the system, whereas for $\Phi < \Phi_c$ the spanning cluster does not exist and the system is made of many small clusters. At the percolation threshold several power laws can be tested. For the conductivity and the dielectric constant the power law assumes the following shape $\sigma_{eff} \sim \sigma_{conductor}(\Phi-\Phi_c)^t$ for $\Phi > \Phi_c$ and $\varepsilon_{eff} \sim \varepsilon_{matrix}|\Phi-\Phi_c|^{-s}$ for $\Phi < \Phi_c$ and $\Phi > \Phi_c$, respectively. The s and t are the critical exponents and are assumed to be universal, i. e., they only depend on the dimensionality of the domain. Near the percolation threshold the dependence of the dielectric constant and the conductivity on the frequency can also be tested: a power relation near a critical frequency is expected[11-13].
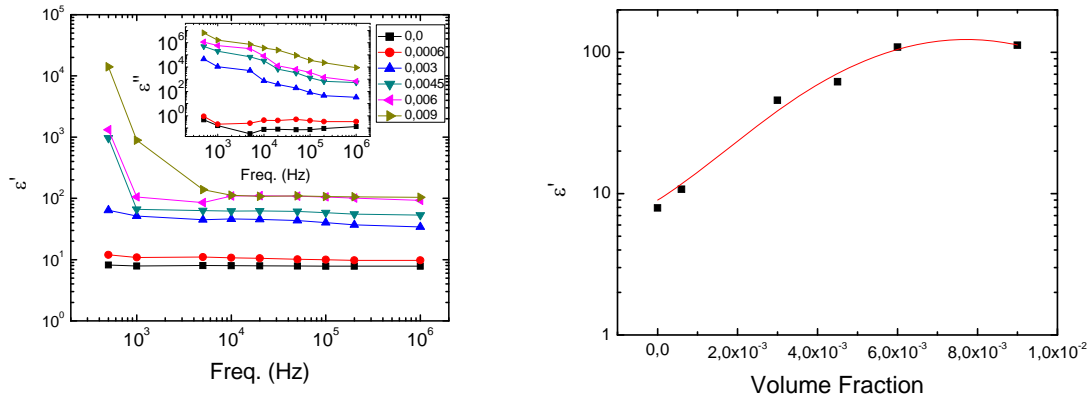
Figure 3. 2- Left: real and imaginary part (inset) of the permittivity versus frequency for several volume fractions. Right: dielectric constant variation versus volume fraction. The line represents a Gaussian fit on the data.

No power law relation in the behavior of the dielectric constant with the frequency, (Figure 3.2, left) was found. Also in the same figure it is possible to observe a larger increase of the value of the dielectric constant between 0.0006 and 0.003 volume fraction. The power law relating the volume fraction and the dielectric constant ($\varepsilon_{eff} \sim \varepsilon_{matrix}|\Phi\text{-}\Phi_c|^{-s}$) was inconclusive, and the best fit is a Gaussian function (R^2=0.96, Figure 3.2 right) relating the dielectric constant and the volume fraction. From these results it can be concluded that the increase found in the dielectric constant cannot be explained simply by the percolation theory but by the formation of a capacitive network[14].

To further test the latter conclusions, the conductivity values were analyzed and fitted with the percolation power law for the DC conductivity (Figure 3.3, inset (a)). The linear fit in the log-log plot results in a critical exponent (*t*) of 4.54 ± 0.35 for Φ_c equal to 6.2E-4 and $\sigma_{conductor} \approx 3.2E6\ S/cm$. The fit R^2 was 0.97. The critical exponent (*t*) deviates from the universal value which is approximately 2[15], the problem of non-universal values has already been addressed in previous works[16, 17]. This deviation is interpreted as a result of interparticle tunneling and the formation of a percolation network with a mean tunneling distance.

The Φ_c found in this work also deviates from the predictions of the excluded volume theory. Using the values provided by the manufacturer[4], the excluded volume[18] predicts, for an average aspect ratio of the VGCNF of 433, the following

bounds: *0.002 ≤ Φ_c ≤ 0.003*, in volume fraction. The experimental *Φ_c* is an order of magnitude lower than theoretical predictions whereas the conductivity value found from the power law (3.2E6 S/cm) is two orders of magnitude higher than the manufacturer value for the VGCNF.
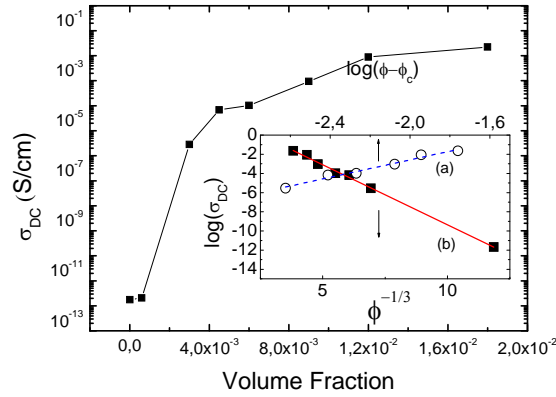
Figure 3. 3- DC conductivity versus volume fraction displayed in a log-linear scale. Inset (a): Fit of the percolation law $\sigma_{eff} \sim \sigma_{conductor}(\Phi-\Phi_c)^t$. Inset (b): Fit of a single tunneling junction expression in a log-linear plot.

From the latter it is possible to conclude that the main mechanism for the composites could be the interparticle tunneling. In order to test the latter claim we fit the conductivity values with the single tunnel junction expression $\sigma_{DC} = \sigma_0 \exp(-2\chi_t d)$ [19]. Where $\chi_t = \sqrt{2mV(T)/\hbar^2}$, "m" the mass of the charge carriers , "d" the barrier width and "V(T)" the temperature modified barrier height[20],(Figure 3.3 inset (b)). Assuming a random distribution of the particles it was demonstrated that $d \propto \Phi^{-1/3}$ [21]. The results of the application of the latter expression in a log - linear plot are presented in Figure 3.3 (inset). The R^2 was 0.996, the value found for σ_0 (1.49E3 S/cm) was very similar to the VGCNF conductivity values (1E3 – 1E4 S/cm)[2]. The fit error plus the σ_0 indicate that the main conduction mechanism in this type of composites could be attributed to tunneling through a potential barrier of varying height due to local temperature fluctuations[22].

3.4- Conclusions

In summary, we reported conductivity values of 10^{-2} S/cm for 3 wt.% in composites produced in a simple way. We also demonstrate that the good cluster distribution seems to be more important than the VGCNF dispersion. Finally, these results, point out inter-particle tunneling as the main conduction mechanism in VGCNF/epoxy composites.

References

1. Fink, J.K., Reactive Polymers Fundamentals and Applications - A Concise Guide to Industrial Polymers. 2005: William Andrew Publishing/Plastics Design Library.

2. Al-Saleh, M.H. and U. Sundararaj, A review of vapor grown carbon nanofiber/polymer conductive composites. Carbon, 2009. **47**(1): p. 2-22.

3. Tibbetts, G.G., et al., A review of the fabrication and properties of vapor-grown carbon nanofiber/polymer composites. Composites Science and Technology, 2007. **67**(7-8): p. 1709-1718.

4. ASI. Applied Sciences Inc.; Available from: http://www.apsci. com/ppi-pyro3.html.

5. Patton, R.D.P., Jr C. U. Wang, L. Hill, J. R., Vapor grown carbon fiber composites with epoxy and poly(phenylene sulfide) matrices Composites Part A: Applied Science and Manufacturing, 1999. **30**(9): p. 1081-1091.

6. Zhou, Y., F. Pervin, and S. Jeelani, Effect vapor grown carbon nanofiber on thermal and mechanical properties of epoxy. Journal of Materials Science, 2007. **42**(17): p. 7544-7553.

7. Allaoui, A., S.V. Hoa, and M.D. Pugh, The electronic transport properties and microstructure of carbon nanofiber/epoxy composites. Composites Science and Technology, 2008. **68**(2): p. 410-416.

8. Prasse, T., J.-Y. Cavaillé, and W. Bauhofer, Electric anisotropy of carbon nanofibre/epoxy resin composites due to electric field induced alignment. Composites Science and Technology, 2003. **63**(13): p. 1835-1841.

9. Lafdi, K., et al., Effect of carbon nanofiber heat treatment on physical properties of polymeric nanocomposites: part I. J. Nanomaterials, 2007. **2007**(1): p. 1-6.

10. Leer, C., et al. On the Dispersion of Carbon Nanofibre-Based Suspensions in Simple Shear: An Experimental Study. in Materials Science Forum. 2008.

11. Stauffer, D. and A. Aharony, eds. Introduction to percolation theory. 2nd edition ed., ed. T.a. Francis. 1991: London.

12. Stroud, D. and D.J. Bergman, Frequency dependence of the polarization catastrophe at a metal-insulator transition and related problems. Physical Review B, 1982. **25**(3): p. 2061-2064.

13.   Nan, C.-W., Physics of inhomogeneous inorganic materials. Progress in Materials Science, 1993. **37**(1): p. 1-116.

14.   Simoes, R. and et al., Low percolation transitions in carbon nanotube networks dispersed in a polymer matrix: dielectric properties, simulations and experiments Nanotechnology, 2009. **20**(3): p. 8.

15.   Kirkpatrick, S., Percolation and Conduction. Reviews of Modern Physics, 1973. **45**(4): p. 574-588.

16.   Balberg, I., Tunneling and nonuniversal conductivity in composite materials. Physical Review Letters, 1987. **59**(12): p. 1305-1308.

17.   Vionnet-Menot, S., et al., Tunneling-percolation origin of nonuniversality:Theory and experiments. Physical Review B, 2005. **71**(6): p. 12.

18.   Celzard, A., et al., Critical concentration in percolating systems containing a high-aspect-ratio filler. Physical Review B, 1996. **53**(10): p. 6209.

19.   Ezquerra, T.A., M. Kulescza, and F.J. Baltá-Calleja, Electrical transport in polyethylene-graphite composite materials. Synthetic Metals, 1991. **41**(3): p. 915-920.

20.   Dekker, M., Carbon Black-Polymer Composites, ed. E. Sichel. 1982, New York.

21.   Kübler, J. and K.H. Höck, H. Böttger, V. V. Bryksin, Hopping Conduction in Solids, VCH-Verlagsgesellschaft, Weinheim, Deerfield Beach-Florida 1985. 398 Seiten, Preis: DM 140,—. Berichte der Bunsengesellschaft für physikalische Chemie, 1987. **91**(1): p. 77-77.

22.   Sheng, P., E.K. Sichel, and J.I. Gittleman, Fluctuation-Induced Tunneling Conduction in Carbon-Polyvinylchloride Composites. Physical Review Letters, 1978. **40**(18): p. 1197-1200.

4. Quantitative evaluation of the dispersion ability of different preparation methods and DC electrical conductivity of vapor grown carbon nanofiber/epoxy composites

The aim of this work is to quantitatively analyze the dispersion ability of different methods for the preparation of vapor grown carbon nanofiber - epoxy composites. Four different dispersion methods were used, differing in stress level intensity: blender mixing, capillary rheometry mixing, 3 roll milling and planetary centrifuge mixing. Furthermore, the relationship between dispersion and DC conductivity of the composites was evaluated. For the dispersion analysis, four nanofiber concentrations ranging from 0.1 to 3.0 wt.% were prepared for each method, while the DC measurements were performed for eight concentrations, ranging from 0 to 4.0 wt.%. The dispersion was analyzed by transmitted light optical microscopy and greyscale analysis, following a methodology previously established. The results show that as the VGCNF content increases the dispersion level decreases, as indicated by the increase of the variance of the corresponding greyscale histograms. The 3 roll-mill method produces the samples with the highest dispersion levels, whilst the samples from the remaining methods show large VGCNF agglomerates. The dispersion was also estimated and calculated along the length of the samples, indicating a symmetric variation of dispersion from the center. The dispersion method also strongly influences the overall composite electrical response. No relationship was found between the electrical conductivity and the greyscale analysis achieved by the different methods. Thus, this method for the quantification of dispersion works well for lengthscales around 0.1 μm, but this is above the relevant scale that determines the electrical response.

4.1- Introduction

Nanoscience has grown strongly over the last twenty years and the importance of nanotechnology will increase as miniaturization becomes more important in areas such as computing, sensors, biomedical and many other applications. The development of polymer nanocomposites has opened a new research field in the area of materials science [1]. Many research works have been performed in order to improve polymer composite properties after the discovery and development of novel carbon structures.

CNT and VGCNF are promising multifunctional nanofillers for polymer composites due to their exceptional mechanical, electrical and thermal properties [2]. VGCNF have received less research attention than CNT as nanofillers, as CNT have superior mechanical properties, smaller diameter and lower density than VGCNF. However, the availability and relatively low price of VGCNF, in combination with good properties, makes them an excellent alternative to CNT. In fact, currently MWCNT are 2-3 times more expensive than VGCNF and SWCNT are even more expensive [3]. VGCNF are low-cost, discontinuous filaments, with diameters in the nanometer range, i.e., about a hundred times smaller than conventional carbon fibers [4]. The incorporation of VGCNF into polymer matrices offers the opportunity to transfer their intrinsic properties to the polymer at low fiber contents due to their large surface to volume ratio, which increases particle–matrix interactions.

The ultimate performance of polymer nanocomposites strongly depends on the dispersion and distribution of the VGCNF in the polymer matrix.VGCNF tend to agglomerate in clusters, due to the dominant intermolecular Van der Waals interactions between them, which may affect in a negative way some of the composites properties. The quality of nanofillers dispersion in the polymer matrix is directly correlated to its efficiency in the improvement of mechanical, electrical and thermal properties, amongst others. The properties of a composite are also intimately linked to the aspect ratio and surface-to-volume ratio of the filler[5]. The homogeneous dispersion of nanofiller particles in the polymer matrix, as well as the quality of the interface between filler and polymer, play also a key role as lack of adhesion between the two phases will result in less efficient property enhancement and e.g. premature failure [6]. For instance, the mechanical and thermal properties are largely enhanced by a homogeneous dispersion of the nanofillers [7-9]. The dispersion level of nanoparticles has been shown to

influence other physical properties such as the dielectric constant [10, 11], the electrical conductivity [12-16], the ionic conductivity [17], the coercive force [18], the refractive index [19], the UV resistance [20] and abrasion resistance [21], among others [22, 23].With respect to the electrical properties, it is not consensual that the electrical properties are strictly related to a good dispersion of nanofillers, some studies claiming that filler distribution seems to be more important than dispersion [24-27], or even that a good dispersion of the fillers may be disadvantageous [14].

Composite processing methods and conditions influence filler distribution, dispersion, orientation and aspect ratio [3]. Several methods of dispersing VGCNF in thermoplastic matrices have been reported [4], such as injection molding [28], and single [29] and twin [30] screw extrusion. To produce nanocomposites based on VGCNF and thermosets, distinct methods can be used, such as dilution of the epoxy resin in acetone [31] and tetrahydrofuran [32] to promote the nanofillers infusion, blending of the nanofibers with the resin followed by roll milling [31] and high shear mixing [33]. All methods were successful in dispersing nanofillers, except high shear mixing, where the nanofibers could not completely penetrate into the matrix and, consequently, modest improvements in mechanical properties were obtained despite the enhancement of thermal conductivity[4].

Several characterization techniques have been used to quantify dispersion. SEM, TEM, SPM and TOM have been classically used to visualize the nanofillers dispersion in the host matrix [34]. However, if the goal of the study is to quantify rather than qualify the dispersion or distribution of the nanofillers in the matrix, there is a need to use specific image techniques and mathematical tools to achieve it. Even if TEM can provide direct information on nanofiller layers in the real space, it can only explore very small volumes of the sample and may not be representative. It is also important to use TOM to expose the overall dispersion/distribution at the macroscopic level [35]. The drawback of this technique is that it just reaches length scales of a few microns. The quantification of CNF dispersion in thermoplastic (high impact polystyrene - HIPS) and thermosetting (epoxy resin) matrices has been also been done by nanomechanical characterization: a rule-of-mixtures (ROM) formulation was developed to determine the fraction of dispersed nanofibers, which yielded a dispersion limit of 3.0 and 3.5 vol.% of CNF in HIPS and epoxy resin, respectively [36]. As for correlations between dispersion and electrical properties, no definite conclusions have been drawn [37].

There is insufficient information in the literature about structure–property relationships for nanofiller/polymer composites. This is partly due to the difficulty in characterizing the aspect ratio of nanofillers before and after mixing without making use of destructive techniques to quantify the degree of nanofiller dispersion [3].

The mixing quality of VGCNF in epoxy can be properly evaluated by means of TOM and GSA, yielding a quantitative description of the CNF dispersion/distribution in the matrix [38-40]. In this work, this technique is used to investigate the dispersion of VGCNF in epoxy achieved by four different methods, namely blender mixing, capillary rheometry mixing, 3 roll milling and planetary centrifuge mixing. In addition, the degree of dispersion is correlated with the electrical conductivity.

4.2- Experimental

4.2.1- Preparation of the VGCNF/epoxy composites

VGCNF Pyrograf III^{TM} PR-19-XT-LHT were supplied by ASI. The epoxy resin was Epikote^{TM} Resin 862 and the curing agent was Ethacure 100 Curative, supplied by Hexion Specialty Chemicals and Albemarle, respectively. Samples made with Epon Resin 862 from Hexion Specialty Chemicals as epoxy resin and Epikure W from Resolution Performance Products as a curing agent were also used. The two types of resins and curing agents share the same CAS. The weight ratio of resin to curing agent was 100:26.4. The dispersion of the VGCNF in the epoxy resin was performed by the following methods:

Method 1: Mixing in a Haeger blender for two minutes [24], where the velocity field and stress levels should generate a predominantly distributive mixing.

Method 2: Using a Rosand RH7 capillary rheometer to perform a four pass extrusion through a series of dies with alternating diameters, thus generating a series of converging-diverging flows with a strong extensional stress component [41, 42]; this flow field should generate good distribution but limited dispersion.

Method 3: Roll milling (using a Lehmann 3 roll mill) for 5 minutes, with a gap of 25.4 μm between the first and second rolls and 600 rpm for the third roll, where the ratio of the rotational speeds is 1:3:6 from the first to the third roll; which is expected to result in good dispersion levels and a relatively good distribution.

Method 4: Using a planetary-type Thinky ARE-250 mixer, at revolution and rotation speeds of 2000 rpm and 800 rpm, respectively, for 10 minutes and a good distribution should be expected.

After mixing the VGCNF with the epoxy, the corresponding amount of curing agent was added and blender mixed during two minutes. Then, all samples were subjected to a 20 mbar pressure, cast into a mold and cured at 80 °C and 150 °C for 90 minutes [24]. For each dispersion method, composites with eight VGCNF concentrations were prepared, ranging from 0 to 4.0 wt.%. All samples were casted rectangular molds with 1mm thickness, 10 mm width and 70 mm length.

4.2.2- Greyscale analysis

A group of samples from each method was selected for the morphological study. One aim was to study the effect of VGCNF content on dispersion for blender mixed samples at concentrations close to the percolation found in previous reports [24, 25, 27], which is 0.1 and 0.5 wt.%, and also 1.0 and 3.0 wt.%. The second aim criterion was to investigate the effect of the methods on dispersion at constant VGCNF content (1.0 wt.%). The selected samples were cut at the center, in a crosswise direction. In the particular case of the sample produced with method 1 and having 1.0 wt.% VGCNF, six of these cuts were performed at regular lengthwise intervals to study eventual variations in its characteristics in this direction. A 10 μm thick slice was removed from each sample using a Leitz 1401 microtome equipped with a glass knife. Each slice was placed between a microscope glass slide and cover glass using Canada balsam (Alfa Aesar, CAS# 8007-47-4) as a fixing resin. All samples were left to cure for at least 12 hours prior to analysis. Their thickness was determined by the homogeneity of the cut and the need of transparency even in the areas with higher VGCNF concentration, thus becoming more difficult as the concentration increases.

An Olympus BH2 transmission microscope with an integrated X-Y stage, a digital camera Leica DFC 280 and corresponding software were used to capture and record images from each slice. To obtain a representative sample area in terms of VGCNF dispersion, an array of N rows and M columns of optical micrographs were captured and recorded, avoiding image overlap. Close to 100 micrographs were captured, each with 1280 x 1024 pixels, each pixel being a square with a side of 131

nm. The dispersion of the VGCNF in the epoxy resin was estimated from a GSA based on the TOM. In this method, the value of variance is related to the width of the curve of the greyscale histogram. The histogram presents values proportional to the number of pixels of the micrograph at each gray scale, versus the corresponding greyscale value, for a certain lengthscale. In turn, the latter is related to the size of each pixel of the micrograph, so that the lower the lengthscale value the higher the micrograph resolution. Using 8-bit greyscale images, the greyscale value varies from 0 to 255, corresponding to black (0) and white (255), respectively. The variance is nil in the absence of dispersion and equal to 1 for perfect dispersion. The methodology is explained in more detail in [39].

4.2.3- Electrical measurements

For the electrical measurements, the samples were coated on both sides by thermal evaporation with circular Al electrodes of 5 mm in diameter. The characteristic *I-V* curves at room temperature were measured with a Keithley 6487 picoammeter/voltage source and the volume DC electrical conductivity was calculated taking also into account the geometric factors.

4.3- Results

4.3.1- Greyscale analysis

A greyscale analysis was performed on all samples. For ease of comparison, all TOM micrographs presented in Figures 4.1-4.3 and 4.5 have a 512x640 pixels resolution, where each pixel is a square with 0.26x0.26 μm^2 and the histograms presented correspond to this resolution. Figure 4.1(a) maps 96 micrographs with an 8-bit greyscale of a cross-section located at the center of the sample with 0.5 wt.% of VGCNF and prepared using method 1. A simple visual observation identifies several VGCNF clusters with different shapes and sizes ranging from a few to almost a hundred micrometers, which are reasonably well distributed. Figure 4.1(b) presents four adjacent micrographs extracted from Figure 4.1(a), in order to better evidence the size and distribution of the VGCNF clusters. The greyscale histograms corresponding to the micrographs of Figure 4.1(b) are presented Figure 4.1(c). Big clusters of VGCNF are

visible as black spots occupying a reasonable area of the image and their presence is indicated in the histograms as peaks for lower greyscale values. As the VGCNF becomes better dispersed, the resulting greyscale histogram will shift towards an increasingly narrower 'peak' distribution around a medium grey value. In the bottom right, top left and top right histograms of Figure 4.1(c) the small peak at the lower end of the greyscale values indicates the presence of big clusters that are visible in the corresponding micrographs. In the bottom left histogram no such peak exists, and no large clusters can be detected in the corresponding micrograph. The three histograms presenting two peaks have higher variances than the one with only one peak, intuitively demonstrating the existing quantitative correlation between dispersion level and the variance of the corresponding greyscale distribution.
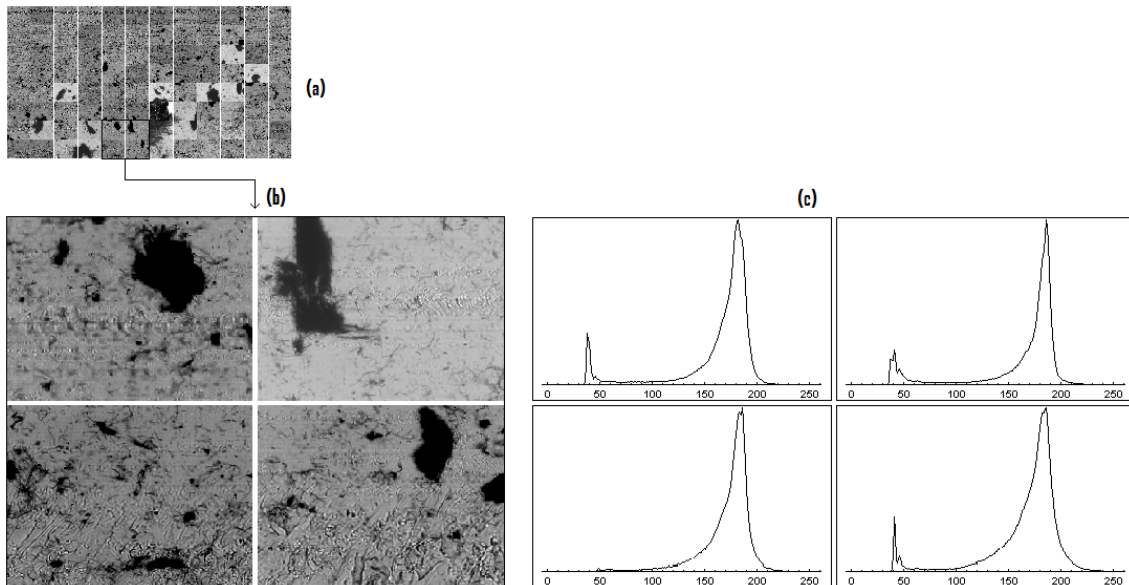
Figure 4. 1- Dispersion of sample with 0.5 wt.% VGCNF and preparation method 1: (a) array of 8 rows and 12 columns of TOM micrographs with a total area of 2.16 mm^2, (b) 4 adjacent micrographs from this array and (c) corresponding greyscale histograms.
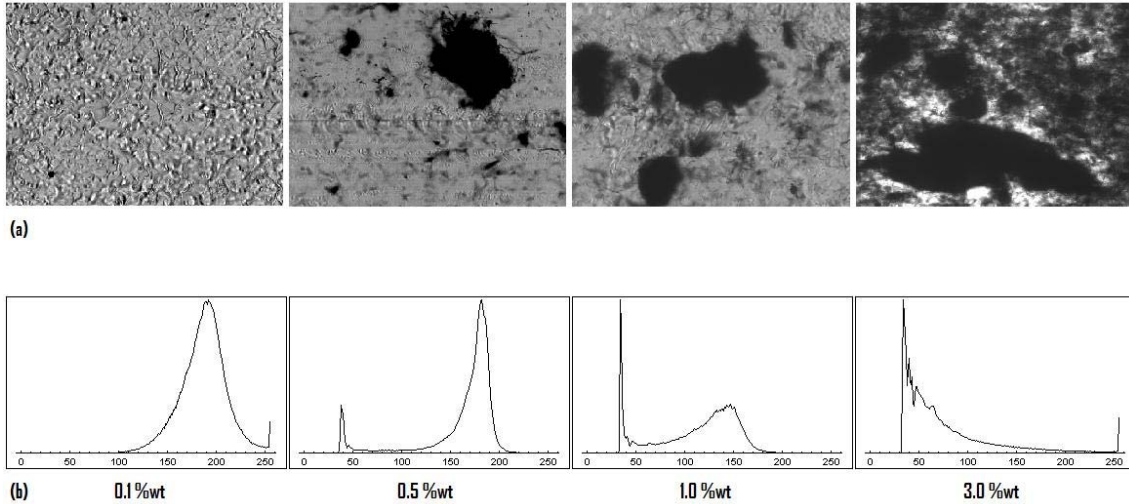
Figure 4. 2- TOM (a) micrographs and (b) corresponding greyscale histograms of samples with 0.1, 0.5, 1.0 and 3.0 wt.%VGCNF prepared with method 1.

The effect of CNF concentration on dispersion is shown in Figure 4.2, where the micrographs and greyscale histograms correspond to sample cross-sections taken at the center of the samples. Figure 4.2(b) indicates that only samples with 0.1 wt.% VGCNF do not exhibit a peak at low values in the greyscale, which means the absence of large clusters. As the VGCNF content increases, the dispersion level decreases: the histograms show a gradual increase of the peak, which also broadens for 3.0 wt.%. The histograms for 0.1 and 3.0 wt.% also contain a peak at the highest value of the greyscale, which corresponds to the white spots observed in the respective micrographs, corresponding to the polymer matrix with low levels of VGCNF.

The dispersion ability of the different methods at fixed VGCNF concentration (1.0 wt.%) is displayed in Figure 4.3. The histogram presented in Figure 3(b) for method 1 is similar to that for method 2. This is in agreement with the VGCNF dispersion, agglomerate size and distribution qualitatively observed in the corresponding micrographs. Only the sample from method 3 has no peak for low values of greyscale. Again, this is confirmed by the respective micrograph, which shows better dispersed VGCNF agglomerates.
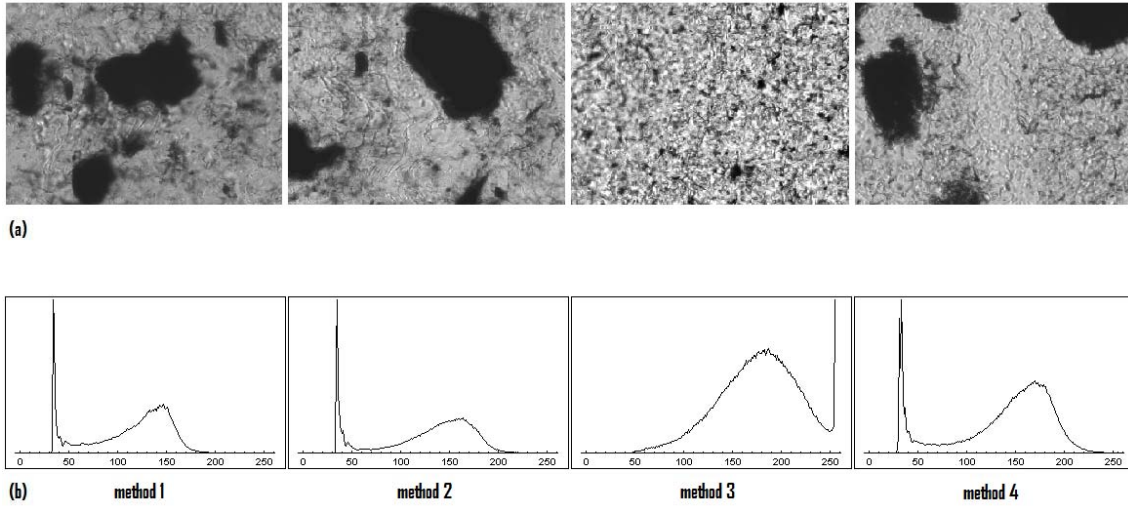
Figure 4. 3- TOM (a) micrographs and (b) corresponding greyscale histograms of samples with 1.0 wt.% of samples produced by all methods.

Figure 4.4(a) and (b) present the variance as a function of the length scale for the samples represented in Figure 4.2 and 4.3, respectively.
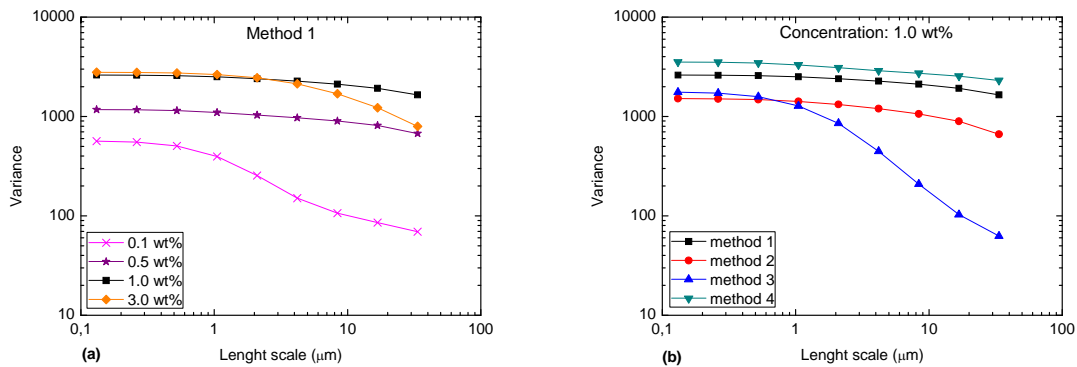
Figure 4. 4- Variance as a function of length scale for (a) method 1 with 0.1, 0.5, 1.0 and 3.0 wt.%VGCNF concentration and (b) 1.0 wt.% for the 4 methods.

Figure 4.4(a) shows that the variance increases as the VGCNF content increases. This is related to a decrease in the dispersion level, which is in agreement with what was observed in the analysis of Figure 4.2. As the length scale increases, the breath of the variance decreases with increasing VGCNF content, except for the samples with 3.0 wt.%. This particular behavior is due to the contrast shown in the corresponding

micrograph between the regions with and without VGCNF clusters. The sharp transitions from black to white regions are noticed for length scale low values, but are smoothed out as the length scale increases. As for the curves in Figure 4.4(b), the major change of the variance occurs for the sample produced by method 3. This means that, as the observation length scale increases, this method produces more homogenous nanocomposites than the remaining. Conversely, Figure 4.4(b) also shows that method 4 creates materials with higher values of the variance, i.e., that it is the less performing in terms of dispersion. This is confirmed in Figure 4.3(b), where the histogram of the sample from method 4 shows more pronounced peaks at both high and low gray values.

It can be concluded from Figure 4.4 that the curves of samples with 0.1 wt.% from method 1 and 1.0 wt.% from method 3 show the steeper decrease in variance as the length scale increases. The micrographs and histograms of these two samples (see Figure 4.2 and 4.3) show that dispersion is indeed much higher than that in the remaining samples.

Figure 4.5 presents data from three of the 5 cross-sections equally spaced that were obtained along the length of the sample with 1.0 wt.% prepared by method 1 (see Figure 4.5(d)). Figure 4.5(a) and (c) show micrographs and histograms at locations 1, 3 and 5.
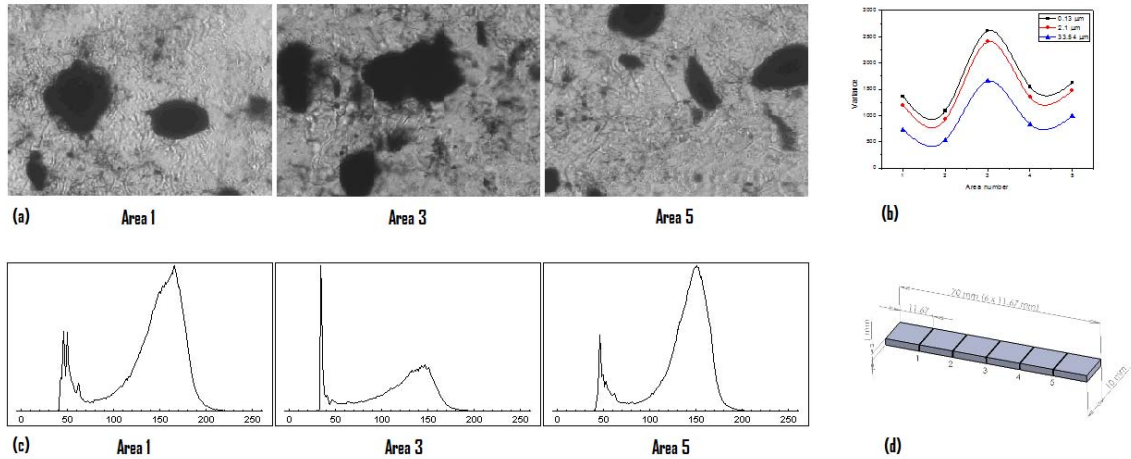
Figure 4. 5- Analysis along the length of an individual sample (1.0 wt.%, method 1). (a) TOM micrographs of areas 1, 3 and 5, (b) variance as a function of the sample area for the lowest (0.13 μm), medium (2.1 μm) and highest (33.54 μm) value of the length scale, (c) greyscale histograms of areas 1, 3 and 5 and (d) location of the areas studied in the sample.

The micrographs and histograms of areas 1 and 5 show nearly the same patterns whilst the histogram of area 3 is slightly different. Although all histograms have the same number and location of the peaks in the greyscale, the weight of the peaks varies. The highest peak in the histogram of area 3 is the one at lower greyscale numbers, while for areas 1 and 5 it occurs at higher greyscale levels. The three curves in Figure 4.5(b) show a peak in variance for area 3, at the center of the sample. In all cases, the variance decreases as the length scale increases.

Figure 4.6 depicts the effect of VGCNF concentration on variance, for all mixing methods at two length scales. At small length scales in Figure 4.6(a), the variance increases with concentration for method 1 and for method 2 evidences an almost linear behavior. For method 3 the variance increases from 0.5 to 1.0 wt.% and then slightly decreases somewhat, while for method 4 variance decreases with increasing concentration. Contrariwise, Figure 4.6(b) shows that, with the exception of method 3, the variance decreases when the concentration increases from 1 to 3 wt.%. Therefore, a change in the length scale strongly influences the histograms and, hence, the variance curves.
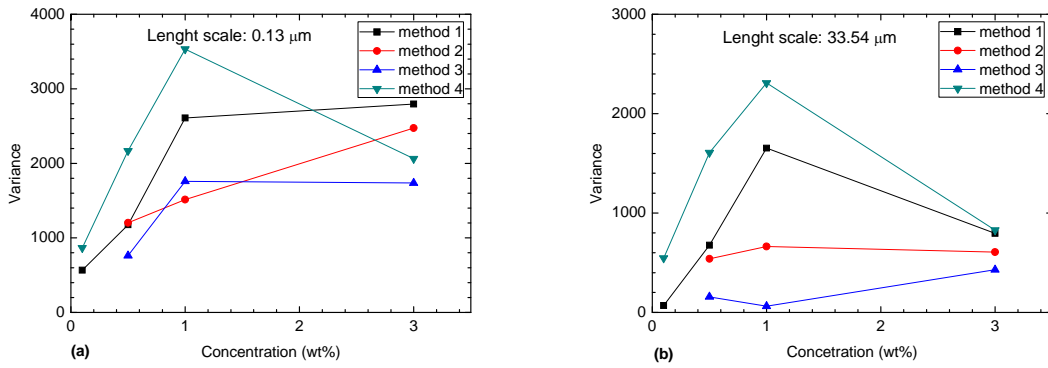
Figure 4. 6- Variance as a function of VGCNF concentration for all the methods with (a) 0.13 μm and (b) 33.54 μm of length scale.

4.3.2- Electrical measurements

The electrical measurements presented in Figure 4.7(a) and (b) consist of DC electrical current (I) versus voltage (V) and DC conductivity (σ) versus VGCNF concentration, respectively. The first shows the current measured as a function of the voltage applied to the electrodes of samples from method 2 with 0.5, 1.5 and 3.0 wt.%, as well as the neat sample (inset). The second refers to curves of DC conductivity as a function of VGCNF concentration for the four mixing methods.
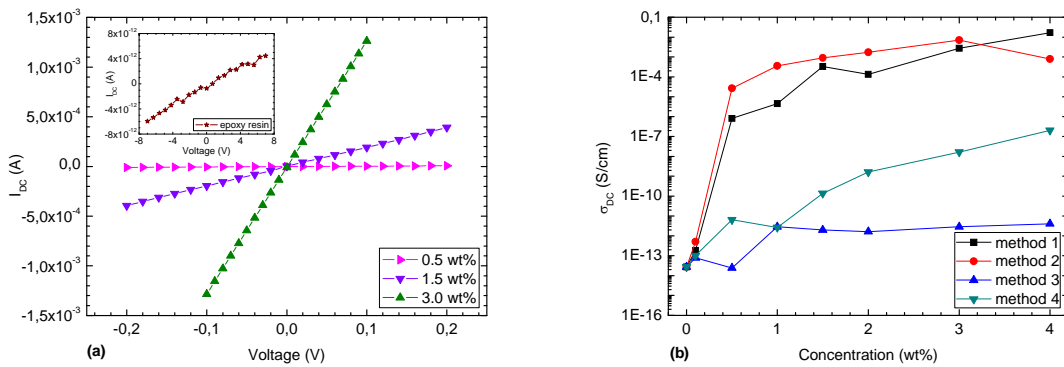
Figure 4. 7- DC measurements: (a) current versus voltage for samples from method 2, with different VGCNF concentrations and (b) conductivity versus VGCNF concentration for the four mixing methods.

Figure 4.7(a) indicates a linear relation between the measured current and the applied voltage for all samples. As expected, there is an increase of conductivity as the VGCNF content increases, as shown by the increased slope of the curves. The curves in Figure 4.7(b) show that, for the same VGCNF content, methods 1 and 2 generate higher values of conductivity than methods 3 and 4. In the case of method 3, the difference escalates with increasing VGCNF content. The behavior shown for methods 1 and 2 reveals a percolation threshold between 0.1 to 0.5 wt.% due to an increase in conductivity in seven and eight orders of magnitude, respectively. For the curve of method 3, the increase in conductivity is very small and almost independent of the VGCNF content. This can be explained within the scope of the network theory, by the formation of a capacitor network [43, 44].Although in the case of method 4 the increase in conductivity is considerably higher, no percolation threshold was found [27].

4.4- Discussion

The greyscale analysis utilized in this work is able to quantify and differentiate the dispersion levels of VGCNF in the epoxy resin for samples prepared by four mixing methods entailing different residence times, velocity patterns and stress levels. Three roll milling seems to be the most effective method to disperse the VGCNF in the epoxy resin, as inferred from the micrographs and histograms of Figure 4.3 and the variance graphs of Figure 4.4(b). The plots of variance versus length scale (Figure 4.4) show that the better the VGCNF are dispersed in the sample, the bigger the changes of the variance with the increase of the length scale. Figure 4.4(a) quantifies the dispersion of samples produced by method 1 with different filler concentrations and confirms that dispersion decreases as concentration increases. The greyscale analysis performed on samples from methods 1 and 2 demonstrates that the two methods create similar dispersion levels regardless of the concentration. This is confirmed both qualitatively and quantitatively, by analyzing the corresponding micrographs and histograms presented in Figure 4.3 and the variance diagram of Figure 4.4(b).

From the analysis of the histograms, micrographs and plots of Figure 4.5, it can be concluded that the dispersion of VGCNF is uniform throughout the entire volume of the sample. Probably, this is extensive to all samples from all methods.

With respect to the electrical response, the I-V characteristic curves are linear and the percolation threshold for samples from methods 1 and 2 ranges between 0.1 and 0.5 wt.%[27]. This linearity is observed both below and above the percolation threshold, though non-linearities are sometimes observed regarding internal field emission associated with various tunneling processes between isolated conducting clusters [45].

The conductivity performance as a function of the dispersion method presented in Figure 4.7(right) and the analysis performed in [27] show that the dispersion method strongly influences the overall composite electrical response [25, 26]. It can be suggested that the mechanism of electrical conductivity of samples from methods 1 and 2 as well as of samples with high concentrations from method 4, is dominated by hopping between the nearest VGCNF, giving rise to a weak disorder regime. For samples from method 3 and lower concentrations from method 4, the mechanism is the development of a capacitive network.

A comparative analysis of the curves in Figure 4.6 and Figure 4.7(b) indicates that there is no direct correlation between variance and DC conductivity. The DC conductivity curves for the blender and capillary rheometer samples show a similar behavior, while the variance curves of these methods are distinct with respect to the concentration variation. The DC conductivity curves for the samples from 3 roll milling and planetary centrifuge mixing methods are different from the corresponding variance curves. In the same way, no correlation could be found between the maximum achieved conductivity at a given concentration and the dispersion level obtained. In general, it can be concluded that the method of quantification of dispersion adopted here provides reliable comparisons at length scales that might be relevant to discuss certain characteristics and properties of the nanocomposites, but cannot be used to provide insights into the electrical conductivity of these materials.

4.5- Conclusions

VGCNF/epoxy composites have been prepared by different mixing methods including blender mixing, capillary rheometer mixing, 3 roll milling and planetary centrifugal mixing. TOM and greyscale analyses were used to quantitatively analyze the corresponding dispersion achieved, based on the calculation and comparison of the variance. It could be concluded that the best dispersion was obtained by the 3 roll

milling method and that the proposed dispersion assessment method allows an effective quantification of dispersion at a lower resolution level of 0.13 μm. However, the quantification of dispersion at this level is not sufficiently detailed to gain an insight on the electrical response of the materials.

The composites prepared using either the blender or the capillary rheometer show higher DC conductivity than those prepared by the 3 roll mill and planetary centrifugal mixing methods. It is interesting to note that the higher values of the DC conductivity are for the samples with better nanofiber distribution instead of better dispersion.

References

1.   Kuilla, T., et al., Recent advances in graphene based polymer composites. Progress in Polymer Science, 2010. 35(11): p. 1350-1375.

2.   Sharma, A., C.E. Bakis, and K.W. Wang, A new method of chaining carbon nanofibers in epoxy. Nanotechnology, 2008. 19(32): p. 5.

3.   Al-Saleh, M.H. and U. Sundararaj, A review of vapor grown carbon nanofiber/polymer conductive composites. Carbon, 2009. 47(1): p. 2-22.

4.   Tibbetts, G.G., et al., A review of the fabrication and properties of vapor-grown carbon nanofiber/polymer composites. Composites Science and Technology, 2007. 67(7-8): p. 1709-1718.

5.   Stankovich, S., et al., Graphene-based composite materials. Nature, 2006. 442(7100): p. 282-286.

6.   Šupová, M., G.S. Martynková, and K. Barabaszová, Effect of Nanofillers Dispersion in Polymer Matrices: A Review. Science of Advanced Materials, 2011. 3(1): p. 1-25.

7.   Coleman, J.N., et al., Small but strong: A review of the mechanical properties of carbon nanotube-polymer composites. Carbon, 2006. 44(9): p. 1624-1652.

8.   Manchado, M.A.L., et al., Thermal and mechanical properties of single-walled carbon nanotubes–polypropylene composites prepared by melt processing. Carbon, 2005. 43(7): p. 1499-1505.

9.   Garg, P., et al., Effect of dispersion conditions on the mechanical properties of multi-walled carbon nanotubes based epoxy resin composites. Journal of Polymer Research, 2011. 18(6): p. 1397-1407.

10.   Rao, Y., A. Takahashi, and C.P. Wong, Di-block copolymer surfactant study to optimize filler dispersion in high dielectric constant polymer-ceramic composite. Composites Part A: Applied Science and Manufacturing, 2003. 34(11): p. 1113-1116.

11.   Khastgir, D. and K. Adachi, Rheological and dielectric studies of aggregation of barium titanate particles suspended in polydimethylsiloxane. Polymer, 2000. 41(16): p. 6403-6413.

12. Choi, Y.-K., et al., Mechanical and physical properties of epoxy composites reinforced by vapor grown carbon nanofibers. Carbon, 2005. 43(10): p. 2199-2208.

13. Sandler, J.S., M. S. P. Prasse, T. Bauhofer, W. Schulte, K. Windle, A. H., Development of a dispersion process for carbon nanotubes in an epoxy matrix and the resulting electrical properties. Polymer, 1999. 40(21): p. 5967-5971.

14. Andrews, R., et al., Fabrication of Carbon Multiwall Nanotube/Polymer Composites by Shear Mixing. Macromolecular Materials and Engineering, 2002. 287(6): p. 395-403.

15. Schueler, R., et al., Agglomeration and electrical percolation behavior of carbon black dispersed in epoxy resin. Journal of Applied Polymer Science, 1997. 63(13): p. 1741-1746.

16. Jimenez, G.A. and S.C. Jana, Electrically conductive polymer nanocomposites of polymethylmethacrylate and carbon nanofibers prepared by chaotic mixing. Composites Part A: Applied Science and Manufacturing, 2007. 38(3): p. 983-993.

17. Okamoto, M., S. Morita, and T. Kotaka, Dispersed structure and ionic conductivity of smectic clay/polymer nanocomposites. Polymer, 2001. 42(6): p. 2685-2688.

18. Guo, Z., et al., Fabrication and characterization of iron oxide nanoparticles reinforced vinyl-ester resin nanocomposites. Composites Science and Technology, 2008. 68(6): p. 1513-1520.

19. Imai, Y., et al., Transparent poly(bisphenol A carbonate)-based nanocomposites with high refractive index nanoparticles. European Polymer Journal, 2009. 45(3): p. 630-638.

20. Essawy, H.A., N.A. Abd El-Wahab, and M.A. Abd El-Ghaffar, PVC–laponite nanocomposites: Enhanced resistance to UV radiation. Polymer Degradation and Stability, 2008. 93(8): p. 1472-1478.

21. Dasari, A., et al., Clay exfoliation and organic modification on wear of nylon 6 nanocomposites processed by different routes. Composites Science and Technology, 2005. 65(15-16): p. 2314-2328.

22. Bocchini, S., et al., Influence of nanodispersed hydrotalcite on polypropylene photooxidation. European Polymer Journal, 2008. 44(11): p. 3473-3481.

23. Adhikari, A. and K. Lozano, Effects of carbon nanofibers on the crystallization kinetics of polyethylene oxide. Journal of Polymer Research, 2011. 18(5): p. 875-880.

24. Cardoso, P., et al., The dominant role of tunneling in the conductivity of carbon nanofiber-epoxy composites. Physica Status Solidi a-Applications and Materials Science, 2010. 207(2): p. 407-410.

25. Cardoso, P., et al., The influence of the dispersion method on the electrical properties of vapor-grown carbon nanofiber/epoxy composites. Nanoscale Res Lett, 2011. 6(1): p. 370-370.

26. Aguilar, J.O., J.R. Bautista-Quijano, and F. Avilés, Influence of carbon nanotube clustering on the electrical conductivity of polymer composite films. eXPRESS Polymer Letters, 2010. 4(5): p. 292–299.

27. Cardoso, P., et al., The role of disorder on the AC and DC electrical conductivity of vapour grown carbon nanofibre/epoxy composites. Composites Science and Technology, 2012. 72(2): p. 243–247.

28. Tibbetts, G.G. and J.J. McHugh, Mechanical properties of vapor-grown carbon fiber composites with thermoplastic matrices. Journal of Materials Research, 1999. 14: p. 2871-2880.

29. Hattum, F.W.J.v., et al., PROCESSING AND PROPERTIES OF CARBON NANOFIBER / THERMOPLASTIC COMPOSITES, in SAMPE 2004. 2004: Long Beach, CA, USA. p. 7.

30. Zeng, J., et al., Processing and properties of poly(methyl methacrylate)/carbon nano fiber composites. Composites Part B: Engineering, 2004. 35(2): p. 173-178.

31. Patton, R.D.P., Jr C. U. Wang, L. Hill, J. R., Vapor grown carbon fiber composites with epoxy and poly(phenylene sulfide) matrices Composites Part A: Applied Science and Manufacturing, 1999. 30(9): p. 1081-1091.

32. Chyi-Shan, W. and A.M. D, Method of forming conductive polymeric nanocomposite materials, O. University of Dayton (Dayton, Editor. 2004.

33. Rice, B.P., T. Gibson, and K. Lafdi. DEVELOPMENT OF MULTIFUNCTIONAL ADVANCED COMPOSITES USING A VGNF ENHANCED MATRIX. in 49th International SAMPE symposium proceedings. 2004. Long Beach.

34. Peter, T.L. and et al., A quantitative assessment of carbon nanotube dispersion in polymer matrices. Nanotechnology, 2009. 20(32): p. 7.

35. Xie, S., et al., Quantitative characterization of clay dispersion in polypropylene-clay nanocomposites by combined transmission electron microscopy and optical microscopy. Materials Letters, 2010. 64(2): p. 185-188.

36. Gershon, A., et al., Nanomechanical characterization of dispersion and its effects in nano-enhanced polymers and polymer composites. Journal of Materials Science, 2010. 45(23): p. 6353-6364.

37. Kumar, S.K. and R. Krishnamoorti, Nanocomposites: Structure, Phase Behavior, and Properties, in Annual Review of Chemical and Biomolecular Engineering, Vol 1, J.M. Prausnitz, M.F. Doherty, and M.A. Segalman, Editors. 2010, Annual Reviews: Palo Alto. p. 37-58.

38. Spowart, J.E.M., B. Miracle, D. B., Multi-scale characterization of spatially heterogeneous systems: implications for discontinuously reinforced metal-matrix composite microstructures. Materials Science and Engineering: A, 2001. 307(1-2): p. 51-66.

39. Hattum, F.v., et al. Quantitative assessement of mixing quality in nanoreinforced polymers using a multi-scale image analysis method. in 38th ISTC. 2006. Dallas, Texas.

40. Leer-Lake, C. and e. al., Quantifying Dispersion in Carbon Nano Materials Composites by Grey Scale Analysis. submitted to Comp. Sci. Techn., 2012.

41. Paiva, M. and J.Covas et. al. The influence of extensional flow on the dispersion of functionalized carbon nanofibers in a polymer matrix. in Proc ChemOnTubes. 2008. Zaragoza:

   digital.csic.es/.../ChemOnTubes2008_Book%20of%20Abstracts.pdf, pag 126.

42. Novais, R.M., J.A. Covas, and M.C. Paiva, The effects of flow type and chemical functionalization on the dispersion of carbon nanofibers in polypropylene. submitted to Composites Part A, 2012.

43. Simoes, R. and et al., Low percolation transitions in carbon nanotube networks dispersed in a polymer matrix: dielectric properties, simulations and experiments Nanotechnology, 2009. 20(3): p. 8.

44.   Simoes, R., et al., Influence of fiber aspect ratio and orientation on the dielectric properties of polymer-based nanocomposites. Journal of Materials Science, 2010. 45(1): p. 268-270.

45.   He, L. and S.-C. Tjong, Nonlinear electrical conduction in percolating systems induced by internal field emission. Synthetic Metals, 2011. 161(5-6): p. 540-543.

5. The role of disorder on the AC and DC electrical conductivity of vapor grown carbon nanofiber/epoxy composites

Four dispersion methods were used for the preparation of VGCNF/epoxy composites. It is shown that each method induces certain levels of VGCNF dispersion and distribution within the matrix, and that these have a strong influence on the composite electrical properties. A homogenous VGCNF dispersion does not necessarily imply higher electrical conductivity. In fact, it is concluded that the presence of well distributed fibers, rather than a fine dispersion, is more important for achieving larger conductivities for a given VGCNF concentration. It is also found that the conductivity can be described by a weak disorder regime.

5.1- Introduction

Epoxy resins have a wide range of applications in materials science and engineering [1]. By incorporating high aspect ratio fillers like CNT [2] or VGCNF [3], the epoxy mechanical and electrical properties are enhanced and the range of applications is extended. The VGCNF electrical and mechanical properties are relatively lower than those obtained with CNT but, on the other hand, they typically are more cost-efficient and are readily available in large quantities with consistent quality [3]. VGCNF can be prepared with diameters in the nanometer range, resulting in high aspect ratios [4-6].

The focus of recent research related to VGCNF/epoxy composites has been on the development of processing methods able to generate a homogenous dispersion of the VGCNF within the polymer matrix. For instance, Allaoui *et.al.*[7] prepared VGCNF/epoxy composites using a combination of ultrasonication and mechanical mixing, concluding that the composite conductivity can be attributed to the formation of a tunneling network with a low percolation threshold (0.064 wt.%). In fact, one of the earlier works with VGCNF/epoxy [8] revealed, by dispersing the VGCNF via acetone solvent/epoxy solution and mixing, that the degree of VGCNF dispersion is relevant for the composite mechanical strength.The mechanical properties of VGCNF/epoxy composites were also studied by Zhou *et. al.*[9], who investigated the effect of loading on the thermal and mechanical properties of the composites, using high-intensity ultrasonication to disperse the VGCNF. The effect on the composite's mechanical, thermal, and electric properties of preparation methods involving heat treatment of the fibers was also reported by Lafdi *et. al.*[10]. In turn, Prasse *et. al.*[11] used sonication and conventional stirring to disperse the VGCNF. Anisotropy has an effect on the electrical properties: composites with VGCNF preferentially parallel to the electric field show lower electrical resistance and higher dielectric constant [12]. This effect can be explained by the formation of a capacitor network, as demonstrated by Simões *et. al.*[12, 13] for CNT/polymer composites. Furthermore, studies of systems such as VGCNF/poly(vinylidene fluoride) showed that the characteristics of the matrix, such as crystallinity or phase type, also influence the type of conduction mechanism in VGCNF/polymer composites [14].

In a previous work [15], the electrical properties of VGCNF/epoxy composites prepared by simple hand mixing were studied, and it was confirmed that the conductivity is due to the formation of a tunneling network. Although the homogenous dispersion of VGCNF in the matrix is important for the mechanical properties, a good distribution seems to be more significant for the electrical properties, as discussed in [15]. By exploring different methods for dispersing the VGCNF, the present work demonstrates that, for a given concentration, a good VGCNF distribution indeed produces higher electrical conductivity than a highly dispersion level.

5.2- Experimental

The VGCNF Pyrograf III^{TM} PR-19-LHT-XT were supplied by ASI. Epoxy resin Epikote^{TM} Resin 862 and curing agent Ethacure 100 Curative were supplied by Albemarle. Samples with Epon Resin 862 from Hexion Specialty Chemicals and Epikure W from Resolution Performance Products, as a curing agent, were also used. The two types of resins and curing agents share the same CAS. The weight ratio of resin to curing agent was 100:26.4. The dispersion of the VGCNF in the epoxy resin was achieved by four different methods: Method 1: mixing with a Haeger blender for two minutes [15], the velocity field and stress levels should generate a predominantly distributive mixing; Method 2: four-pass extrusion through a Capillary Rheometer fitted with a series of pairs of rings with alternate high and low diameters (8 and 2 mm, respectively) [16], which generate converging-diverging flows with strong extensional fields (thus, good distribution but limited dispersion are anticipated); Method 3: roll milling (using a Lehmann 3 roll miller) for 5 minutes, forcing the material through a gap of 25.4 μm, which is expected to result in good dispersion and relatively good distribution; Method 4: using a planetary-type Thinky ARE-250 mixer for 10 minutes, at simultaneous revolution and rotation speeds of 2000 rpm and 800 rpm, respectively, being that these conditions should induce a good distribution. For each pre-mixture, the corresponding amount of curing agent was added and hand mixed during 2 minutes [15]. After mixing, all samples were degassed at a 20 mbar absolute pressure during 10 minutes, then cast into a rectangular mold (1 x 10 x 70 mm) and cured at 80 °C and 150 °C for 90 minutes at each stage. Composites with seven VGCNF concentrations in epoxy resin (from 0.1 to 4.0 wt.%) were prepared, as well as neat resin samples.

VGCNF dispersion and distribution in the matrix was evaluated by observing surface and cross section imageswith a SEM Phillips X230 FEG. The DC volume electrical resistivity was measured at room temperature with a Keithley 487 picoammeter/voltage source. The capacity and tan(δ) (dielectric loss) were measured at room temperature in the range of 500 Hz to 1 MHz with an applied signal of 0.5 V, using an automatic Quadtech 1929 Precision LCR meter and the A.C. electrical conductivity was calculated from the data. For the electrical measurements, the samples were coated on both sides, in the thickness direction, by thermal evaporation with 5 mm diameter Al electrodes.

5.3- Results

Figure 5.1 represents the log-log plot of conductivity versus frequency for the samples produced with the different dispersion methods. Based on this data, method 1 produced a percolation threshold between 6E-4 and 3E-3 volume fraction and conductivity independent of frequency for volume fractions higher than the percolation threshold. Method II induces a percolation threshold similar to that of Method I and the same independence of conductivity relative to frequency. In contrast, a percolation threshold cannot be identified for Method III, while the conductivity follows a power law with respect to the frequency for all volume fractions. Similarly, no percolation threshold was found for Method IV and, as for Method III, a power law relates well the conductivity to the frequency.
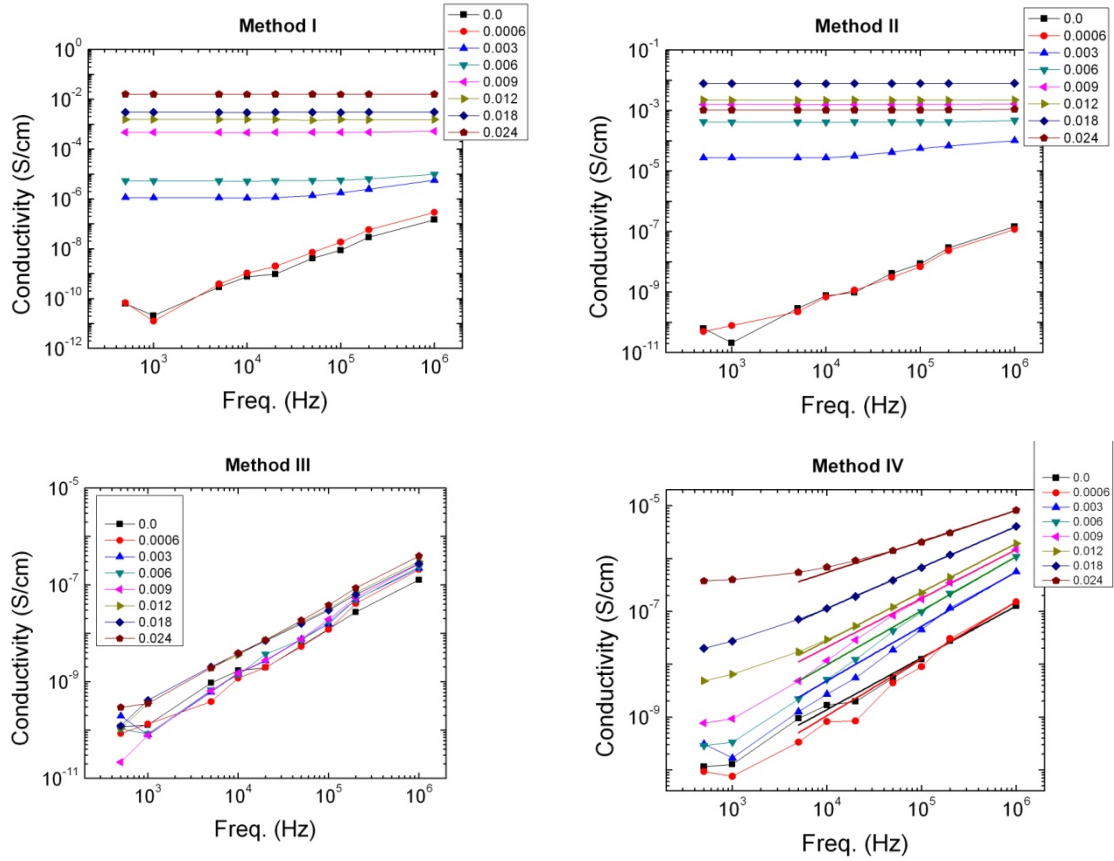
Figure 5. 1- Log-log plot of conductivity versus frequency for the different dispersion methods and composites. The straight bold lines in Method IV are fits to a power law with $R^2 \approx 0.99$.

In order to assess the effect of the different dispersion methods on the composite conductivity, the latter (at 1 kHz) was plotted as a function of the VGCNF volume fraction for the different methods in Figure 5.2. In the samples prepared by Methods I and II, the AC conductivity shows an increase of five and six orders of magnitude for volume fractions of 6E-4 and 3E-3, respectively (Figure 5.2 left). Moreover, the same samples also reveal a strong increase in the DC conductivity of 6 and 8 orders of magnitude respectively, at similar volume fractions (Figure 5.2, right). In fact, the highest conductivity values are achieved with these two methods. When using Method III to disperse the VGCNF, both the AC and DC conductivities are very low and almost independent of the volume fraction. This behavior will be related later to the formation of a capacitive network [12, 13]. In the case of Method IV, the composites conductivity (AC and DC) shows a slight increase with volume fraction, but the highest value is only three orders of magnitude higher than the AC conductivity and seven orders of

magnitude higher than the DC conductivity of the epoxy resin, respectively. Furthermore, no percolation threshold was found.
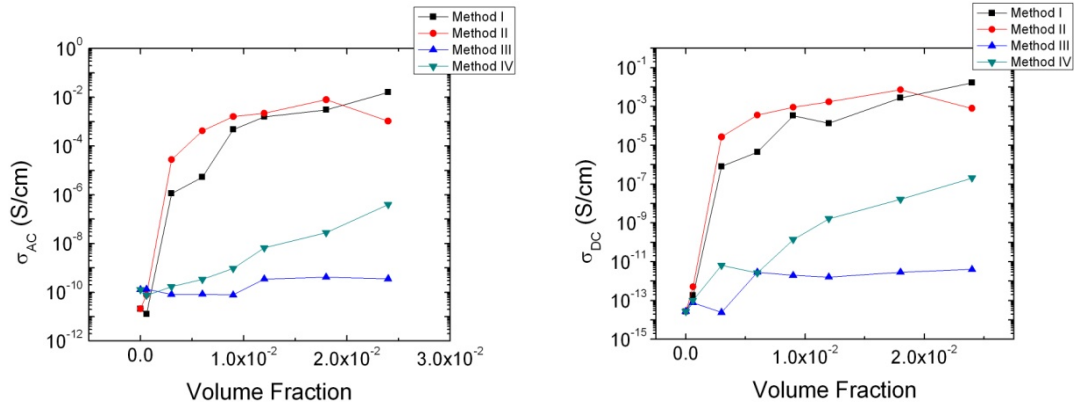
Figure 5. 2- Log-linear plot of conductivity versus volume fraction for the different dispersion methods. Left: AC conductivity (1 kHz), right: DC conductivity.

In view of the above, it is clear that the processing conditions (more specifically, the dispersion method), strongly influence the overall composite electrical response. The actual level of VGCNF distribution and dispersion in the matrix achieved in each case was estimated from SEM images (Figure 5.3). Methods I and II seem to have produced composites with some degree of agglomeration of the nanofibers, but with a relatively good cluster distribution (Figure 5.3, top left and top right). Method III yields apparently a homogeneous VGCNF dispersion (Figure 5.3, bottom left). Conversely, Method IV produces better VGCNF dispersion than methods I and II but with worst cluster dispersion (Figure 5.3, bottom right). The larger clusters are hollow, with the matrix clearly visible in their interior.

Method I: Blender
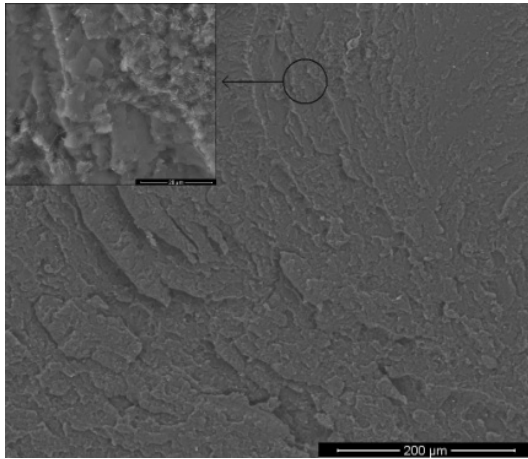
Method II: Converging-diverging flows
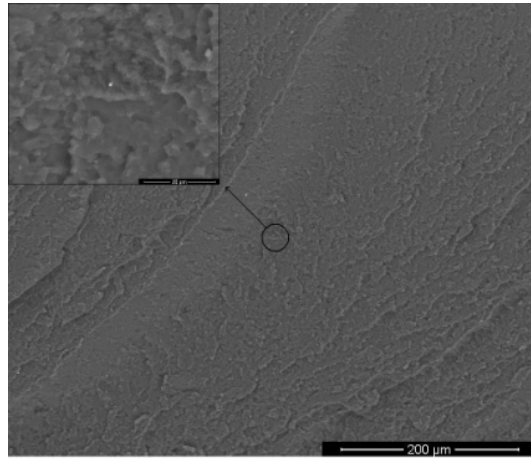
Method III: Roll milling
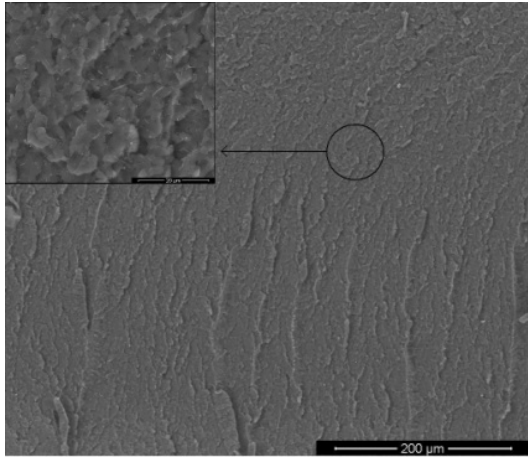
Method IV: Planetary mixer
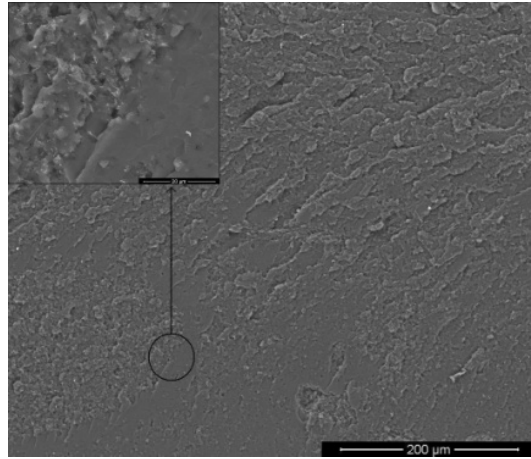
Figure 5. 3- SEM images of sample cross-sections for the 0.018 volume fraction composite prepared with the four different mixing methods.

5.4- Discussion

As demonstrated in Figure 5.1, for Methods III and IV the composite conductivity as a function of frequency follows a power law. This type of behavior is usually explained in the framework of the percolation theory [17, 18], which predicts that $\sigma_{AC} \propto \omega^{\beta}$, where β is a critical exponent that depends only on the system dimension. The typical value of β obtained from numerical simulations of random resistor networks is ≈ 0.73 [18]. The results presented in Figure 5.1 show that $0.94 \leq \beta \leq 1.1$ for Method III and $0.78 \leq \beta \leq 1.03$ for Method IV. Thus, these values are not only in disagreement with the expected theoretical one, but they are not unique, as

predicted by the percolation theory. In addition to the dependency of conductivity on frequency, the percolation theory also predicts an exponential relationship between conductivity and volume fraction:

$$\sigma \propto \sigma_0 \left(\Phi - \Phi_c \right)^t, \text{ for } \Phi > \Phi_c, \qquad (5.1)$$

The universal critical exponent t depends only on the system dimension, Φ is the volume fraction and Φ_c is the critical concentration at which an infinite cluster appears. For $\Phi > \Phi_c$ a cluster spans the system, whereas for $\Phi < \Phi_c$ the system contains many small clusters. Fits of equation (5.1) to the data of Figure 5.2 were inconclusive. For fibers with a capped cylinder shape, the theoretical framework developed by Celzard [19], based on the Balberg model [20], provides the bounds for the percolation threshold. In general, the percolation threshold is defined within the following bounds:

$$1 - e^{\frac{-1.4V}{\langle V_e \rangle}} \leq \Phi_c \leq 1 - e^{\frac{-2.8V}{\langle V_e \rangle}} \qquad (5.2)$$

Equation (5.2) links the average excluded volume, $\langle V_e \rangle$, i.e., the volume around an object in which the centre of another similarly shaped object is not allowed to penetrate, averaged over the orientation distribution, with the critical concentration (Φ_c), where 1.4 corresponds to the lower limit, i.e., infinitely thin cylinders, while 2.8 corresponds to spheres. These values were obtained by simulation. Using the values provided by the manufacturer of the VGCNF used in this work [4], equation (5.2) predicts the bounds *2E-3 ≤ Φc ≤ 3E-3* for an average aspect ratio of 433. The Φ_c found in this work for Methods I and II (*6E-4 <Φc< 3E-3*) includes the predictions of the theory, with exception of the upper bound. This indicates that a network is formed, but it does not necessarily imply a physical contact between the VGCNF. It has previously been shown [21] that the range *0.8 < β <1.0* is characteristic of hopping in a disorder material. Through the application of the network theory to VGCNF composites, namely by mapping fillers to vertices and edges to the gaps between fillers, a formula relating the composite conductance to the network disorder has been deduced [22]:

$$G_{eff} = G_{cut} \exp\left(\frac{-l_{opt}}{(N_{max}\Phi)^{\frac{1}{3}}}\right) \qquad (5.3)$$

In this equation, l_{opt} is the length of the optimal path that is the single path for which the sum of the weights along the path is the minimum. When most of the links of the path contribute to the sum, the system is said to be in the "weak disorder" regime [23]. Conversely, the situation where a single link dominates the sum along the path is called the strong disorder limit [23]. In equation (5.3), N_{max} is the maximum number of fillers in the domain and G_{cut} is the effective conductance of the system before a bond with maximum conductance is added to (or removed from) the system [23]. The l_{opt} parameter is related to the disorder strength when the system is in the weak disorder regime. At the weak disorder regime the disorder strength is just the inverse of the scale over which the wave function decays in the polymer (x_0), as expressed by the hopping conductivity equation at room temperature [24, 25]:

$$\sigma_{ij} = \sigma_0 \exp\left(-\frac{x_{ij}}{x_0}\right) \qquad (5.4)$$

In Equation (5.4), σ_0 is the dimension coefficient and x_{ij} is the distance between two fillers. As described in [22], applying Equation (5.4) to the gap between the fillers (described as the minimum distance between two rods), and thus defining the conductivity by hopping between adjacent fillers, results in Equation (5.3). As stated before, the range $0.8 < \beta < 1.0$ is characteristic of hopping in a disordered material [21]. This agrees well with recent results [22], which demonstrate that hopping between adjacent fillers gives rise to the expression $\log(\sigma) \propto \Phi^{-\frac{1}{3}}$, as given by equation (5.3), which corresponds to a weak disorder regime. This relation is also found in fluctuation-induction tunneling [26] for the DC conductivity. In order to prove the latter assumptions, the $\log(\sigma) \propto \Phi^{-\frac{1}{3}}$ dependence was tested for the composite AC conductivity at 1 kHz (Figure 5.4, left), and for the DC measurements (Figure 5.4, right).
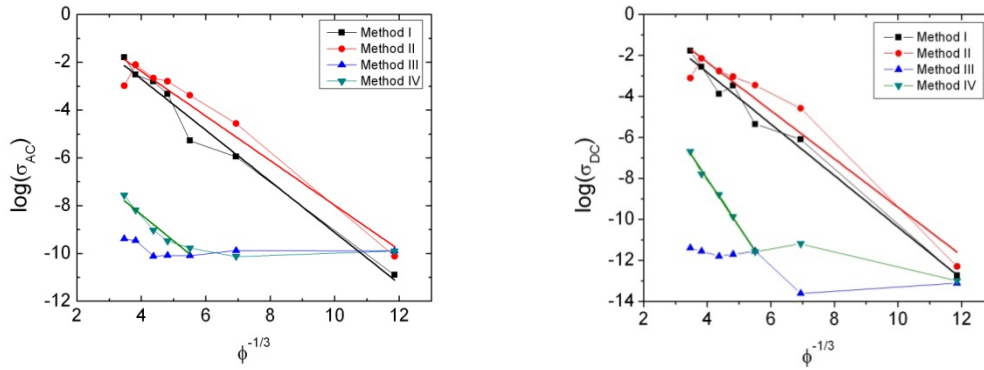
Figure 5. 4- Left: Logarithm of the AC conductivity at 1 kHz versus volume fraction for the different mixing Methods. The thick lines are linear fits to the data where $R^2 \approx [0.97, 0.95, 0.91]$. Right: Logarithm of the DC conductivity versus volume fraction for the different methods. The thick lines are linear fits to the data where $R^2 \approx [0.98, 0.92, 0.99]$.

As can be observed in Figure 5.4, there is a linear relation between the logarithm of the conductivity and the volume fraction for Methods I and II. This indicates that the composite conductivity is in the weak disorder regime [22]. On the other hand, the data for Method IV shows the same linear behavior, the $\log(\sigma) \propto \Phi^{-\frac{1}{3}}$ dependence, but only for the higher volume fractions and deviating for the lower volume fractions. This deviation from the linear relation can be described by equation (5.3), when the conductive network is not yet formed, which implies that $G_{eff} = G_{cutt}$ [22], i.e., the effective conductance is controlled by the matrix conductance. This fact indicates that the network is only formed by capacitors in lower volume fractions and the matrix dominates the overall conductivity.

Hopping between nearest fillers explains the deviation from the percolation theory; the overall composite conductivity is explained by the existence of a weak disorder regime. The formation of a capacitor network [13], where the plates of each capacitor are VGCNF pairs, explains the deviation from the expected linear relation between the logarithm of the conductivity and volume fraction, as predicted by the weak disorder regime. It is also associated to the better filler dispersion, characteristic of Methods III and IV, as demonstrated by SEM images (Figure 5.3). On the other hand, a good dispersion of the clusters, characteristic of Methods I and II, results in better conductive properties. In [15] it was speculated that a good nanofiller distribution would

result in improved conductive properties. This point of view was theoretically supported in [22]. From the present work, it is possible to conclude that indeed good cluster dispersion (nanofiller distribution) will enhance the nanocomposite conductivity.

5.5- Conclusions

Four dispersion methods were used for the preparation of VGCNF/epoxy composites. It was shown that each method induces a certain level of VGCNF dispersion and distribution in the matrix, and that these have a strong influence on the composite electrical properties. A homogenous VGCNF dispersion does not necessarily imply higher electrical conductivity, in contrast with mechanical properties, where a good distribution of the fillers results in better overall mechanical properties. In fact, it was concluded that the presence of well dispersed clusters is more important for achieving higher electrical conductivity. It was also found that the conductivity of well dispersed clusters can be described by hopping between nearest fillers, giving rise to a weak disorder regime.

These results provide important insights into the usefulness of each method for specific applications. More importantly, they improve our understanding of the relationships between VGCNF dispersion and electrical properties, which is a vital step to pave the way for further research into tailoring the properties of these nanocomposites for specific applications.

References

1.   May, C.A. and G.Y. Tanaka, Epoxy Resins Chemistry and Technology, ed. M. Dekker. 1987, New York, USA.

2.   Moniruzzaman, M. and K.I. Winey, Polymer Nanocomposites Containing Carbon Nanotubes. Macromolecules, 2006. **39**(16): p. 5194-5205.

3.   Al-Saleh, M.H. and U. Sundararaj, A review of vapor grown carbon nanofiber/polymer conductive composites. Carbon, 2009. **47**(1): p. 2-22.

4.   ASI. Applied Sciences Inc.; Available from: http://www.apsci. com/ppi-pyro3.html.

5.   Miyagawa, H., M.J. Rich, and L.T. Drzal, Thermo-physical properties of epoxy nanocomposites reinforced by carbon nanotubes and vapor grown carbon fibers. Thermochimica Acta, 2006. **442**(1-2): p. 67-73.

6.   Uchida, T., et al., Morphology and modulus of vapor grown carbon nano fibers. Journal of Materials Science, 2006. **41**(18): p. 5851-5856.

7.   Allaoui, A., S.V. Hoa, and M.D. Pugh, The electronic transport properties and microstructure of carbon nanofiber/epoxy composites. Composites Science and Technology, 2008. **68**(2): p. 410-416.

8.   Patton, R.D.P., Jr C. U. Wang, L. Hill, J. R., Vapor grown carbon fiber composites with epoxy and poly(phenylene sulfide) matrices Composites Part A: Applied Science and Manufacturing, 1999. **30**(9): p. 1081-1091.

9.   Zhou, Y., F. Pervin, and S. Jeelani, Effect vapor grown carbon nanofiber on thermal and mechanical properties of epoxy. Journal of Materials Science, 2007. **42**(17): p. 7544-7553.

10.   Lafdi, K., et al., Effect of carbon nanofiber heat treatment on physical properties of polymeric nanocomposites: part I. J. Nanomaterials, 2007. **2007**(1): p. 1-6.

11.   Prasse, T., J.-Y. Cavaillé, and W. Bauhofer, Electric anisotropy of carbon nanofibre/epoxy resin composites due to electric field induced alignment. Composites Science and Technology, 2003. **63**(13): p. 1835-1841.

12.   Simoes, R., et al., Influence of fiber aspect ratio and orientation on the dielectric properties of polymer-based nanocomposites. Journal of Materials Science, 2010. **45**(1): p. 268-270.

13. Simoes, R. and et al., Low percolation transitions in carbon nanotube networks dispersed in a polymer matrix: dielectric properties, simulations and experiments Nanotechnology, 2009. **20**(3): p. 8.

14. Costa, P., et al., The effect of fibre concentration on the α to β-phase transformation, degree of crystallinity and electrical properties of vapour grown carbon nanofibre/poly(vinylidene fluoride) composites. Carbon, 2009. **47**(11): p. 2590-2599.

15. Cardoso, P., et al., The dominant role of tunneling in the conductivity of carbon nanofiber-epoxy composites. Physica Status Solidi a-Applications and Materials Science, 2010. **207**(2): p. 407-410.

16. Paiva, M. and J.C.e. al. The influence of extensional flow on the dispersion of functionalized carbon nanofibers in a polymer matrix. in Proc ChemOnTubes. 2008. Zaragoza:
digital.csic.es/.../ChemOnTubes2008_Book%20of%20Abstracts.pdf, pag 126.

17. Stauffer, D. and A. Aharony, eds. Introduction to percolation theory. 2nd edition ed., ed. T.a. Francis. 1991: London.

18. Bergman, D.J. and Y. Imry, Critical Behavior of the Complex Dielectric Constant near the Percolation Threshold of a Heterogeneous Material. Physical Review Letters, 1977. **39**(19): p. 1222-1225.

19. Celzard, A., et al., Critical concentration in percolating systems containing a high-aspect-ratio filler. Physical Review B, 1996. **53**(10): p. 6209.

20. Balberg, I., et al., Excluded volume and its relation to the onset of percolation. Physical Review B, 1984. **30**(7): p. 3933.

21. Dyre, J.C. and T.B. Schrøder, Universality of ac conduction in disordered solids. Reviews of Modern Physics, 2000. **72**(3): p. 873-892.

22. Silva, J. and et al., Applying complex network theory to the understanding of high-aspect-ratio carbon-filled composites. EPL (Europhysics Letters), 2011. **93**(3): p. 37005.

23. Sreenivasan, S., et al., Effect of disorder strength on optimal paths in complex networks. Physical Review E, 2004. **70**(4): p. 6.

24. Ambegaokar, V., B.I. Halperin, and J.S. Langer, Theory of hopping conductivity in disordered systems. Journal of Non-Crystalline Solids, 1972. **8-10**(0): p. 492-496.

25.   Miller, A. and E. Abrahams, Impurity Conduction at Low Concentrations. Physical Review, 1960. **120**(3): p. 745-755.

26.   Connor, M.T., et al., Broadband ac conductivity of conductor-polymer composites. Physical Review B, 1998. **57**(4): p. 2286–2294.

6. Effect of filler dispersion on the electromechanical response of epoxy/vapor grown carbon nanofiber composites

The piezoresistive response of epoxy/vapour grown carbon nanofiber composites prepared by four different dispersion methods achieving different dispersion levels has been investigated. The composite response was measured as a function of carbon nanofiber loading for the different dispersion methods. Strain sensing by variation of the electrical resistance was tested through 4-point bending experiments and the dependence of the gauge factor as a function of the deformation and velocity of deformation was calculated as well as the stability of the electrical response. The composites demonstrated an appropriate response for being used as a piezoresistive sensor. Specific findings were that the intrinsic piezoresistive response was only effective around the percolation threshold and that good cluster dispersion was more appropriate for a good piezoresistive response than a uniform dispersion of individual nanofibers. The applications limits of these materials for sensors applications are also addressed.

6.1- Introduction

Smart materials include solid-state transducers that have piezoelectric, pyroelectric, electrostrictive, magnetostrictive, piezoresistive or other sensing and actuating properties. Piezoelectric ceramics, electroactive polymers and shape memory alloys present a number of limitations that hinder their application in certain areas [1-3], such as the requirement of high voltage or high currents, brittleness (in the case of ceramic materials), or limited range of strain or actuation forces. Smart nanoscale materials may circumvent these limitations and represent a new route to generate and measure motion in devices and structures [4].

An emerging and attractive strain sensing method is self-sensing, i.e., the material itself is the sensor, no attachments or embedded components being needed. This is attractive because of its low cost, high durability, large sensing area and no loss of mechanical performances. The ability of structural materials to sense their own strain has been reported for carbon fiber polymer–matrix composites [4].

Carbon nanotubes and nanofibers are commonly available and synthesized using commercial CVD techniques. The main types of carbonaceous fillers used for smart materials applications are SWCNT, MWCNT and CNF. It has been shown that by incorporating these high aspect ratio fillers, the mechanical and electrical properties of epoxy are enhanced and the range of applications extended [5]. Thermoset matrix systems loaded with very small volume contents of conductive nanofillers exhibit interesting piezoresistive properties, enabling the electrical measurement of mechanical deformation of the composite specimen [1].

In one of the first studies on this topic using epoxy composites with carbon black and short graphite fibers as fillers, Carmona et al [6] reported that the relationship between the relative resistance change and pressure depends only on the nature of the latter, suggesting that the components of the composite do not need to exhibit intrinsic piezoresistive properties. In this way, the study of piezoresistance will simultaneously allow the development of smart sensors and establishment of quantitative information about the conduction mechanisms [7]. It has been demonstrated that the electrical properties of VGCNF/epoxy composites strongly depend on the dispersion method [8], as a homogenous VGCNF dispersion does not necessarily imply higher electrical conductivity. In fact, the presence of well-distributed nanofiber clusters seems to be the

key parameter for increasing electrical conductivity. The piezoresistive mechanism is usually explained in terms of variations in the tunneling resistance and in the nature of the percolation network when a strain occurs. The slightly non-linear response of resistance to strain decreases in sensitivity for concentrations above the percolation threshold [9].

In the present work, the effect of the preparation method of epoxy/VGCNF composites on the piezoresistive response is investigated. The methods used generate systems with different filler dispersion and distribution levels, thus providing the opportunity to correlate mixing with sensing. This investigation represents a step forward in the understanding and potential industrialization of epoxy nanocomposite based self-sensing materials.

6.2- Experimental

6.2.1- Materials and processing conditions

The VGCNF Pyrograf III™ PR-19-LHT-XT were supplied by ASI, while epoxy resin Epikote™ Resin 862 and curing agent Ethacure 100 Curative were supplied by Albemarle. Samples with Epon Resin 862 from Hexion Specialty Chemicals and Epikure W from Resolution Performance Products, as a curing agent, were also used. The two types of resins and curing agents share the same CAS. The weight ratio of resin to curing agent was 100:26.4. Eight different concentrations of VGCNF varying from 0 to 4.0 wt.% in the epoxy resin and hardener were prepared. The corresponding amount of curing agent was added to each of the pre-mixes and mixed by hand during two minutes. The dispersion of the VGCNF in the epoxy resin was achieved by four different methods:

Method I: mixing with a Haeger blender for 2 min, the velocity field and stress levels should generate a predominantly distributive mixing;

Method II: four-pass extrusion through a Capillary Rheometer fitted with a series of pairs of rings with alternate high and low diameters (8 and 2 mm, respectively), which generate converging–diverging flows with strong extensional fields;

Method III: roll milling (using a Lehmann 3 roll miller) for 5 min, forcing the material through a gap of 25.4 μm, which is expected to result in good dispersion and relatively good distribution;

Method IV: using a planetary-type Thinky ARE-250 mixer for 10 min, at simultaneous revolution and rotation speeds of 2000 rpm and 800 rpm, respectively.

For each pre-mixture, the corresponding amount of curing agent was added and hand mixed during 2 min. After mixing, all samples were degassed at a 20 mbar absolute pressure during 10 min, then cast into a rectangular mold (1x10x70 mm) and cured at 80 ºC and 150 ºC for 90 min at each stage. Composites with seven VGCNF concentrations in epoxy resin (from 0.1 to 4.0 wt.%) were prepared, as well as neat resin samples.

6.2.2- Morphological and thermal characterization

VGCNF dispersion in the polymer was observed by cross section images of samples with 1.0 wt.% from the four methods, taken with a SEM Phillips X230 FEG scanning electron microscope.

DSC studies were performed using a Perkin-Elmer Diamond DSC apparatus in order to assess the glass transition of the epoxy resin and to correlate it with the temperature dependence of the electromechanical response. During the DSC analysis the samples were ramped from 20 °C to 200 °C under a dry N_2 environment at a rate of 10 °C/min, then maintained at isothermal conditions for 10 minutes at 200 °C and cooled at a rate of 10 °C/min to 20 °C.

6.2.3- Electrical conductivity measurement

The DC electrical resistance was measured at room temperature with a Keithley 487 picoammeter/voltage source. Circular Au electrodes (diameter of 5 mm) were deposited by magnetron sputtering onto the top and bottom faces, and copper wire was attached to the electrodes to ensure a good electrical contact. The volume resistivity ρ_V (Ω/cm) was calculated by:

$$\rho_v = R\frac{A}{d} \qquad (6.1)$$

In equation 6.1, R is the volume resistance, A is the electrode area and d is the distance between the electrodes (sample thickness).

6.2.4- Electromechanical Characterization

The sensitivity of a piezoresistive sensor can be represented by the gauge factor, GF, which represents the relative change in electrical resistance due to mechanical deformation:

$$GF = \frac{dR/R}{dl/l} \qquad (6.2)$$

In equation 6.2, R is the steady-state material electrical resistance before deformation and dR is the resistance change caused by the variation in length dl[10]. The resistance change under strain results from the contribution of the dimensional change (geometrical effect) is ΔR_D and from the intrinsic piezoresistive effect is ΔR_I. Therefore,for the surface mode measured in the present investigation (Figure 6.1), the GF can be written as[10]:

$$\begin{aligned} GF &= \frac{dR/R}{\varepsilon_l} = \Delta R_D + \Delta R_I \\ &= 1 + \upsilon + \frac{d\rho/\rho}{\varepsilon_l} \end{aligned} \qquad (6.3)$$

In equation 6.3 $dl/l = \varepsilon_l$, where ε is the strain, υ is the Poisson ratio and ρ is the resistivity.

The experiments were performed in 4-point-bending mode using a Shimadzu-AG-IS universal testing machine. Figure 6.1 presents a schematic of the 4-point bending set-up.
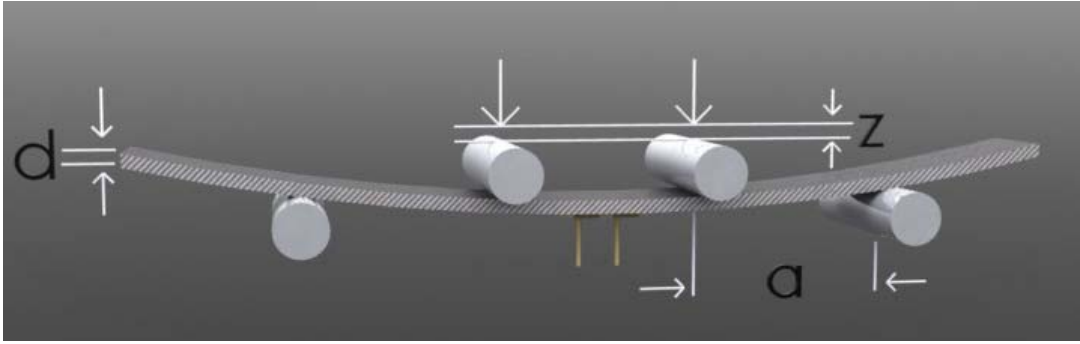
Figure 6. 1- Schematic of the 4-point bending test, where *z* is the vertical displacement of the piston, *d* is the sample thickness (~1 mm) and *a* is the distance between the two bending points (15 mm). The electrodes are placed in the bottom surface of the sample.

Assuming pure bending of a plate to a cylindrical surface, the strain between the inner loading points can be calculated from [4, 11]:

$$\varepsilon = \frac{3dz}{5a^2} \qquad (6.4)$$

Tests were performed with different settings of z-displacement, displacement rates (velocities), and temperature and consisted of several loading/relaxation cycles. The *GF* was calculated for each cycle from the z-displacement and the electrical resistance curves by taking the best fit curve by linear regression. Finally, the average *GF* value was calculated for each sample. The value of the *GF* for the loading and unloading mechanical cycles at a given set of conditions was the same, unless indicated.

6.3- Results and discussion

6.3.1- Nanocomposites morphology

The VGCNF distribution and dispersion in the epoxy matrix achieved by the four preparation methods has been previously investigated by greyscale analyses of transmission optical microscopy images [12] and was characterized in the present work by SEM images of the samples with 1.0 wt.% (Figure 6.2) [8]. Methods I and II produced composites with some agglomeration of the nanofibers within clusters, but

with a relative good filler distribution (Figure 6.2(a) and (b)). Method III yielded a homogeneous mixing (Figure 6.2(c)). On the other hand, method IV generated poor dispersion and the worst distribution as compared with the other methods (Figure 6.2(d)). The large clusters were hollow, with the matrix clearly visible inside the cluster. The qualitative evaluation of the SEM images is in agreement with the quantitative analyses of the dispersion presented in [12] and demonstrated the different dispersion ability of the used methods.

(a) Method I: Blender mixing
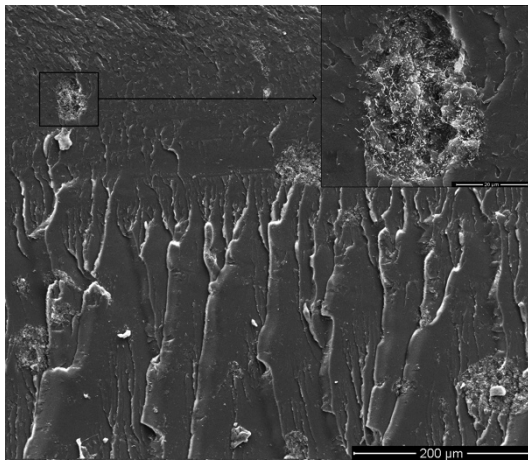
(b) Method II: Capillary Rheometer
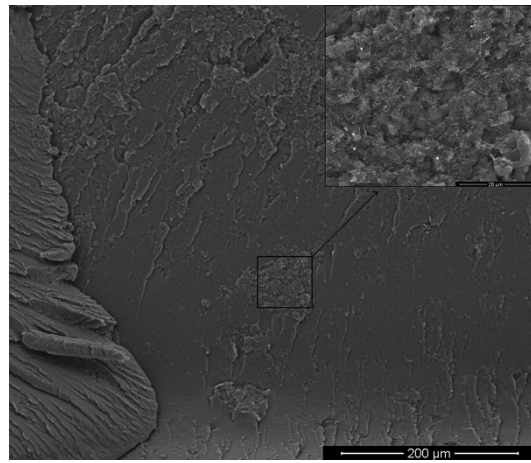
(c) Method III: Roll milling
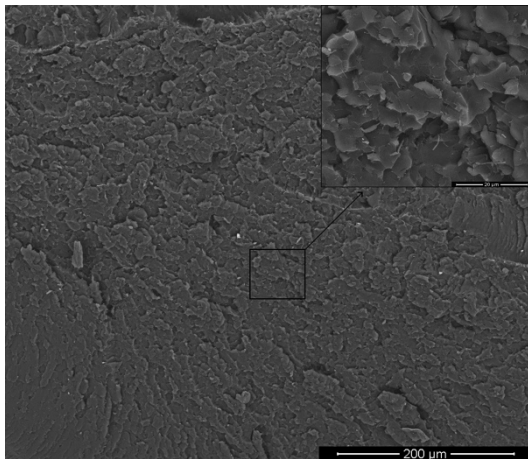
(d) Method IV: Thinky ARE-250 mixer
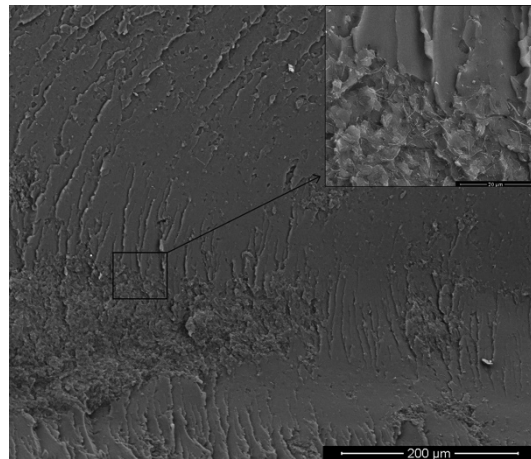
Figure 6. 2- SEM images of Cross-section of the 1.0 wt.% CNF samples. The insets represent the enlargement of the indicated area.

By increasing filler content, it is expected the composite to undergo a transition from insulator to conductor [13] that will, in turn, affect the piezoresistive response [4,

10, 14]. In this way, it is important to study the dependence of electrical conductivity on filler concentration.

6.3.2- Electrical Conductivity

Representative *I-V* curves for the epoxy composites with different VGCNF loadings are shown in Figure 6.3(a). The effect of VGCNF concentration on the electrical volume conductivity is presented in Figure 6.3(b) for samples prepared by the four different methods.

(a)   (b)
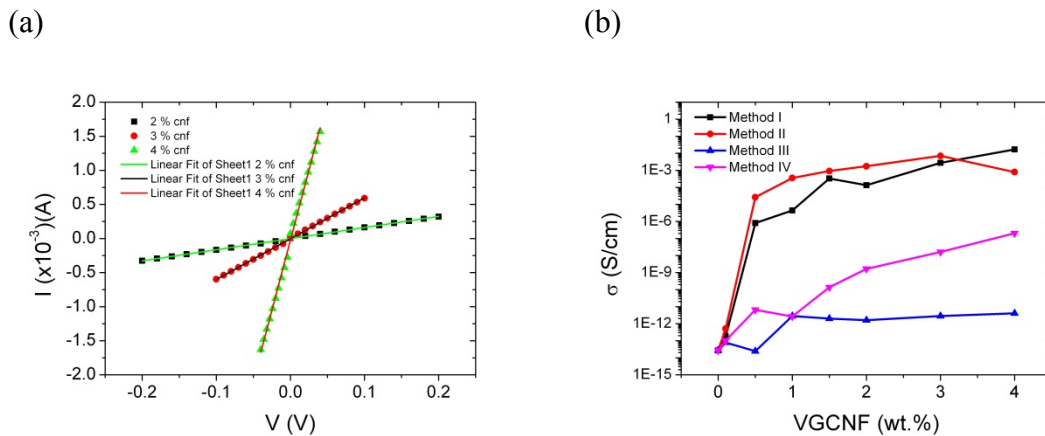
Figure 6. 3- (a) Representative I-V curves for the different nanocomposites (Method I), (b) Electrical conductivity values versus weight percentage of VGCNF for all preparation methods.

It was observed that as the carbon nanofiber content increased, there was an increase of the electrical conductivity by several orders of magnitude for the methods of preparation I and II, but this effect was not observed for the preparation methods III and IV. It is important to stress at this point that the only difference between the samples was the dispersion method used, while all the materials used for the composite preparation were the same. From the applied point of view, it is important to notice the low percolation threshold (≤0.5%) obtained by the dispersion methods I and II, comparing to the values typically obtained in the literature [13]. The electrical results in these types of composites have been generally discussed in the scope of the percolation theory [13]. Further, the correlation of the current-voltage *I-V* curves should give insight

on the conduction mechanism: linear *I-V* relationships should arise from direct contact between fillers, whereas a power law should result from a tunneling mechanism [13, 15, 16]. On the other hand, it has been shown that composites with tunneling type conductivity also obey the Ohm´s law and, therefore, show linear *I-V* relationships [17]. The AC and DC electrical behavior for the composites shown in figure 3 have been discussed previously based on the network theory [18]and the role of disorder has been analyzed. It was concluded that the presence of well dispersed clusters is more important than a good filler dispersion to achieve higher electrical conductivity. Further, the conductivity of the well dispersed clusters cannot be described by the percolation theory, instead, hopping between nearest fillers explainsthe observed deviation from the percolation theory; the overall composite conductivity being then explained by the existence of a weak disorder regime that establishes a path for conduction in contrast with the percolation theory that predicts the formation of a contact network[8].

6.3.3- Electromechanical response

Figure 6.4 shows a typical example (2.0 wt.% VGCNF, Method I) of the data obtained from the strain tests performed on the samples prepared by the different methods and for all concentrations: four loading/unloading cycles were applied (z-displacements of 1 mm at 2 mm/min at room temperature) with simultaneous measurement of the electrical resistance. For the lower strain (deformation) values a fairly linear piezoresistive behavior is observed, becoming slightly nonlinear for the higher deformation values (Figure 6.4 (b)). The *GF* was then calculated applying equation 6.2 (Figure 6.4(b)) by fitting with a linear regression in the linear part of the data.

(a) (b)
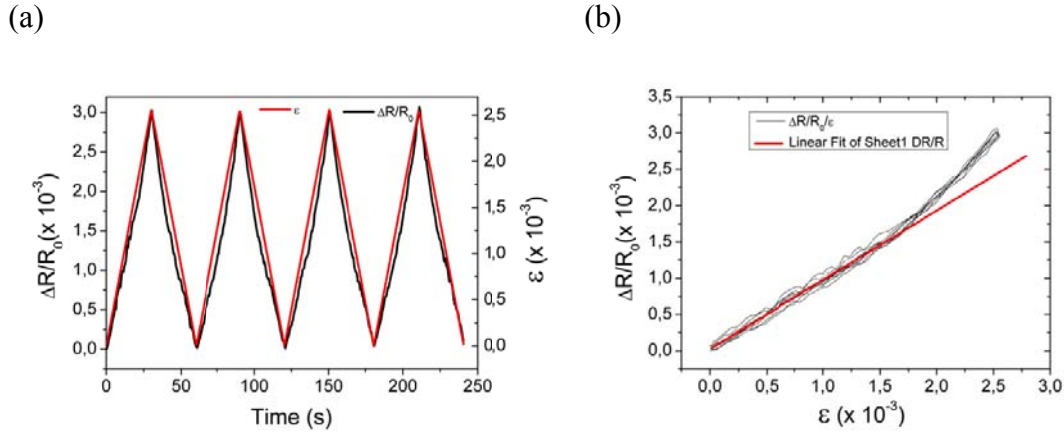
Figure 6. 4- (a) Representative cyclic strain applied to a sample and the corresponding resistance variation over time. (b) Relative change in electrical resistance due to mechanical deformation, for four up-down cycles applied to a sample with 2.0 wt.% VGCNF, Method I, z-deformation of 1 mm, deformation velocity of 2 mm/min at room temperature. The R-square of the fit is 0.99.

Figure 6.5(a), (b) and (c) shows the experimental results of the fractional change in surface resistance on the tension side of epoxy/CNF composites for progressively increasing flexural stress amplitudes of epoxy/CNF composites with 2.0 wt.% content as a function of time for the preparation methods I, II, and 3.0 wt.% for method III. It was observed that method IV gives no measurable piezoresistive response due to the high values of the electrical resistance even for samples with higher VGCNF concentrations. Methods I and II, on the other hand, give similar results, with the larger values of the GF close to the percolation threshold.
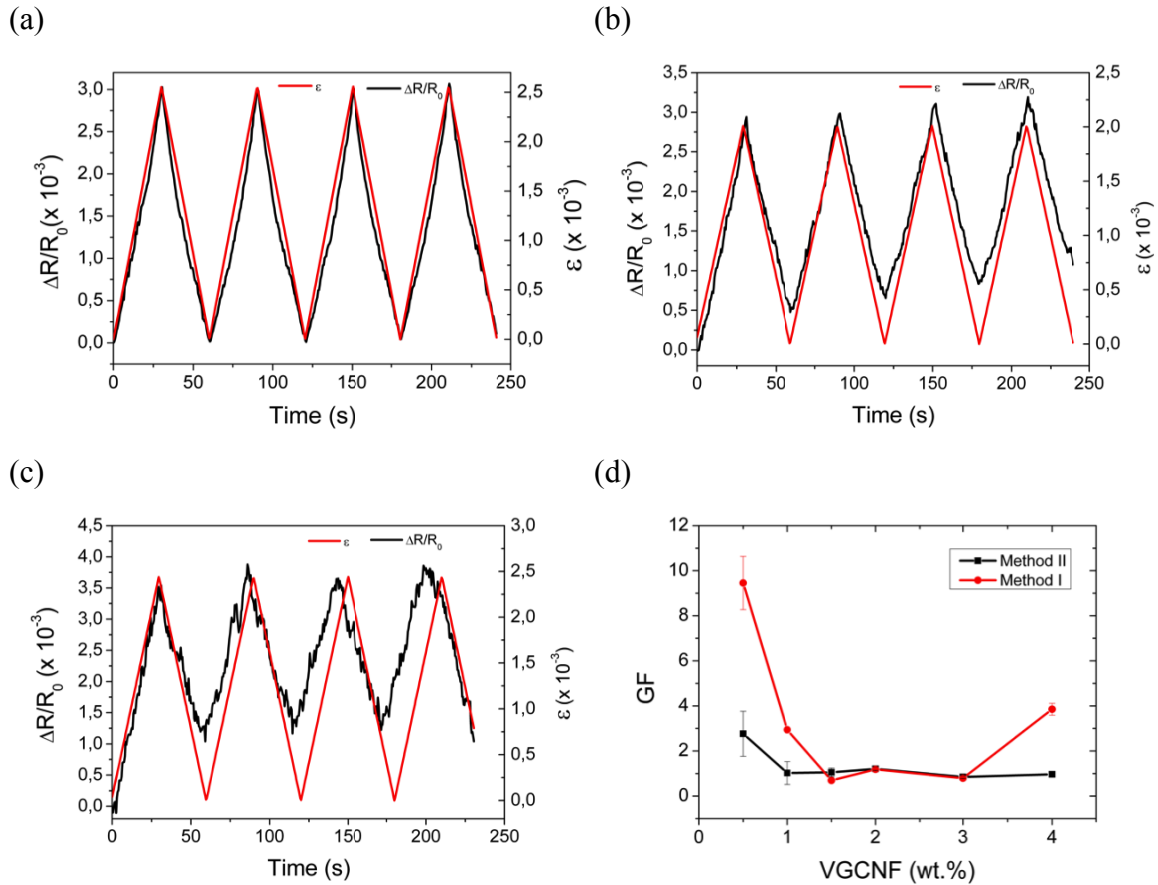
Figure 6. 5- Cyclic piezoresistive response as a function of time for samples with 2.0 wt.% from (a) Method I and (b) Method II; (c) for sample with 3.0 wt.% of Method III; (d) the Gauge factor dependence for samples with different VGCNF concentrations for the methods I and II for the following conditions: bending of 1 mm, deformation velocity of 2 mm/min at room temperature.

In spite of the fact that the piezoresistivity of conducting particle-reinforced insulating matrix has been previously studied, there are still not definitive conclusions about this subject. In general, it is assumed an exponential dependence of the resistance change versus strain as a consequence of interparticle tunneling model [7]. This exponential behavior can be adjusted with a linear trend for small strains, such as the case shown in this study, so the *GF* can be calculated with a linear fit (Figure 6.4 (b)).

According to the theory of pure bending of a plate to a cylindrical surface, there are two different effects contributing to the gauge factor: i) the intrinsic piezoresistive effect and ii) the geometric effect (equation 6.3). For this kind of materials the Poisson ratio is usually close to 0.35, which means that the geometric effect contribution to *GF* is

around 1.35 [19]. Figure 6.5(d) shows that for CNF concentrations above 1.5 wt.%, the geometric factor is the dominant one, but just below 1.0 wt.% CNF, the intrinsic contribution to the *GF* is dominant and its value reaches 9.8 for method I and 2.7 for method II. In this way, the intrinsic contribution is relevant just in samples around the percolation threshold. Moreover, it is observed that the region near 0.5 wt.% CNF at which the conductivity increases heavily, close to the percolation threshold, is the region with the largest *GF*. These facts are in accordance with previous reports showing that the sensitivity is higher in the surroundings of percolation thresholds [9, 20-22]. Close to the percolation threshold, the deformation induced reversible configurations of the conductive network result in strong variations of the electrical conductivity.

It is important to notice that the better conductivity values and therefore the best values of the GF are obtained for the samples with the better cluster dispersion (Figure 6.2).

Despite the conductivity in carbonaceous composites is still under discussion and direct contact [13], tunneling [7] or hopping [18], are being proposed as possible conduction mechanisms, in the following, the piezoresistive response will be discussed in terms of tunneling, as it is the most consolidated mechanism for the interpretation of the piezoresistive response in this type of materials, and it is supported, in our case, by the slight non-linear dependence of the resistance change versus strain [7]. It is to notice, nevertheless, that a model based on hopping should show similar overall response [18].

According to a heterogeneous fibril model, the general resistance *(R)* of carbon nanofibers is determined by the following relationship of tunneling resistance *(R$_T$)* and the VGCNFs band-gap change-dependent resistance *(R$_B$)*[23]:

$$R = \frac{L_T}{A_T} R_T + \frac{L_B}{A_B} R_B \quad (6.5)$$

$$R_T = R_m \left(1 + \exp\left(\frac{E_g}{k_B T} \right) \right) \quad (6.6)$$

$$R_B = R_t \exp\left(\frac{E_a}{k_B T}\right) \quad (6.7)$$

The paremeters L_T and A_T are the effective length and effective cross-sectional area involving the part of conducting electricity. R_T represents the intrinsic resistance and R_B the junction resistance, R_m and R_t are proportional constants, E_a is the tunnel activation energy and E_g is the band gap energy of CNF, k_B is the Boltzmann constant and T is temperature [23, 24]. The equation (6.5) can be rewritten as

$$R(T) = R_m\left(1 + \exp\left(\frac{E_g}{k_B T}\right)\right) + R_t \exp\left(\frac{E_a}{k_B T}\right) \quad (6.8)$$

In this approach, the conducting pathways are assumed to be connected in parallel and the resistance of pathways perpendicular to the current is neglected. If conduction is dominated by tunneling through the polymer gaps separating the CNFs and the resistance of the polymer matrix is much higher than the resistance of the particles, R_B, the resistance of the fillers can be neglected, $(R_B \approx 0)$ [23]. Thus, assuming that R_m is constant, the resistance change under stress can be expressed by

$$\frac{R(\varepsilon)}{R_0} = \exp(2\alpha d_0 \varepsilon) \quad (6.9)$$

$$\alpha = \frac{2\pi}{\hbar}\sqrt{2m\phi} \quad (6.10)$$

The parameters $R(\varepsilon)$ and R_0 are the composite resistance under tensile strain (ε) and the original resistance at $\varepsilon = 0$, respectively; d_0 is the tunneling distance between CNF, $\hbar$ is Planck's constant, m is the mass of the charge carriers, and φ is the tunneling barrier height. The detailed derivation for equations (6.9) and (6.10) can be found in [25]. In this model, if the tunneling distance is responsible for the resistance change under stress, the plot of $ln(R(\varepsilon)/R_0)$ versus tensile strain (ε) should be linear with a slope of $2\alpha d_0$ (Figure 6.6).

(a)   (b)
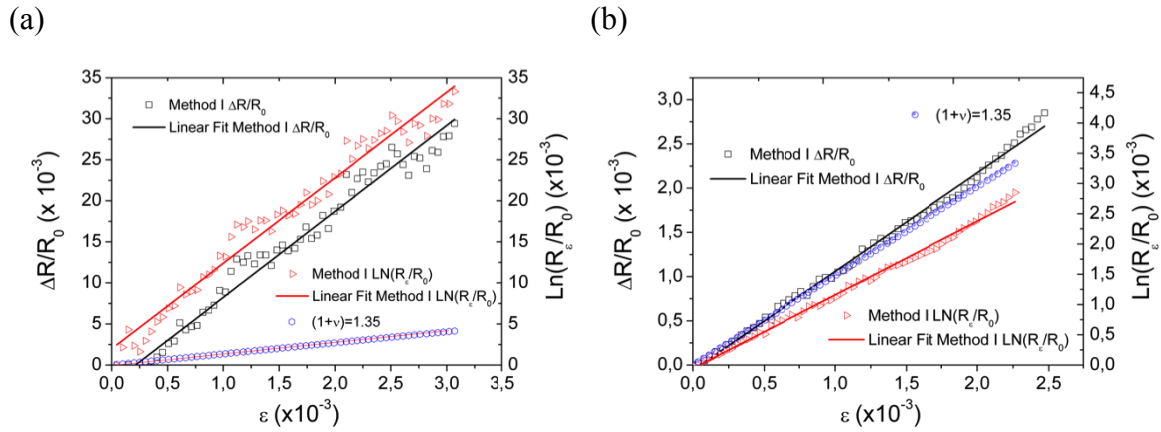
Figure 6. 6- Surface sensing resistance change $\ln(R(\varepsilon)/R_0)$ for methods I as function of stress, (a) 0.5 wt.% CNF and (b) 2.0 wt.% CNF and corresponding fittings with equation 6.9.

For example, for the samples prepared with Method I, the linear regression shows a slope of approximately 10.4 for the concentration of 0.5 wt.%, corresponding to $\alpha d_0 = 5.2$, satisfying the tunneling premise for which it must be $\alpha d_0 > 1$ [25]. On the other hand, for 2.0 wt.%, which is distant from the threshold zone, the linear regression results in approximately 1.2, corresponding to $\alpha d_0 = 0.6$ (< 1). This fact confirms that the tunneling condition does not hold and the piezoresistance relies only on the geometrical contribution (Figure 6.6 (b)).

For sensor applications it is relevant to study the stability of the sensing response (GF) as a function of the number of loading-unloading cycles. Experiments with 32 cyclic 4-point-bending tests were performed (Figure 6.7) and it is possible to observe a general trend to decrease both the resistance response for z = 0 mm and for z = 1 mm with increasing number of cycles, in particular, after 25 loading unloading cycles.

The decrease of the resistance for increasing number or cycles points out to fatigue effects indicative of irreversible variations in the filler network responsible for the conductivity of the composites. This fact is confirmed by the decreases of the *GF* for the higher cycle numbers (Figure 6.7).

(a)

(b)
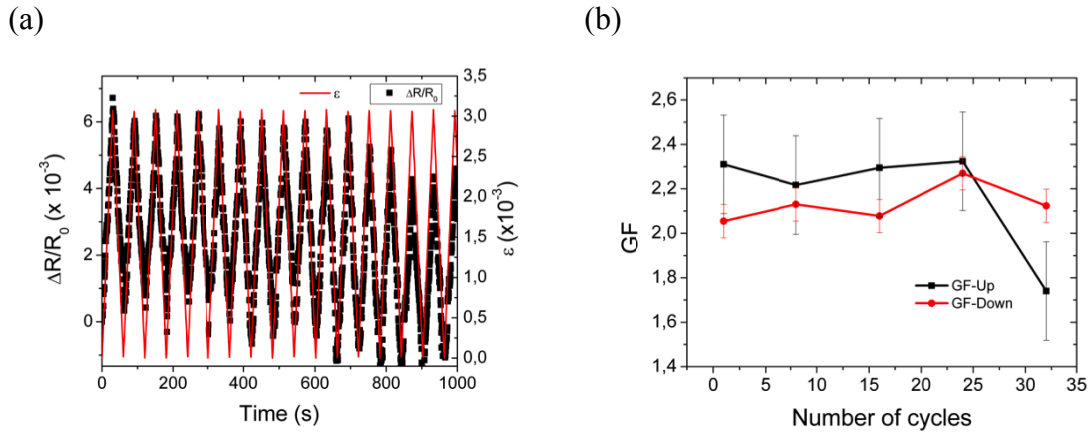
Figure 6. 7- Sensing resistance of the sample at 1.0 wt.% VGCNF of method I as a function of time, during a four-point bending experiment consisting of 32 cycles at 1 mm in z-displacement and 2 mm.min^{-1} at room temperature. Only the first 16 cycles are shown in graphic (a).

Figure 6.8 shows the strain sensing performance of the composite at 1.0 and 2.0 wt.% filler (Method I) loading as a function of z-displacement in mm (figure 6.8 (a)), and the response for the composite applying the same deformation (1 mm z-displacement) at different velocities (figure 6.8 (b)). These samples are representative for the general behavior of the samples prepared by methods I and II and represent samples with contribution from the intrinsic plus geometrical (1.0 wt.%) and just geometrical (2.0 wt.%) piezoresisitive responses. The large error bars for low displacements and high speeds are due to experimental constrains. The plots show variations up to 12% of the *GF* with bending deformation and with deformation speed both for the samples with intrinsic and geometrical and just geometrical responses. This behavior implies that the sensitivity is not constant, but depends on the applied strain, due to larger contributions to the nonlinear behaviour to the piezoresistive response [7], and speed due to the time response of the composite. These facts are in agreement with previous results in epoxy/CNF composites [9] and also with studies focused in carbon-black polymer systems [6, 26, 27].

(a)

(b)

(c)

(d)
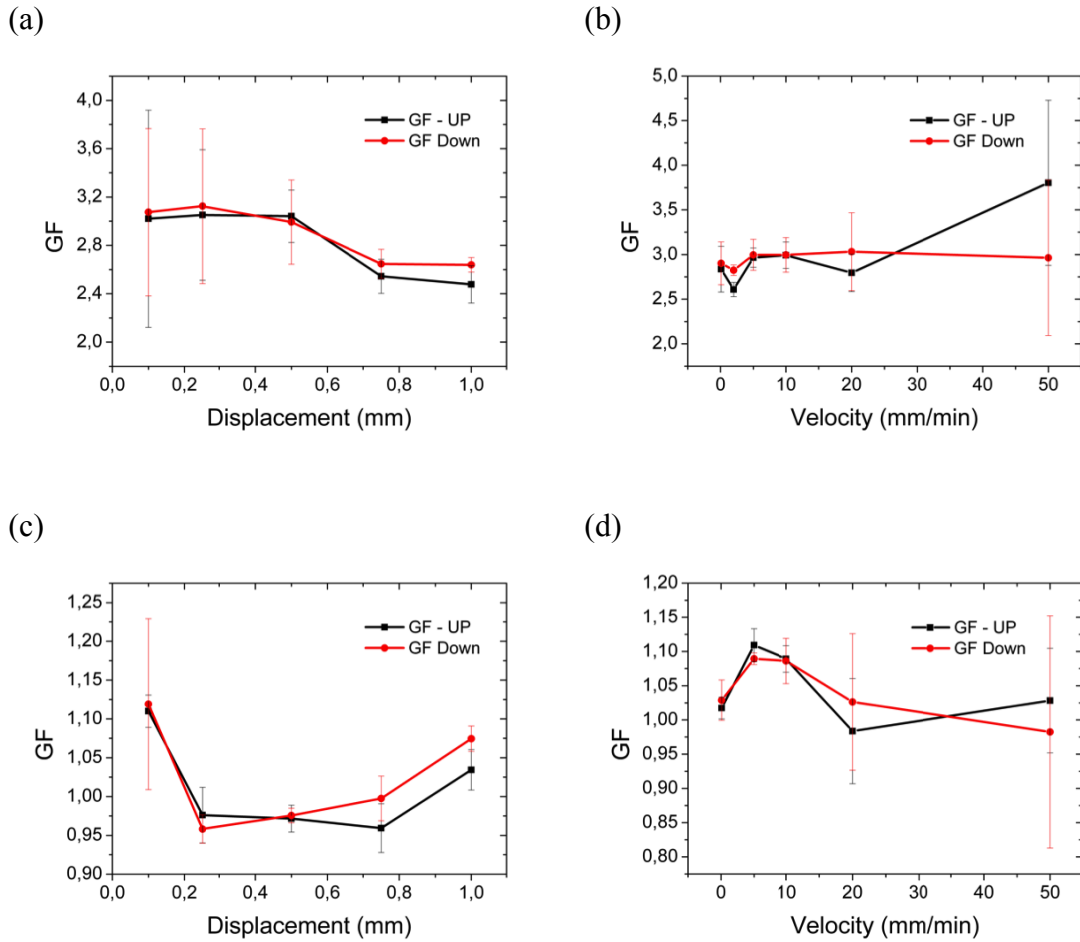
Figure 6. 8- Gage factor of the samples with 1.0 and 2.0 wt.% filler loading (Method I) as a function of z-displacement, (a) and (c); and deformation at different velocity for a given displacement of 1 mm, (b) and (d).

The temperature behavior of the GF calculated after 4 cycles at 1 mm deformation in z direction with a deformation speed of 2 mm/min and the heat flow versus temperature are represented in Figure 6.9.
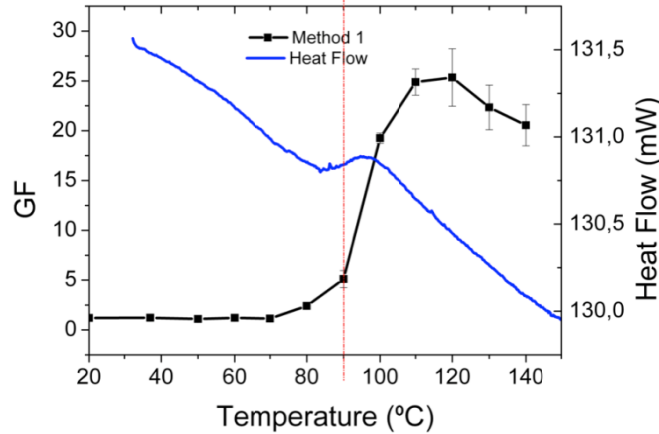
Figure 6. 9- Dependence of the *GF* with increasing temperature for the sample 2.0 wt.% prepared by method 1. The corresponding DSC scan shows the glass transition temperature.

Three distinct regions are observed (Figure 6.9): the *GF* is stable up to temperatures of 75 ºC, increases strongly from approximately 80 ºC to 120 ºC and then decreases with increasing temperature. This behavior was attributed to the amorphous nature of the epoxy resin and is related to the glass transition temperature, T_g[28-30], which depend on cure time and temperature. At T_g the polymer undergoes a transition from a glassy state to a rubbery state, becoming mechanically softer and therefore allowing larger reconfigurations of the CNF network for a given deformation. Therefore this leadsto larger values of the *GF* (Figure 6.9), which are 9 to 10 times larger than the ones at temperatures below the T_g.

6.4- Conclusions

The electrical and piezoresistive response of epoxy/VGCNF composites prepared by different methods has been reported. The dispersion method I and II leads to a better cluster dispersion and to higher electrical conductivity for a given concentration, lower percolation threshold and larger piezoresistive responses. The electrical response was characterized by linear *I-V* curves and a percolation threshold around 0.5 wt.% loading. The piezoresistive response, quantitatively analyzed by the gauge factor, was strongly concentration dependent, reaching the largest values around the percolation threshold, where the deformation induced variations in the conduction

network are the largest. At this concentration, intrinsic contributions to the GF are larger than the geometrical ones and seem to be driven by tunneling mechanism. The maximum value of the gauge factor was approximately 9.8 for method I (blender mixing), and its cycle and thermal stability up to 75 ºC shows the viability of these materials to be used as piezoresistive sensors. The samples show GF variations up to 10% depending on the deformations and deformation velocities used in the present investigation.

References

[1]   Kang I, Heung Y, Kim J, Lee J, Gollapudi R, Subramaniam S, et al. Introduction to carbon nanotube and nanofiber smart materials. Composites Part B: Engineering. 2006;37:382-94.

[2]   Knite M, Teteris V, Kiploka a, Klemenoks I. Reversible Tenso-Resistance and Piezo-Resistance Effects in Conductive Polymer-Carbon Nanocomposites. Advanced Engineering Materials. 2004;6:742-6.

[3]   Adhikari B, Majumdar S. Polymers in sensor applications. Progress in Polymer Science. 2004;29:699-766.

[4]   Zhu S, Chung D. Analytical model of piezoresistivity for strain sensing in carbon fiber polymer–matrix structural composite under flexure. Carbon. 2007;45:1606-13.

[5]   May CA. Epoxy Resins: Chemistry and Technology. New York: Marcel Dekker Inc; 1987.

[6]   Carmona F, Canet R, Delhaes P. Piezoresistivity of heterogeneous solids. Journal of Applied Physics. 1987;61:2550, 7.

[7]   Wichmann MHG, Buschhorn ST, Böger L, Adelung R, Schulte K. Direction sensitive bending sensors based on multi-wall carbon nanotube/epoxy nanocomposites. Nanotechnology. 2008;19:475503.

[8]   Cardoso P, Silva J, Klosterman D, Covas JA, van Hattum FWJ, Simoes R, et al. The role of disorder on the AC and DC electrical conductivity of vapour grown carbon nanofibre/epoxy composites. Composites Science and Technology. (DOI: 10.1016/j.compscitech.2011.11.008).

[9]   Yasuoka T, Shimamura Y, Todoroki A. Electrical Resistance Change under Strain of CNF/Flexible-Epoxy Composite. Advanced Composite Materials. 2010;19:123-9.

[10]   Beeby S, Ensell G, Kraft M, White N. MEMS mechanical sensors. Boston: Artech House; 2004.

[11]   Alpuim P, Marins ES, Rocha PF, Trindade IG, Carvalho MA, Lanceros-Mendez S.Ultra-sensitive shape sensor test structures based on piezoresistive doped nanocrystalline silicon. Vacuum, 2009. 83(10): p. 1279-1282.

[12]   Cardoso P, Klosterman D, Covas JA, van Hattum FWJ, Lanceros-Mendez S. Quantitative evaluation of the dispersion ability of different preparation methods and DC electrical conductivity of vapor grown carbon nanofiber/epoxy composites. Polymer Testing, 2012. 31: p. 697-704.

[13]   Alsaleh M, Sundararaj U. A review of vapor grown carbon nanofiber/polymer conductive composites. Carbon. 2009;47:2-22.

[14]   Wichmann MHG, Buschhorn ST, Gehrmann J, Schulte K. Piezoresistive response of epoxy composites with carbon nanoparticles under tensile load. Physical Review B. 2009;80:1-8.

[15]   Yui H, Wu G, Sano H, Sumita M, Kino K. Morphology and electrical conductivity of injection-molded polypropylene/carbon black composites with addition of high-density polyethylene. Polymer. 2006;47:3599-608.

[16]   Bar H, Narkis M, Boiteux G. The electrical behavior of thermosetting polymer composites containing metal plated ceramic filler. Polymer Composites. 2005;26:12-9.

[17]   Chekanov Y, Ohnogi R, Asai S, Sumita M. Electrical properties of epoxy resin filled with carbon fibers. Journal of Materials Science. 1999; 34(22):5589-5592.

[18]   Silva J, Simoes R, Lanceros-Mendez S, Vaia R. Applying complex network theory to the understanding of high-aspect-ratio carbon-filled composites. EPL (Europhysics Letters). 2011;93(3):37005.

[19]   Miller B. Plastics World 1996.

[20]   Paleo AJ, van Hattum FWJ, Pereira J, Rocha JG, Silva J, Sencadas V, et al. The piezoresistive effect in polypropylene—carbon nanofibre composites obtained by shear extrusion. Smart Materials and Structures. 2010;19:065013.

[21]   Hu N, Karube Y, Yan C, Masuda Z, Fukunaga H. Tunneling effect in a polymer/carbon nanotube nanocomposite strain sensor. Acta Materialia. 2008;56:2929-36.

[22]   Foreman J, Behzadi S, Porter D, Curtis P, Jones F. Hierarchical modelling of a polymer matrix composite. Journal of Materials Science. 2008;43(20):6642-50.

[23]   Cao CL, Hu CG, Xiong YF, Han XY, Xi Y, Miao J. Temperature dependent piezoresistive effect of multi-walled carbon nanotube films. Diam Relat Mat. 2007;16(2):388-92.

[24] Sheng P. Fluctuation-induced tunneling conduction in disordered materials. Physical Review B. 1980;21(6):2180-95.

[25] Dawson JC, Adkins CJ. Conduction mechanisms in carbon-loaded composites. Journal of Physics: Condensed Matter. 1996;8(43):8321.

[26] Wang L, Dang Z-M. Carbon nanotube composites with high dielectric constant at low percolation threshold. Applied Physics Letters. 2005;87:042903.

[27] Celzard A, McRae E, Mare ché JF, Furdin G, Sundqvist B. Conduction mechanisms in some graphite–polymer composites: Effects of temperature and hydrostatic pressure. Journal of Applied Physics. 1998;83:1410.

[28] Tamulevich TW, Moore VE. The Significance Of Glass Transition Temperature on epoxy Resins for Fiber Aplications. In: Epoxy Technology I, editor. Proceedings, EFOC 80 - the first European Fiber Optics e Communications Exposition, July 1,2,3, Paris France. Billerica, Mass 018211980. p. 96-100.

[29] Wisanrakkit G, Gillham JK. The glass transition temperature (Tg) as an index of chemical conversion for a high-Tg amine/epoxy system: Chemical and diffusion-controlled reaction kinetics. Journal of Applied Polymer Science. 1990;41:2885-929.

[30] Zhou J, Lucas JP. Hygrothermal effects of epoxy resin. Part II: variations of glass transition temperature. Polymer. 1999;40:5513-22.

7. Comparative analyses of the electrical properties and dispersion level of VGCNF and MWCNT - epoxy composites

This work focuses on a comparative study of the electrical properties and the dispersion of VGCNF and MWCNT - epoxy resin composites. A blender was used to disperse the nanofillers within the matrix, producing samples with concentrations of 0.1, 0.5 and 1.0 wt.% for both nanofillers. The dispersion of the nanofillers was analyzed using SEM and TOM together with a GSA. The electrical conductivity and the dielectric constant were evaluated. The percolation threshold of MWCNT in epoxy composites was found to be lower than 0.1 wt.% while in the case of VGCNF it was found to lie between 0.1 and 0.5 wt.%. The observed difference on the dispersion of the two nanofillers is due to their intrinsic characteristics such as aspect ratio and surface characteristics, which influences both the composite electrical conductivity and the interaction of the nanofillers with the matrix. Celzard's theory was shown to be suitable to calculate the bounds of the percolation threshold for the VGCNF composites but not for the MWCNT composites, indicating that intrinsic characteristics of the nanofillers beyond the aspect ratio are determinant for the MWCNT composites electrical conductivity.

7.1- Introduction

In the past years one of the main focuses of industrial and academic research has been the development of conductive nanocomposites where a polymeric matrix is reinforced with nanofillers. These nanofillers provide the polymeric matrix with a wide range of properties as compared to the pristine polymeric matrix [1-3]. The nanocomposites based on carbon nanoscale fillers such as SWCNT and MWCNT, as well as VGCNF, are already commercially significant. Carbon based nanofillers provide polymer composites with improved mechanical, electrical and thermal properties. These high aspect ratio nanofillers have a large specific surface area (SSA) several orders of magnitude higher (up to 1300 m^2/g for CNT) than the conventional reinforcement fibers (SSA $<<$ 1 m^2/g for short carbon fibers). The single most important physical characteristic of CNT and VGCNF nanofillers is their aspect ratio (AR) that can range from a small number to several thousands. In the case of CNT, the SSA is also dependent on the diameter and the number of sidewalls [4]. The AR of these nanofillers is intrinsically related to the surface area and act as desirable interface for stress transfer, also inducing strong attractive forces between nanotubes, leading to agglomeration of the nanofillers mainly due to Van der Waals forces. Among the carbonaceous nanofillers, CNT is widely used in both academic research and industrial applications, although VGCNF have their own interest and applications. In fact, the VGCNF electrical and mechanical properties are generally lower than those obtained with CNT as a reinforcement but, on the other hand, they have significant lower cost (3 to 10 lower than CNT) [5].

Epoxy resins are thermosetting polymers often used to produce composites with a wide range of applications [6]. By incorporating high aspect ratio fillers like CNT [7, 8] or VGCNF [5], the mechanical, thermal and electrical properties of the expoy resin are enhanced and the range of applications extended [9]. The physical properties of a nanocomposite are also intimately linked to the aspect ratio and surface-to-volume ratio of the filler [10], as stated before. Also, the dispersion levels of filler nanoparticles are known to influence the physical properties of the composite such as mechanical [11], thermal [12], dielectric response [13, 14], electrical conductivity [15-19], ionic conductivity [20], coercive force [21], refractive index [22], UV resistance [23] and wear resistance [24], among other properties [25-28]. With respect to the electrical

properties it is not consensual that the response is strictly related to a good dispersion of nanofillers in the matrix, as recent studies demonstrate that filler distribution is more important than dispersion [29-32] for obtaining large electrical conductivity with low percolation thresholds. Moreover, there is a study [17] mentioning that a good dispersion of nanofillers in the matrix might be disadvantageous for the electrical properties. It should be noted that the methodology to produce nanocomposites reinforced with high aspect ratio fillers strongly influences the nanofillers distribution, dispersion, orientation and even aspect ratio [5] and hence the overall nanocomposite response.

To produce nanocomposites based on carbon nanofillers and thermosets, several different methods are found in literature, such as dilution of the epoxy resin with acetone [33] and tetrahydrofuran [34] to promote the nanofillers infusion, blending of the nanofibers with the resin followed by roll milling [33] and high shear mixing [35]. Solution processing, in situ polymerization, melt and bulk mixing are common preparation methods found for CNT/polymer composites [8, 36]. VGCNF/thermoset composites have been produced using methods ranging from simple [37], direct [38], bulk [39] and solution mixing [40], to calendaring [41] and roll milling [42].

Once the nanocomposites are produced, the characterization of the morphological properties is usually performed by using SEM, TEM, scanning probe microscope (SPM) and TOM. The latter techniques have been mostly used to visualize the nanofillers dispersion in the host matrix [43, 44]. However, if the goal of the morphological study is to quantify rather than qualify the dispersion or distribution of the nanofillers in the matrix, there is a need to use specific image techniques and mathematical tools to achieve it. Some methods like SAXS and wide-angle X-ray scattering(WAXS), Raman spectroscopy, AC impedance spectra, ^{13}C NMR, ESR spectroscopy, UV-VIS spectra, neutron reflection and scattering have been used to quantify the dispersion of different nanofillers, including VGCNF and CNT [44]. TOM, by means of GSA, has been also applied in epoxy/VGCNF composites [45], but a clear relationship between dispersion level and macroscopic properties of the composite is still to be achieved.

The aim of this work is to comparatively analyze the dispersion level of both VGCNF and MWCNT - epoxy resin composites prepared under the same conditions and to compare to their electrical properties. Composites were prepared by dispersing 0.1, 0.5 and 1.0 wt.% nanofillers with a blender as this method is known to produce

highly conductive composites with lower percolation threshold when compared to other dispersion methods [30, 32].

7.2- Experimental

7.2.1- Preparation of composite samples

MWCNT, NC7000, were supplied by Nanocyl[TM]. The NC7000 MWCNT have an average diameter of 9.5 nm, average length of 1.5 μm, produced in industrial large-scale using catalytic carbon vapor deposition (CCVD) process, with a carbon purity of 90% and a surface area of 250-300 m^2/g [46]. The VGCNF Pyrograf III[TM], PR-19-XT-LHT, were supplied by Applied Sciences (Applied Sciences Inc, Ohio, USA). They are a highly graphitic form of VGCNF with stacked-cup morphology [7, 47].The epoxy resin was an Epikote[TM] 862 Resin and the curing agent was Ethacure 100 Curative, supplied by Hexion Specialty Chemicals and Albemarle, respectively. The weight ratio of resin to curing agent was 100:26.4. The dispersion of both VGCNF and MWCNT in the epoxy resin was performed with a Haeger blender for two minutes [29], where the velocity field and stress levels should generate a predominantly distributive mixing.For each pre-mixture thecorresponding amount of curing agent was added and blender mixedduring two minutes. After mixing, all samples were subjected to a 20 mbarabsolute pressure, to remove air enclosures, and then cast into a mold and cured at subsequently 80 °C and 150 °C for 90 minutes each [48].A neat resin sample and composites with VGCNF and MWCNT concentrations of 0.1, 0.5 and 1.0 wt.% were prepared. The samples were in the form of rectangular bars with 1mm thickness, 10 mm width and 70 mm length.

7.2.2- Morphological analysis

The samples with 1.0 wt.% of VGCNT and MWCNT were selected for the morphological study because this content is above the electrical percolation threshold and it is convenient to observe the nanofillers conductive network throughout the matrix. These samples were cut perpendicular to the length direction and SEM and TOM images were taken. A Phillips X230 FEG apparatus was used to acquire cross-

sectional SEM images after coating the samples with a gold layer by magnetron sputtering.

To prepare the samples for the TOM analyses, one slice with a thickness of 10 μm was cut using a Leitz 1401 microtome equipped with a glass slicing knife. Each sample slice was placed between a microscope glass slide and cover glass. To prevent them from curling up or corrugating, Canada balsam (Alfa Aesar, CAS# 8007-47-4) was used as a fixing resin. All samples were left to cure under a simple weight pressure during at least 12 hours prior to analysis. The thickness of the sample slices is determined by the homogeneity of the cut and the need for a minimum transparency in the areas with higher concentration of VGCNF.

An Olympus BH2 transmission microscope with an integrated X-Y stage, a digital camera Leica DFC 280 and corresponding software were used to capture and record images from each slice. To obtain a representative sample area in terms of nanofillers (MWCNT or VGCNF) dispersion, an array of N rows and M columns of optical micrographs were captured and recorded, avoiding image overlap. Close to 100 micrographs were captured, each with 1280 x 1024 pixels, each pixel being a square with a side of 131 nm. The nanofillers dispersion in the epoxy resin was estimated from a greyscale analysis (GSA) based on the transmission light optical micrographs (TOM). The histogram presents values proportional to the number of pixels of the micrograph at each gray scale, versus the corresponding greyscale value, for a certain lengthscale. In turn, the latter is related to the size of each pixel of the micrograph, so that the lower the lengthscale value the higher the micrograph resolution. Using 8-bit greyscale images, the greyscale value varies from 0 to 255, corresponding to black (0) and white (255), respectively. The methodology is explained in more detail in [45].

7.2.3- Electrical measurements

The electrical measurements were performed on the cured samples with four concentrations of VGCNF and MWCNT, ranging from 0 to 1.0 wt.%. The dielectric response was obtained by measuring the capacity and tan δ (dielectric loss) at room temperature in the range of 500 Hz to 1 MHz with an applied signal of 0.5 V, using an automatic Quadtech 1929 Precision LCR meter. Samples were coated on both sides by thermal evaporation with circular Al electrodes of 5 mm diameter. The volume AC

electrical conductivity (σ_{AC}) and the real component of the dielectric constant (ε') were then calculated from the measurements, taking into account the geometrical factors. The volume DC electrical conductivity was obtained by a two-probe method, measuring thecharacteristic *I-V* curves at room temperature with aKeithley 6487 picoammeter/voltage source and taking into account the sample geometric characteristics.

7.3- Results

7.3.1- Morphological analysis

In Figure 7.1(a) a layout of 90 micrographs with an 8-bit greyscale is presented of a cross-section located at the center of the sample with 1.0 wt.% of VGCNF dispersed in epoxy resin. The TOM micrographs presented in Figure 7.1(b) have 512x640 pixels, where each pixel is a square with 0.26x0.26 μm^2. The correspondinghistograms are shown in Fig 7.1(c).
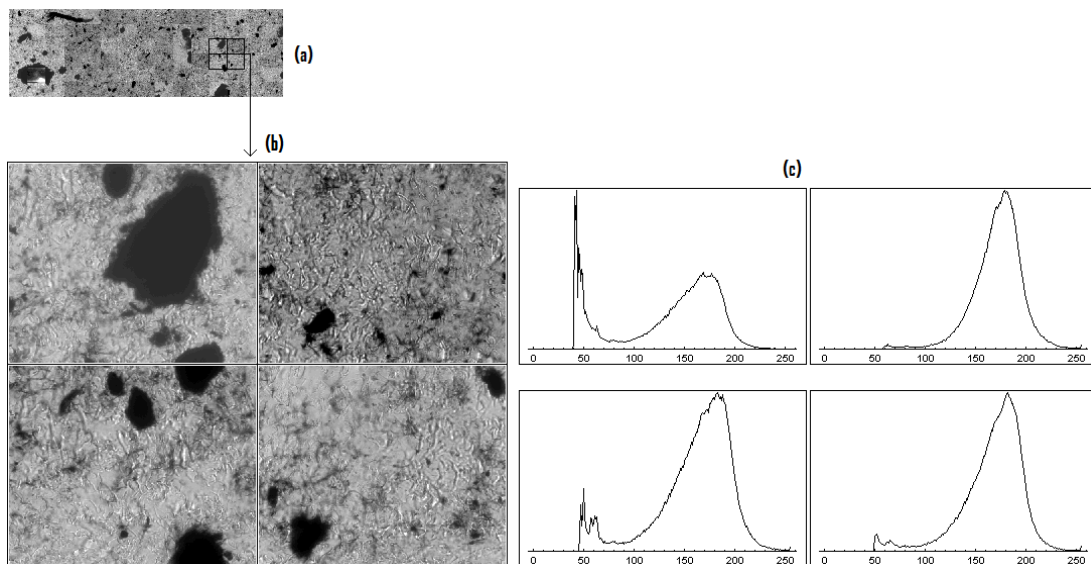

Figure 7. 1- Sample with 1.0 wt.% of VGCNF, (a) array of 6 rows and 15 columns of TOM micrographs with a total area of 1.99 mm^2, (b) 4 adjacent micrographs from this array and (c) the corresponding greyscale histograms.

In the array of TOM images presented in Figure 7.1(a) it is possible to observe VGCNF clusters of different sizes and shapes, which are distributed along the array. Observing the four micrographs shown in Figure 7.1(b), clusters of VGCNF with different sizescan be better distinguished. In fact, the cluster with a high number of VGCNF, black spots in Figure 7.1(b), can be detected in the corresponding histograms from Figure 1(c) as peaks at lower greyscale values. For example, the top left histogram of Figure 7.1(c) shows a strong peak close to 50 in the greyscale axis due to the amount of agglomerated VGCNF, observed in the corresponding micrograph. In the same figure, in the bottom left histogram a peak with a small height for the same value of the grayscale is observed, due to the fact that the area of the corresponding micrograph filled with agglomerates is smaller. Something similar can be confirmed in the two remaining histograms: the height of the peak at 50 in proportional to the area of the filler agglomerates. All the histograms of Figure 7.1(c) demonstrate a peak between 150 and 200 in the greyscale, meaning that there are many gray pixels in the micrographs due to the presence of a background network of VGCNF clusters.

In Figure 7.2(a) a layout of 105 micrographs with an 8-bit greyscale is presented of a slice located in the middle of the sample length which was prepared by dispersing 1.0 wt.% of MWCNT in the epoxy resin. TOM micrographs of Figure 7.2(b) have 512x640 pixels, where each pixel is a square with 0.26x0.26 μm^2 and the corresponding histograms are presented in Figure 7.2(c).
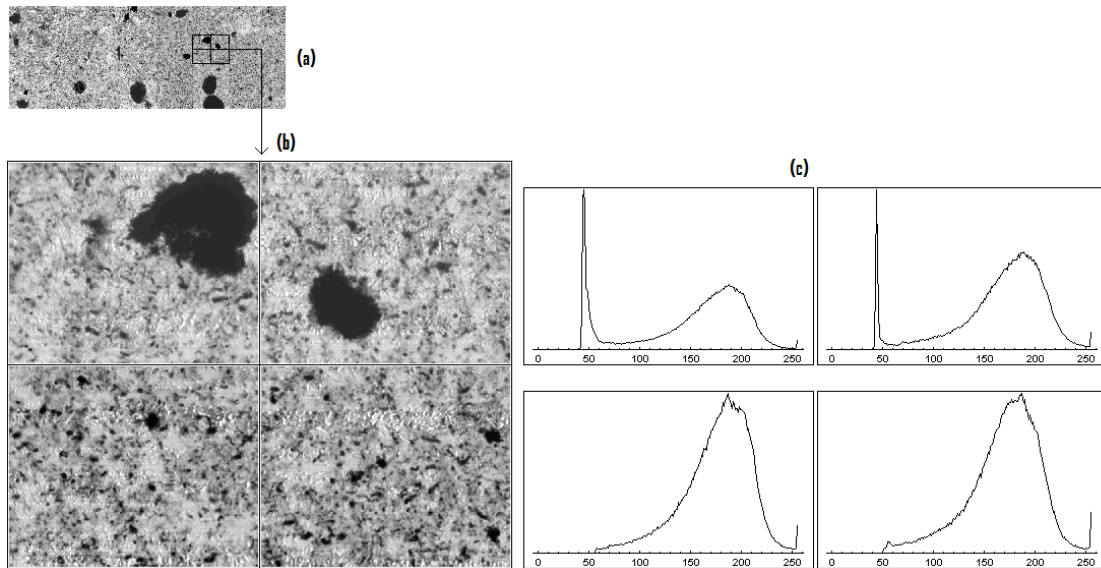
Figure 7. 2- Sample with 1.0 wt.% of MWCNT, (a) array of 7 rows and 15 columns of TOM micrographs with a total area of 2.33 mm^2, (b) 4 adjacent micrographs from this array and (c) the corresponding greyscale histograms.

A qualitative analysis of the array of TOM images of Figure 7.2(a) indicates the presence of large agglomerates reasonably distributed along the sample, with different sizes and geometries. Only in the top left and right micrographs of Figure 7.2 (b) large agglomerates of MWCNT are observed and this is noticed in the corresponding histograms of Figure 7.2(c), through the presence of strong peaks for the greyscale value close to 50. The small agglomerates of MWCNT observed in bottom left and right micrographs of Figure 7.2(b) have a small influence on the corresponding histograms, as no peak for low values of the grayscale can be observed. Instead, both histograms show a pronounced and wide peak for gray values in the middle of the greyscale, meaning that the majority of the pixels of the respective micrographs are at this level of gray and the range of these gray levels is quite large. All the micrographs have gray areas corresponding to the background network of MWCNT and they are noticed in all histograms as a peak for greyscale values between 150 and 200. The latter findings indicate the presence of background network of MWCNT which is not resolved at this lengthscale as it is for the case of VGCNF composite.

In Figure 7.3, SEM images of the cross-section area perpendicular to the length direction of the VGCNF and MWCNT composites with 1.0 wt.% are presented. Both

SEM images presented in this figure have insets on the top right corner with a higher amplification of a specific region of the main image.
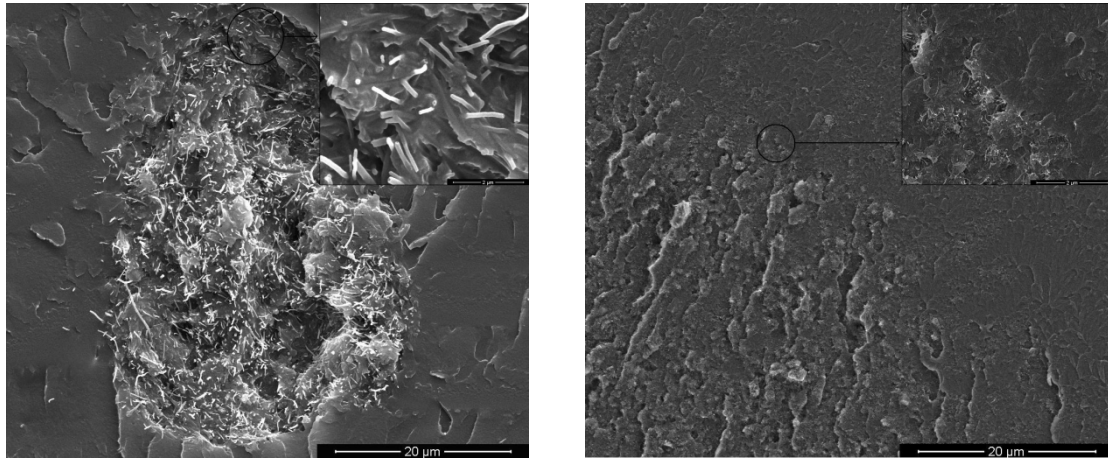
Figure 7. 3- SEM images of samples with 1.0 wt.% of (left) VGCNF and (right) MWCNT. Insets: SEM images with higher amplification of the same sample.

The SEM images of Figure 7.3 give an insight in how both nanofillers are dispersed in the polymer matrix. Although the agglomerate of VGCNF shown in Figure 7.3(left) is much larger than the agglomerates of MWCNT presented in Figure 3(right), the TOM images presented in Figure 7.1 and 7.2 show that they have almost of the same dimensions and distribution along the samples, when a larger representative area is considered. The observations provided by TOM images of Figure 7.2 about the existence of small agglomerates of nanofillers are also found in the corresponding SEM images. It is to be noticed that the differences of VGCNF and MWCNT dimensions are both in average diameter and length: VGCNF and MWCNT have average diameters of 150 and 9.5 nm, respectively, and the length varies from 50 to 200 μm for the VGCNF, while the average length of MWCNT is 1.5 μm.

7.3.2- Electrical measurement

The top left and right graphics of Figure 7.4 show the evolution of conductivity and real part of the dielectric constant with frequency for the VGCNF samples, while the bottom left and right graphics show the same data for the MWCNT.
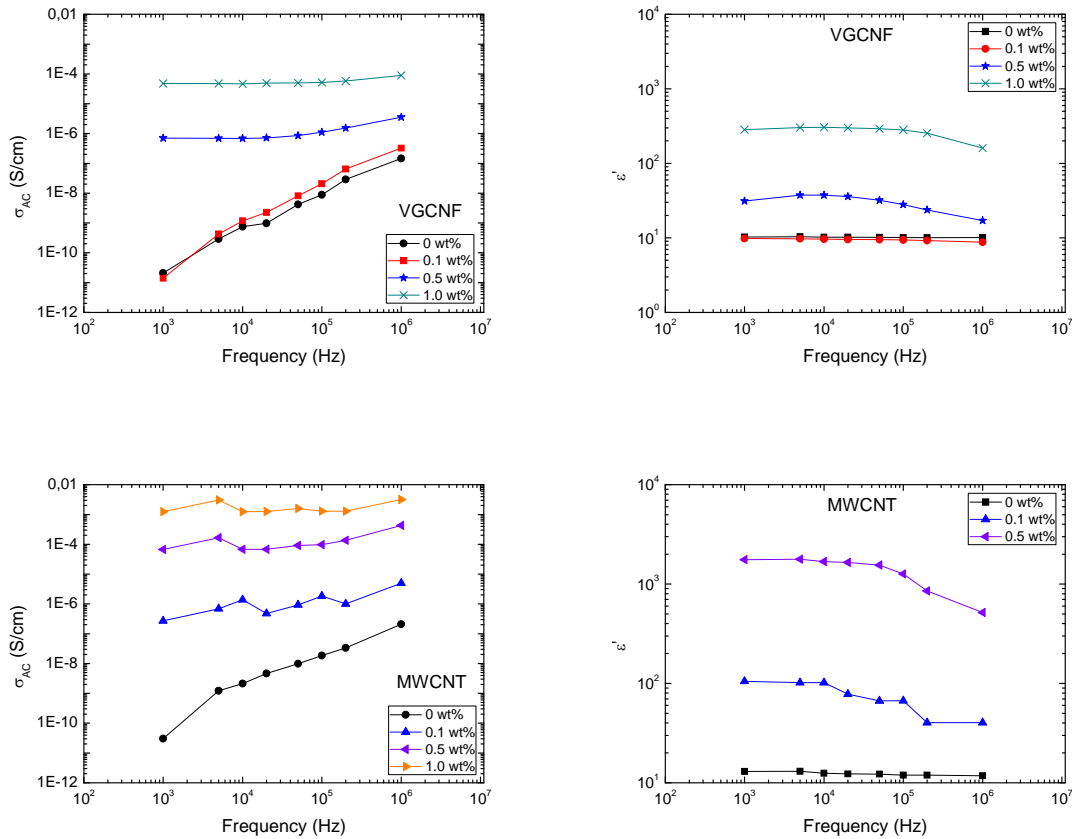
Figure 7. 4- Log-log plots of:top left and right - AC conductivity and dielectric constant versus frequency for VGCNF, respectively. Bottom left and right - AC conductivity and dielectric constant versus frequency for MWCNT, respectively.

The top left graphic of Figure 7.4 shows that the conductivity is dependent of the frequency for the neat sample and the sample with 0.1 wt.% of VGCNF, but it is independent for samples with 0.5 and 1.0 wt.%. The bottom left graphic of Figure 7.4 shows that only the neat sample conductivity is frequency-dependent and the 0.1, 0.5 and 1.0 wt.% MWCNT samples are almost independent of the frequency. Comparing the curves from top and bottom left graphics of Figure 7.4 it can be observed that, regardless of the frequency, AC conductivity is always higher for the MWCNT samples than for the VGCNF samples. It is also noticed that the conductivity always increases with increasing frequency, but this increase is lower for samples with higher filler content. Both top and bottom right graphics of Figure 7.4 show that the dielectric constant of MWCNT and VGCNF samples decreases with frequency, but the values of the dielectric constant from the MWCNT sample are significantly higher than the values

from the VGCNF sample with the same filler content. The main conduction mechanism for the VGCNF/epoxy composite and its increase with the frequency has been discussed in a recent work [32].

Figure 7.5 shows the AC (left) conductivity at 1 kHz and DC (right) conductivity curves versus nanofiller content for the composite samples with MWCNT and VGCNF fillers.
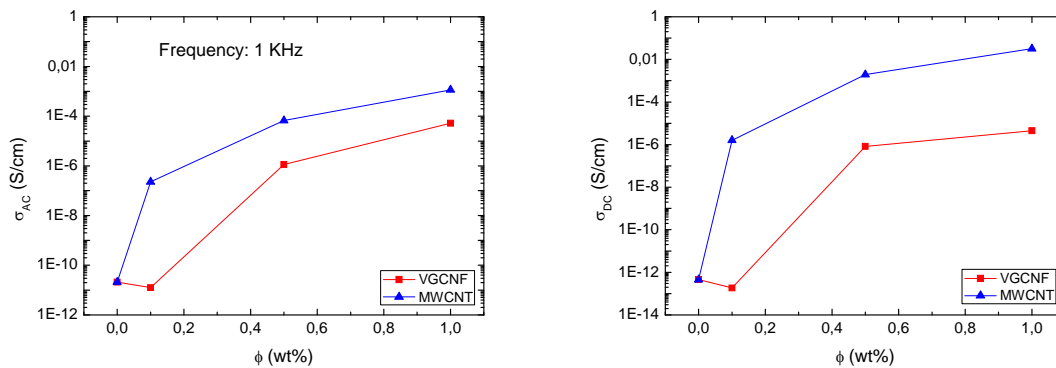
Figure 7. 5- Log-linear plots of the electrical conductivity as a function of weight fraction for MWCNT and VGCNF - epoxy composites: left and right - AC (1 kHz) and DC conductivity versus weight percentage, respectively.

The graphics of Figure 7.5 show that AC and DC conductivity of VGCNF and MWCNT composites increases with increasing concentration. On both figures, the curves of the MWCNT samples always present higher conductivity values in comparison to the values for the VGCNF curves for the same concentration. The higher increase on both AC and DC conductivity for the VGCNF curve is between 0.1 and 0.5 wt.%, in accordance with recent works [30, 32] that use the same preparation method, while for the MWCNT curves this phenomenon happens below 0.1 wt.%.

7.4- Discussion

The analysis of SEM and TOM images demonstrate that the MWCNT samples have smaller agglomerates than the ones reinforced with VGCNF. Both MWCNT and VGCNF composites were produced with exactly the same polymer matrix and processing method. Therefore, the reasons for the difference on the dispersion of the

nanofillers are the intrinsic characteristics of the nanofillers (structure, shape and dimension) and, as a consequence, the interaction (physical, chemical) of the nanofillers with the matrix and among them.

To calculate the percolation threshold for the VGCNF and MWCNT composites the theoretical framework developed by Celzard et al. [49] can be used. This work [49]was based on the Balberg [50] model and allows the calculations of the bounds for the percolation threshold for fibers with a capped cylinder shape. According to this theory, the bounds of the percolation threshold can be calculated using equation 7.1:

$$1-e^{\frac{-1.4V}{\langle V_e \rangle}} \le \Phi_c \le 1-e^{\frac{-2.8V}{\langle V_e \rangle}} \quad (7.1)$$

In equation 7.1, $<V_e>$ is the average excluded volume (the volume around an object in which the center of another similar object is excluded, averaged over the orientation distribution), V is the average volume of a single filler and Φ_c is the critical concentration of the percolation threshold. The values 1.4 and 2.8 found in the equation 7.1, obtained by simulation, are the lower and upper limits corresponding to infinitely thin cylinders and to spheres, respectively.

Using the values provided by the VGCNF manufacturer [51] and applying equation (7.1), the calculated $\Phi_c$is between 0.3 and 0.5 wt.% for an average aspect ratio of 433. Analyzing the top left graphic of Figure 7.4 and the VGCNF curves of both graphics from Figure 7.5, it can be observed that the higher increase in conductivity is between 0.1 and 0.5 wt.% and also that the conductivity is almost frequency-independent for the 0.5 wt.% and 1.0 wt.% composites. This means that the experimental Φ_c is between 0.1 and 0.5 wt.% which includes the predictions of the theory, meaning the calculated percolation bounds feat the experimental data. This analysis was confirmed in previous studies carried out with the same VGCNF composites [30, 32].

Assuming the data provided by the MWCNT manufacturer and applying equation 7.1, the calculated $\Phi_c$is between 0.7 and 1.5 wt.%. Analyzing the bottom left graphic of Figure 7.4 and the MWCNT curves of Figure 7.5 it is found that experimental bounds for the critical concentration are very distant from the corresponding calculated values, as the larger increase in electrical conductivity and therefore the percolation threshold occurs below 0.1 wt.%. The difference between the

calculated and the experimental bond values for the critical concentration is large, so it can be concluded that this model is not appropriate for the current MWCNT composites. The reasons for this mismatch are not clear, but it has to be pointed out that despite being widely used in literature, the used theoretical model has strong limitations. The model is based on the physical contact between fillers and the aspect ratio is the main factor to be considered in explaining the percolation threshold, so other factors such as the formation of clusters and its interaction with the matrix are neglected. The experimental results and the strong deviations confirm that more research is needed to determine the true nature of the relevant interactions determining the percolation threshold of these type of composites, being the clustering and cluster distribution a very important factor [29-32].

In the graphics of Figure 7.4 and 7.5, the curves of the MWCNT samples always present higher conductivity values in comparison to the values for the VGCNF curves for the same concentration. The difference in conductivity is due to the intrinsic characteristics of the nanofillers (aspect ratio, nanofillers conductivity, etc.), which is also related to the dispersion ability of the nanofillers in the matrix, as mention previously. In fact, in a recent work [52] it is demonstrated that the existence of good dispersion of clusters could promote the conductivity of the sample and in fact, the TOM micrographs from the MWCNT sample shows a better dispersion of the clusters than the VGCNF ones.

7.5- Conclusions

VGCNF and MWCNT - epoxy composites with 0.1, 0.5 and 1.0 wt.% and a neat sample, were produced by the same method. SEM and TOM images were taken to characterize the dispersion of the nanofillers. The DC and AC electrical conductivity and the dielectric constant were measured.

TOM micrographs and histograms of VGCNF and MWCNT composites demonstrated the formation of agglomerates with different sizes and geometries, which in the case of MWCNT samples, the clusters are better dispersed: the amount of small agglomerates of nanofillers is higher for the composites with MWCNT than with VGCNF. The difference on the dispersion of the two nanofillers is due to their intrinsic characteristics, which influences the composite electrical conductivity.

Although the Celzard's theory is suitable to calculate the bounds of the percolation threshold for the VGCNF composites, it does not fit for the MWCNT composites produced in the same way. In this way, the assumptions of this model (contact between nanofillers and its aspect ratio) are not valid and other factors such as nanofillers distribution have to be taken into account, as the percolation threshold is lower for samples with better nanofillers distributions (cluster dispersion).

References

1. Breuer, O. and U. Sundararaj, Big returns from small fibers: A review of polymer/carbon nanotube composites. Polymer Composites, 2004. **25**(6): p. 630-645.

2. Winey, K.I. and R.A. Vaia, Polymer Nanocomposites. MRS Bulletin, 2007. **32**: p. 314-322.

3. Maruyama, B. and H. Alam, Carbon nanotubes and nanofibers in composite materials. SAMPE Journal, 2002. **38**(3): p. 59–70.

4. Peigney, A., et al., Specific surface area of carbon nanotubes and bundles of carbon nanotubes. Carbon, 2001. **39**(4): p. 507-514.

5. Al-Saleh, M.H. and U. Sundararaj, A review of vapor grown carbon nanofiber/polymer conductive composites. Carbon, 2009. **47**(1): p. 2-22.

6. May, C.A. and G.Y. Tanaka, Epoxy Resins Chemistry and Technology, ed. M. Dekker. 1987, New York, USA.

7. Martone, A., et al., The effect of the aspect ratio of carbon nanotubes on their effective reinforcement modulus in an epoxy matrix. Composites Science and Technology, 2011. **71**(8): p. 1117-1123

8. Moniruzzaman, M. and K.I. Winey, Polymer Nanocomposites Containing Carbon Nanotubes. Macromolecules, 2006. **39**(16): p. 5194-5205.

9. Hussain, F., et al., Review article: Polymer-matrix Nanocomposites, Processing, Manufacturing, and Application: An Overview. Journal of Composite Materials, 2006. **40**(17): p. 1511-1575.

10. Stankovich, S., et al., Graphene-based composite materials. Nature, 2006. **442**(7100): p. 282-286.

11. Coleman, J.N., et al., Small but strong: A review of the mechanical properties of carbon nanotube-polymer composites. Carbon, 2006. **44**(9): p. 1624-1652.

12. Zhou, T., et al., Study of the thermal conduction mechanism of nano-SiC/DGEBA/EMI-2,4 composites. Polymer, 2008. **49**(21): p. 4666-4672.

13. Rao, Y., A. Takahashi, and C.P. Wong, Di-block copolymer surfactant study to optimize filler dispersion in high dielectric constant polymer-ceramic composite. Composites Part A: Applied Science and Manufacturing, 2003. **34**(11): p. 1113-1116.

14. Khastgir, D. and K. Adachi, Rheological and dielectric studies of aggregation of barium titanate particles suspended in polydimethylsiloxane. Polymer, 2000. **41**(16): p. 6403-6413.

15. Choi, Y.-K., et al., Mechanical and physical properties of epoxy composites reinforced by vapor grown carbon nanofibers. Carbon, 2005. **43**(10): p. 2199-2208.

16. Sandler, J.S., M. S. P. Prasse, T. Bauhofer, W. Schulte, K. Windle, A. H., Development of a dispersion process for carbon nanotubes in an epoxy matrix and the resulting electrical properties. Polymer, 1999. **40**(21): p. 5967-5971.

17. Andrews, R., et al., Fabrication of Carbon Multiwall Nanotube/Polymer Composites by Shear Mixing. Macromolecular Materials and Engineering, 2002. **287**(6): p. 395-403.

18. Schueler, R., et al., Agglomeration and electrical percolation behavior of carbon black dispersed in epoxy resin. Journal of Applied Polymer Science, 1997. **63**(13): p. 1741-1746.

19. Jimenez, G.A. and S.C. Jana, Electrically conductive polymer nanocomposites of polymethylmethacrylate and carbon nanofibers prepared by chaotic mixing. Composites Part A: Applied Science and Manufacturing, 2007. **38**(3): p. 983-993.

20. Okamoto, M., S. Morita, and T. Kotaka, Dispersed structure and ionic conductivity of smectic clay/polymer nanocomposites. Polymer, 2001. **42**(6): p. 2685-2688.

21. Guo, Z., et al., Fabrication and characterization of iron oxide nanoparticles reinforced vinyl-ester resin nanocomposites. Composites Science and Technology, 2008. **68**(6): p. 1513-1520.

22. Imai, Y., et al., Transparent poly(bisphenol A carbonate)-based nanocomposites with high refractive index nanoparticles. European Polymer Journal, 2009. **45**(3): p. 630-638.

23. Essawy, H.A., N.A. Abd El-Wahab, and M.A. Abd El-Ghaffar, PVC–laponite nanocomposites: Enhanced resistance to UV radiation. Polymer Degradation and Stability, 2008. **93**(8): p. 1472-1478.

24. Dasari, A., et al., Clay exfoliation and organic modification on wear of nylon 6 nanocomposites processed by different routes. Composites Science and Technology, 2005. **65**(15-16): p. 2314-2328.

25. Bocchini, S., et al., Influence of nanodispersed hydrotalcite on polypropylene photooxidation. European Polymer Journal, 2008. **44**(11): p. 3473-3481.

26. Jana, S.C. and S. Jain, Dispersion of nanofillers in high performance polymers using reactive solvents as processing aids. Polymer, 2001. **42**(16): p. 6897-6905.

27. Gorrasi, G., et al., Vapor barrier properties of polycaprolactone montmorillonite nanocomposites: effect of clay dispersion. Polymer, 2003. **44**(8): p. 2271-2279.

28. Zhu, A., et al., Film characterization of poly(styrene-butylacrylate-acrylic acid)–silica nanocomposite. Journal of Colloid and Interface Science, 2008. **322**(1): p. 51-58.

29. Cardoso, P., et al., The dominant role of tunneling in the conductivity of carbon nanofiber-epoxy composites. Physica Status Solidi a-Applications and Materials Science, 2010. **207**(2): p. 407-410.

30. Cardoso, P., et al., The influence of the dispersion method on the electrical properties of vapor-grown carbon nanofiber/epoxy composites. Nanoscale Res Lett, 2011. **6**(1): p. 370-370.

31. Aguilar, J.O., J.R. Bautista-Quijano, and F. Avilés, Influence of carbon nanotube clustering on the electrical conductivity of polymer composite films. eXPRESS Polymer Letters, 2010. **4**(5): p. 292–299.

32. Cardoso, P., et al., The role of disorder on the AC and DC electrical conductivity of vapour grown carbon nanofibre/epoxy composites. Composites Science and Technology, 2012. **72**(2): p. 243–247.

33. Patton, R.D.P., Jr C. U. Wang, L. Hill, J. R., Vapor grown carbon fiber composites with epoxy and poly(phenylene sulfide) matrices Composites Part A: Applied Science and Manufacturing, 1999. **30**(9): p. 1081-1091.

34. Chyi-Shan, W. and A.M. D, Method of forming conductive polymeric nanocomposite materials, O. University of Dayton (Dayton, Editor. 2004.

35. Rice, B.P., T. Gibson, and K. Lafdi. DEVELOPMENT OF MULTIFUNCTIONAL ADVANCED COMPOSITES USING A VGNF ENHANCED MATRIX. in 49th International SAMPE symposium proceedings. 2004. Long Beach.

36. Spitalsky, Z., et al., Carbon nanotube-polymer composites: Chemistry, processing, mechanical and electrical properties. Progress in Polymer Science, 2010. **35**(3): p. 357-401.

37. Breton, Y., et al., Mechanical properties of multiwall carbon nanotubes/epoxy composites: influence of network morphology. Carbon, 2004. **42**(5-6): p. 1027-1030.

38. Allaoui, A.B., S. Cheng, H. M. Bai, J. B., Mechanical and electrical properties of a MWNT/epoxy composite. Composites Science and Technology, 2002. **62**(15): p. 1993-1998.

39. Guo, P., et al., Fabrication and mechanical properties of well-dispersed multiwalled carbon nanotubes/epoxy composites. Composites Science and Technology, 2007. **67**(15-16): p. 3331-3337.

40. Špitalský, Z., et al., Modification of carbon nanotubes and its effect on properties of carbon nanotube/epoxy nanocomposites. Polymer Composites, 2009. **30**(10): p. 1378-1387.

41. Gojny, F.H., et al., Carbon nanotube-reinforced epoxy-composites: enhanced stiffness and fracture toughness at low nanotube content. Composites Science and Technology, 2004. **64**(15): p. 2363-2371.

42. Thostenson, E.T., S. Ziaee, and T.-W. Chou, Processing and electrical properties of carbon nanotube/vinyl ester nanocomposites. Composites Science and Technology, 2009. **69**(6): p. 801-804.

43. Peter, T.L. and et al., A quantitative assessment of carbon nanotube dispersion in polymer matrices. Nanotechnology, 2009. **20**(32): p. 7.

44. Šupová, M., G.S. Martynková, and K. Barabaszová, Effect of Nanofillers Dispersion in Polymer Matrices: A Review. Science of Advanced Materials, 2011. **3**(1): p. 1-25.

45. Hattum, F.v., et al. Quantitative assessement of mixing quality in nanoreinforced polymers using a multi-scale image analysis method. in 38th ISTC. 2006. Dallas, Texas.

46. Krause, B., et al., Correlation of carbon nanotube dispersability in aqueous surfactant solutions and polymers. Carbon, 2009. **47**(3): p. 602-612.

47.   Tibbetts, G.G., et al., A review of the fabrication and properties of vapor-grown carbon nanofiber/polymer composites. Composites Science and Technology, 2007. **67**(7-8): p. 1709-1718.

48.   Paiva, M. and J.C.e. al. The influence of extensional flow on the dispersion of functionalized carbon nanofibers in a polymer matrix. in Proc ChemOnTubes. 2008.   Zaragoza: digital.csic.es/.../ChemOnTubes2008_Book%20of%20Abstracts.pdf, pag 126.

49.   Celzard, A., et al., Critical concentration in percolating systems containing a high-aspect-ratio filler. Physical Review B, 1996. **53**(10): p. 6209.

50.   Balberg, I., et al., Excluded volume and its relation to the onset of percolation. Physical Review B, 1984. **30**(7): p. 3933.

51.   ASI. Applied Sciences Inc.; Available from: http://www.apsci. com/ppi-pyro3.html.

52.   Silva, J. and et al., Applying complex network theory to the understanding of high-aspect-ratio carbon-filled composites. EPL (Europhysics Letters), 2011. **93**(3): p. 37005.

8. Conclusions and suggestions for future work

8.1- Conclusions

In the study about the electrical properties of VGCNF/epoxy resin composites prepared by mixing with a blender it is demonstrated that a good VGCNF distribution seems to be more important than dispersion for low percolation threshold and high conductivity values. Inter-particle tunneling is proposed as the main conduction mechanism in these composites.

The second study investigates the morphological and electrical properties of VGCNF/epoxy composites prepared by four mixing methods such as blender mixing, capillary rheometer mixing, 3 roll milling and planetary centrifugal mixing. The morphological study is performed by TOM and GSA for a quantitative analysis of nanofillers dispersion in the composites. The DC electrical conductivity is also measured. The 3 roll mill achieved the best nanofiber dispersion level. The method used in this study to assess the dispersion level allows an effective quantification of the nanofibers dispersion at a lower resolution level of 0.13 μm.However, at this level of resolution the quantification of dispersion is not enough to gain an insight on the electrical response of the materials. Therefore, no relationship was found between the electrical conductivity and the greyscale analysis of the composites prepared with different methods. The composites prepared with the blender or capillary rheometer methods exhibit higher DC conductivity than those prepared with the planetary centrifugal mixer and 3 roll mill, confirming the previous study in which higher values of the DC conductivity are obtained for samples with better nanofiber distribution instead of better dispersion.

The third study uses the VGCNF/epoxy composites prepared by the aforementioned methods in order to investigate the influence of dispersion method on the electrical properties, mainly on the conduction mechanism. This study also mentions the importance of having a good distribution of nanofillers in order to achieve higher electrical conductivity, being the conductivity of well distributed VGCNF described by hopping between nearest fillers which results in a weak disorder regime.

In the fourth study, the piezoresistive response of the VGCNF/epoxy composites prepared by the different methods was investigated. The dispersion method leading to a better cluster dispersion also lead to better piezoresistive responses, besides improving the electrical properties. The piezoresisitive response was quantitatively analyzed by the

gauge factor (GF) and it is proved to be strongly dependent on nanofillers concentration, reaching the highest values around the percolation threshold. At this concentration, the intrinsic contributions to the GF are larger than the geometrical one. The maximum value of the gauge factor is close to 9.8 for the blender mixing method composites, and its cycle and thermal stability indicate that these materials can be used as piezoresistive sensors. The composites show GF variations up to 10% depending on the deformation level and deformation velocities used in this study.

In the last study, the comparison of epoxy resin composites with VGCNF and MWNT has been addressed, in terms of morphological and electrical properties. These composites were produced using blender mixing. The morphological analysis was performed by SEM and TOM images in order to evaluate the nanofillers dispersion, while the electrical properties were characterized through AC and DC measurements. The analysis of TOM and SEM images of MWCNT composites shows a better distribution of nanofillers than for VGCNF composites. The nanofillers intrinsic characteristics such as aspect ratio and surface characteristics are responsible for the difference in the dispersion ability, influencing the electrical properties of composites and the interaction between nanofillers and matrix. For the calculation of the percolation threshold bounds for the VGCNF composites, the Celzard's theory was shown to be suitable but it fails for the case of MWCNT composites. This indicates that, beyond the aspect ratio, there are other intrinsic characteristics of MWCNT which have to be taken into account for explaining the composites electrical conductivity.

The overall main conclusions of the present work concerns to the relation between the dispersion of nanofillers and the electrical and electromechanical properties of composites with epoxy resin and VGCNF. One of the most important conclusions of this work is that a good VGCNF distribution (cluster dispersion) seems to be more important than VGCNF dispersion in order to obtain high electrical conductivities and lower percolation thresholds. The method used in this work to quantify of the nanofibers dispersion is successful at low resolution level (0.13 μm), although this scale is not suitable for a correlation with the electrical behavior of composites. The VGCNF/epoxy resin composites prepared with the blender and capillary rheometer methods exhibit higher DC conductivity, while the three roll mill provided the best nanofiber dispersion level. The conductivity of composites with well dispersed clusters is described by hopping between nearest fillers, resulting in a weak disorder regime.

The dispersion methods leading to a better cluster dispersion at VGCNF contents around the percolation threshold also lead to better piezoresistive responses. Finally, it can be concluded that MWCNT composites have better distribution of nanofillers than the VGCNF composites and that the intrinsic characteristics of nanofillers are responsible for the difference in the dispersion ability and electrical properties of composites and also the interaction between nanofillers and matrix.

8.2- Suggestions for future work

An important subject to be investigated in polymer based VGCNF and CNT composites is the relation between the morphology and the electrical properties. This work used a method which was able to quantify the nanofillers dispersion, but not to gain an insight on the electrical properties. Novel techniques and mathematical tool have still to be developed to properly address this important subject at scales more suitable to be correlated to the electrical response of the materials. Further, despite the several models dealing with the electrical response of this types of composites more theoretical and experimental work are needed to disclose the role of the polymer matrix (crystallinity, conductivity, etc.) on the overall electrical response of the composites at the different filler concentrations.

The last study presented in this thesis tried to establish a bridge between the investigation of the electrical and morphological properties for epoxy resin composites with VGCNF and MWCNT. It was mentioned that the intrinsic characteristic considered for the determination of the bounds of the percolation threshold of both VGCNF and MWCNT composites was the aspect ratio. In fact, these bounds were calculated according to a theoretical framework (Celzard's theory) which fits the results of VGCNF composites, but is not consistent for the MWCNT composites. Therefore, it is necessary to study which characteristics can also influence the electrical properties and find a theoretical framework which is, at least, suitable to predict both CNF and CNT composites.